UNIVERSITÉ DU QUÉBEC

THÈSE PRÉSENTÉE À
L'UNIVERSITÉ DU QUÉBEC À TROIS-RIVIÈRES

COMME EXIGENCE PARTIELLE
DU DOCTORAT EN BIOPHYSIQUE (3494)

PAR
Paul BERNAZZANI

Contrôle de la morphologie des systèmes amylose-eau et caractérisation par DSClent et FTIR

MAI 2000

RÉSUMÉ

L'amylose, un des constituants de l'amidon, est un polymère naturel abondant dans la nature qui sert de réserve d'énergie aux plantes et de nourriture aux êtres vivants. Malgré le nombre d'études de nature fondamentale ou appliquée, consacrées à l'amylose depuis plus de cinquante ans, le détail des mécanismes de l'interaction amylose-eau et des changements de phases (gélation, dissolution, rétrogradation, cristallisation) reste encore assez obscur.

Le travail présenté dans cette thèse est une contribution à la compréhension de ces mécanismes basée sur *deux concepts nouveaux* valables pour toutes les molécules en chaîne, *celui de tension et de changement de phase sous tension et celui de la présence d'ordre à courte distance*. Ces concepts ont été élaborés lors d'études antérieures sur des gels et des solutions de polyéthylène (PE). Leur développement a été lié à deux techniques, celle de calorimétrie à balayage lent (DSC_{Lent}) et celle de spectroscopie infrarouge (IR). *Les deux permettent de mesurer quantitativement l'ordre à courte distance et l'ordre tendu* présent dans un échantillon .

L'idée essentielle qui nous a conduit à passer de la calorimétrie à balayage rapide (DSC_{Rapide}) à la DSC_{Lent} pour analyser l'ordre est la suivante: la tension produite dans une partie du polymère dans l'expansion provoquée par la rampe de température, n'est pas une conséquence obligée de la dissolution (ou de la fusion), mais peut être réduite par un chauffage lent. La région du matériau tendue c'est-à-dire celle où les chaînes ne peuvent pas se rééquilibrer rapidement à cause de freins à leur mobilité (enchevêtrements, liaisons cohésives) a été appelée réseau. La température de dissolution (ou de fusion) de l'ordre dans les réseaux est déplacée vers les hautes températures. En conséquence, l'ordre tendu non dissous (ou non fondu), important lors d'une DSC_{Rapide}, conduit à une solution (ou à un état fondu) hétérogène.

L'investigation de l'ordre à courte distance dans les mélanges amylose-eau s'est faite par la même DSC_{Lent} utilisée pour les polyoléfines (article 1). Pour les études IR des systèmes amylose-eau, nous avons dû recourir à une stratégie complexe. En effet, alors que l'ordre à courte distance et l'ordre tendu dans le PE se reconnaissent par des déplacements de bandes pour des films de différentes cristallinité (article 2), les spectres donnés dans la littérature pour des systèmes amylose-eau traités différemment semblaient peu changés.

Pour trouver une réponse à la question de la relation entre spectres IR et composition phasique, nous avons décidé de préparer des échantillons d'histoire très différente et de comparer leur spectre. *L'originalité de ce travail réside dans la préparation d'échantillons dont les spectres sont très différents entre eux et avec ceux de la littérature. Ces échantillons constituent le matériau de base des articles 3 et 4.* Nous avons préparé ces échantillons en procédant à une dissolution très lente jusqu'à une température maximum dite Tmax et en les refroidissant à la même vitesse. L'importance d'une dissolution lente pour faire une solution homogène nous avait été apprise par les conditions nécessaires à la dissolution du réseau (article 1), la nécessité d'une cristallisation lente pour faire de bons cristaux débarrassés des enchevêtrements était bien connue dans la littérature.

La variation des spectres des échantillons traités différemment (valeur de Tmax) nous a permis d'identifier les cinq bandes variables de la région des vibrations d'élongations C-O et C-C étudiée. En faisant des hypothèses, basées sur la littérature ou les résultats de calorimétrie, nous avons associé chacune de ces bandes à une phase, telle la phase caractéristique des gels, des simples et doubles hélices et de l'environnement associé aux cristaux B et V.

La dissolution d'échantillons traités à différents Tmax ont été suivis par DSC_{Rapide} et DSC_{Lent} (article 4). Les chaleurs de dissolution de l'amylose, qu'on attendrait élevées en considérant la

préparation des échantillons et leur cristallinité par diffraction des rayon X (0.4-0.5) sont très faibles (0 à 4 J/g). *Ce résultat montre sans ambiguïté que la méthode de DSC_{Rapide} pourtant largement utilisée ne peut caractériser l'ordre à grande distance dans des systèmes polymère-solvant très cohésifs, comme les mélanges amylose–eau.* Au contraire, la calorimétrie lente qui enregistre pendant une douzaine d'heures le flux de chaleur qui accompagne une dissolution en équilibre, conduit à des chaleurs de dissolution élevées (22 à 148 J/g). Alors que la trace de dissolution d'un système amylose–eau est constituée d'un seul endotherme, celles des échantillons traités se décompose en trois endothermes distincts dont les chaleurs respectives dépendent de Tmax. Ceux-ci correspondent à des réponses différentes des phases du matériau à la tension induite par l'expansion dans la rampe de température, les moins tendues se dissolvant à plus basse température. Nous avons pu faire une corrélation entre l'intensité d'une ou de deux bandes du spectre IR et l'une et l'autre des trois contributions à la chaleur de dissolution. En utilisant deux techniques complémentaires, cette recherche a montré clairement que les concepts de tension et d'ordre à petite distance sont plus importants dans les systèmes amylose–eau que dans les solutions et les gels de polyoléfines. Dans le chapitre cinq (article 4) nous expliquons que si ces concepts sont ignorés la caractérisation du système amylose–eau sera incomplète.

TABLE DES MATIÈRES

LISTE DES FIGURES

LISTE DES TABLEAUX

REMERCIEMENTS

Je tiens à remercier tout particulièrement le professeur Geneviève Delmas Patterson, pour son soutien et surtout pour son enthousiasme contagieux. Je tiens également à remercier le professeur Camille Chapados pour ses conseils et son apport théorique. Un gros merci aux personnels et aux étudiants des deux laboratoires de Macromolécules (UQAM) et de Spectroscopie Moléculaire (UQTR) pour leurs explications et leur compréhension; merci Phuong, Madgid, Karin, Nathalie et Michel, Jean-Joseph, et Christophe.

Énorme merci à T.M., mon épouse, qui s'est montrée compréhensive et flexible dans les moments difficiles, et à ma famille qui croit en moi et ne cesse de grandir.

CHAPITRE 1

1 INTRODUCTION

1.1 L'amylose

L'amylose est un polysaccharide qui contient quelques milliers d'unités glucosidiques et dont la masse molaire varie entre 150 et 600 kDa. L'unité monomérique de l'amylose est l'α-D glucose et les liaisons polymériques se font en position 1 et 4 (Fig. 1A). L'unité répétitive de l'amylose est le maltose, un diglucose (Fig. 1B). La structure primaire des chaînes d'amylose est formée de chaînes linéaires et la structure secondaire est en formation hélicoïdale. L'unité monomérique de la cellulose est la même que celle de l'amylose soit le glucose, mais l'unité répétitive est la cellobiose, un diglucose, qui a un arrangement différent du maltose (Fig. 1C). À cause de cette différence, les propriétés physico–chimiques et physiologiques de l'amylose sont différentes de celles de la cellulose. La cellulose qui est le constituant principal du bois, n'est pas soluble dans l'eau et dans la plupart des solvants organiques et elle n'est pas comestible par les humains. L'amylose, un des principaux constituants de l'amidon, est soluble dans l'eau et dans plusieurs solvants organiques. Dégradable par les enzymes, elle est comestible.

L'amylose est donc un polymère biodégradable. Cette propriété a intéressé de nombreux chercheurs dans des domaines très variés comme le secteur alimentaire et le secteur pharmaceutique. Dans ce dernier secteur, il sert à l'enrobage des médicaments et comme support au principe actif [1-3]. Dans le premier secteur il sert à l'alimentation, et à la modification de l'aspect physique des aliments [4]. La fabrication des sacs pour les résidus alimentaires est en pleine expansion. Ces sacs, qui sont composés d'amylose et de polyoléfine

se dégradent beaucoup plus rapidement que ceux composés uniquement de polyoléfines.

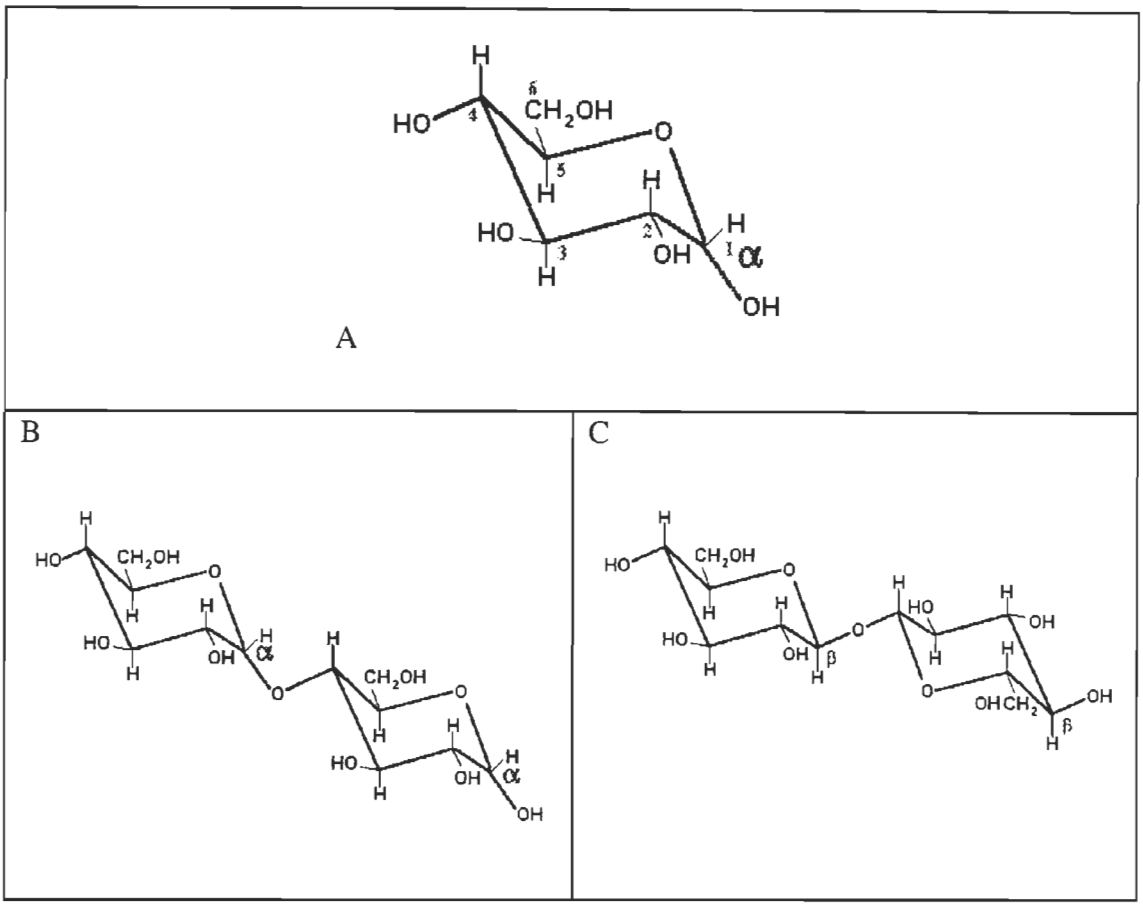

Figure 1. Le monomère et l'unité répétitive de l'amylose et de la cellulose. A, le glucose; B, le maltose qui est l'unité répétitive de l'amylose; C, le cellobiose qui est l'unité répétitive de la cellulose.

Bien que l'amylose soit un composé commercial de première importance, ses caractéristiques physico-chimiques ne sont pas toutes bien comprises et bien contrôlées, surtout celles des mélanges amylose-eau qui sont les plus importantes. Pour développer de nouveaux produits et de nouvelles utilisations de l'amylose, il faut connaître ses caractéristiques physico–chimiques qui permettront de contrôler l'organisation des chaînes du polymère. Avant d'aborder cet aspect qui est l'objet de la thèse, nous parlerons de l'amidon, source de l'amylose et de la

façon d'extraire ce dernier des réserves végétales.

1.2 Source de l'amylose : l'amidon

L'amidon peut être isolé de nombreuses sources: racines, tubercules, tiges, feuilles, graines, fruits et pollen. Toutes ces variétés donnent différents types d'amidon qui ont des propriétés différentes. Les principales sources commerciales de l'amidon sont le maïs, la patate, le blé, le manioc et le maïs ciré. La production mondiale annuelle de l'amidon est estimée à 26 millions de tonnes [5].

L'amidon est un matériau synthétisé dans les cellules des plantes et dans de nombreux micro-organismes. Comme plusieurs glucides naturels, tel le glycogène et la cellulose, l'amidon est un polysaccharide constitué uniquement d'unités glucosidiques. L'amidon est un mélange de deux molécules différentes: l'amylose et l'amylopectine. Ces molécules sont des polymères dont l'unité monomérique est l'α-D–glucose. Les chaînes d'amylose forment facilement des hélices. L'amylopectine a des branchements à tous les 35-30 unités glucose [6, 7].

Outre la présence d'amylose et d'amylopectine, l'amidon renferme également d'autres composés non glucidiques. Dans les amidons de céréales telles que le blé et le maïs, il y a environ 0.8% de lipides et de 0.1 à 0.5% de protéines. Dans les amidons de tubercules et de racines, le contenu en lipides et en protéines est plus petit que 0.1 % [8-13].

Selon la source d'amidon, la quantité d'eau et le rapport amylose/amylopectine varient. Le contenu en amylose de la plupart des amidons, est d'environ de 20 à 30% [14, 15]. Dans certaines espèces de plantes mutagéniques, comme l'amylomaïs, la quantité d'amylose peut être de 80% tandis que dans l'amidon ciré elle diminue à 1%. Ces différences affectent les propriétés physiques de l'amidon et son utilisation.

La densité de l'amidon sec varie entre 1.514 et 1.520 g/cm^3 tandis que celle de l'amidon possédant une quantité d'eau en équilibre varie entre 1.468 et 1.485 g/cm^3 [16]. L'amidon a la propriété d'absorber une certaine quantité d'eau. Par exemple, l'amidon de pomme de terre absorbe jusqu'à 35% de son poids en eau. L'eau est également un agent plastifiant pour l'amidon c'est-à-dire qu'elle baisse considérablement la température de transition vitreuse de ce dernier ce qui rend l'amidon plus facilement malléable à la température de la pièce.

1.2.1 L'intérêt de l'amidon

L'amidon est le produit principal du régime alimentaire de toutes les sociétés humaines. Les diététistes favorisent l'amidon dans les diètes plutôt que les produits raffinés comme les sucres et les matières grasses [17]. Outre leurs apport alimentaires, les polysaccharides constituent d'excellents produits de base qui servent à modifier la consistance et la texture de plusieurs aliments. Pour ces raisons, l'amidon est beaucoup utilisé dans l'industrie de l'alimentation.

Plusieurs industries utilisent l'amidon pour modifier des caractéristiques des aliments (transparence, viscosité, goût). Une suspension d'amidon dans l'eau devient translucide après le gonflement de l'amidon. Cette transparence peut être contrôlée par la température ou par l'ajout d'agents se complexant avec l'amidon [18]. La viscosité des produits alimentaires augmente dans les sauces et les puddings, après l'ajout d'amidon [18]. L'ajout d'amidon dans les aliments modifie le goût [18].

D'autres industries utilisent abondamment l'amidon. Par exemple l'industrie du papier, dont le composé principal est la cellulose, utilise une quantité importante d'amidon comme additif dont l'utilité est de lier les molécules de cellulose pour obtenir un papier plus résistant. L'industrie du textile est un autre grand consommateur d'amidon qui l'utilise dans quatre

grands domaines [18]: a) comme apprêt pour augmenter la force des fils et améliorer leur résistance à l'abrasion; b) dans la finition pour modifier l'apparence du tissu après la décoloration ou la teinture; c) lors de l'impression des tissus, pour augmenter la consistance de la pâte de colorant et d) dans la finition comme composé de polissage. L'importance de l'amidon dans l'industrie et conséquemment de l'amylose, est donc très grande.

1.3 Choix de l'amylose

L'amylose est un polymère linéaire de glucose avec des liens glucosidiques en position 1–4 (Fig. 2A) tandis que l'amylopectine possède, en plus, des liaisons en position 6 (Fig. 2B). À cause de ce point d'ancrage supplémentaire, ce produit est caractérisé par des branchements. La longueur des branches dépend de nombreux facteurs dont le principal est la provenance de l'amidon. L'amylose présente une forme hélicoïdale (Fig. 2C). Les différentes variétés d'amylopectine dont les masses molaires varient entre 10^6 et 10^8 kDa, ont des morphologies arborescentes caractéristiques (Fig. 2D) composées de chaînes en hélices.

À cause des branchements de l'amylopectine et des nombreuses possibilités d'interactions avec les branchements voisins, l'organisation moléculaire de ce polymère est fort complexe [19]. Comme nous le verrons au cours de cette étude, l'organisation de l'amylose est complexe. Cette organisation est cependant beaucoup moins compliquée que celle de l'amylopectine [11, 16, 17, 20]. C'est la raison pour laquelle nous avons choisi d'étudier l'amylose plutôt que l'amylopectine et l'amidon.

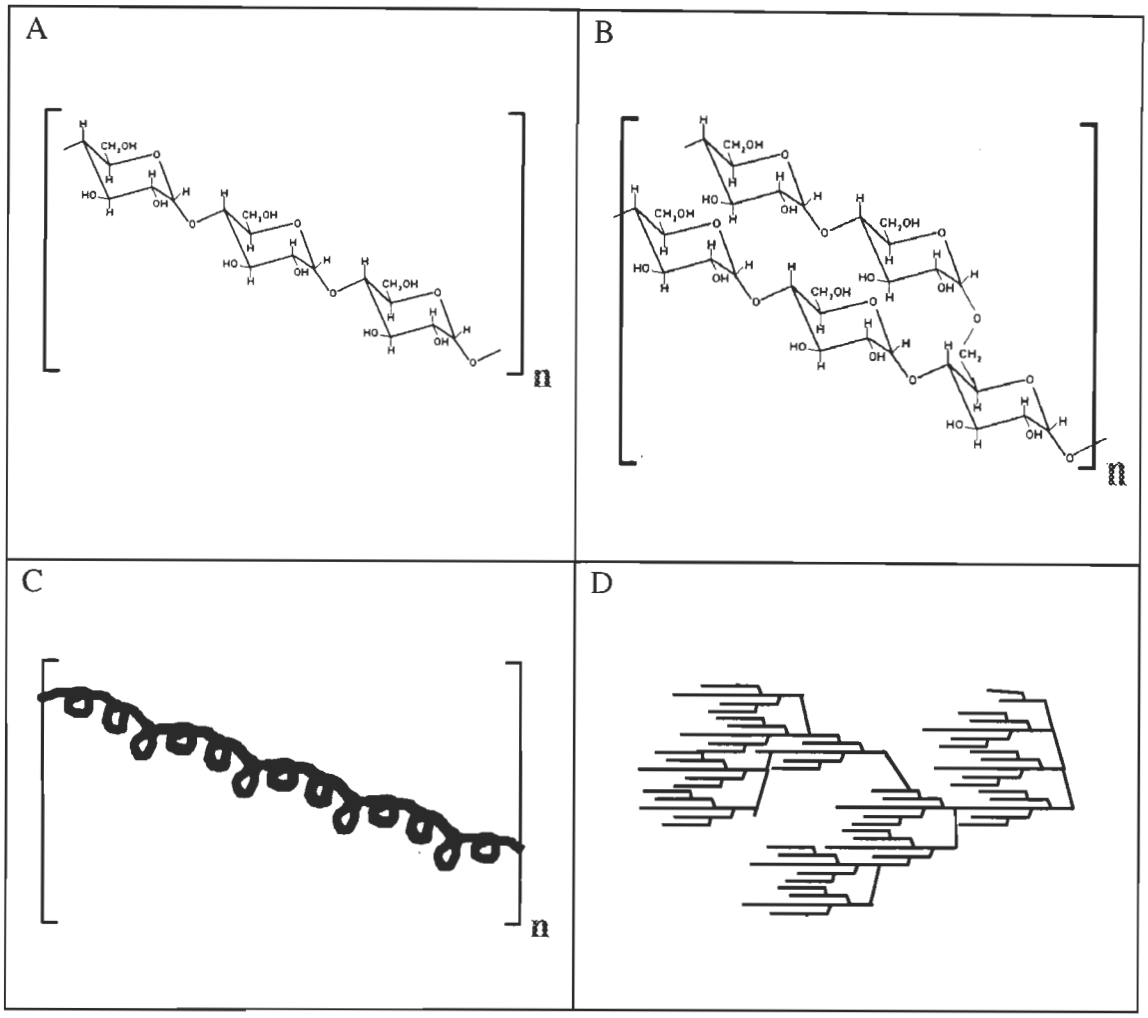

Figure 2. Arrangement moléculaire et morphologique de l'amylose (A, C) et de l'amylopectine (B, D)

1.4 L'intérêt de l'amylose

Dans le cadre de ce projet, nous nous proposons d'étudier l'amylose pour plusieurs raisons: i) l'amylose possède les mêmes phases que celles associées à l'amidon [21]; ii) l'amylose est le constituant le plus simple de l'amidon, il est linéaire et il peut se cristalliser; iii) l'amylose peut être utilisé dans l'alimentation animale et humaine; iv) l'amylose peut être utilisé comme vecteur de médicaments avec des cibles spécifiques.

D'autres facteurs rendent l'amylose intéressant à cause des applications nouvelles qui peuvent

être développées. Son coût de production est faible parce qu'il est obtenu de l'amidon, lequel est la plus importante biomasse produite sur terre après la cellulose [17, 22]. L'amylose, qui est biocompatible, c'est-à-dire qui ne provoque pas de réaction immunitaire chez les humains, est de ce fait un candidat idéal pour de nombreuses applications pharmacologiques comme des matrices de médicament à relarguage lent [21]. En effet, l'amylose réticulé par l'ajout d'épichlorohydrine est utilisé comme matrice polymérique dans les médicaments à relarguage lent depuis le début des années 90 [22]. Cependant il a été trouvé que le relarguage s'effectue de façon non linéaire et dépend du taux de réticulation [23]. Plusieurs auteurs ont supposé que ces propriétés sont associées à la réticulation et à l'enchevêtrement qui sont des paramètres dont dépend la cohésion de la matrice [24-27].

De plus, certains types d'amylose ont une résistance à l'amylase qui est l'enzyme responsable de la dégradation de l'amylose en glucose [28, 29]. Cette propriété ouvre la porte à des applications pharmaceutiques ciblées à des sites spécifiques. En effet, une matrice d'amylose contenant un certain type de médicament pourrait aller le libérer dans un endroit précis qui dépendrait de la résistance au processus de digestion de l'amylose. Des recherches ont montré que des amyloses, traités chimiquement et thermiquement, permettaient un contrôle de la libération de médicaments [30].

Ainsi, bien que l'importance de l'amylose repose sur le fait qu'il est un des constituants de l'amidon, et que ce dernier possède de multiples applications industrielles, l'amylose lui-même possède des qualités et des applications propres qui en font un objet d'études intéressantes.

1.5 L'extraction de l'amylose

Plusieurs méthodes de séparation des principales composantes de l'amidon ont été

développées au cours des cent dernières années. La plupart d'entre elles utilisent la précipitation sélective de l'amylose. La première méthode, développée en 1905 par Maquenne et Roux [31], consiste à laisser reposer la pâte d'amidon préalablement autoclavée à 80 °C. Avec le temps, l'amylose précipite et peut être récupéré par filtration. Une deuxième méthode consiste à faire gonfler des granules d'amidon dans une solution alkaline composée de 1% de NaOH. La neutralisation de la solution provoque la précipitation de l'amylose [32]. Une troisième méthode plus récente, consiste à ajouter une substance organique polaire qui fait précipiter l'amylose sous la forme d'un complexe insoluble. Cette méthode est l'approche favorisée dans l'industrie. L'amylose est obtenu en le complexant avec de l'iode ou du n–butanol [33-37]. Une quatrième méthode pour séparer l'amylose de l'amidon consiste à induire la précipitation de l'amylose par l'addition d'un mauvais solvant. Cette méthode sert à séparer les polymères de poids moléculaires différents [38, 39].

1.6 Caractéristiques du système amylose–eau

Plusieurs études ont montré que la quantité d'eau jouait un rôle important sur la composition phasique et les propriétés physiques de l'amylose [9, 17, 27, 28, 31, 32, 39]. En effet, l'ajout d'eau permet une plus grande mobilité des chaînes d'amylose ce qui rend la modification de la composition phasique plus aisée, mais augmente le nombre d'interactions possible entre les chaînes, d'où une cristallisation plus facile. La plupart des applications de l'amylose utilisent un rapport amylose-eau de 70:30. Nous étudions dans ce projet un système amylose-eau dans lequel on retrouve de façon constante, 30% d'eau. Ceci nous permet de nous assurer que les caractéristiques de l'amylose étudié sont constantes.

Les caractéristiques qui définissent le système amylose-eau peuvent être regroupées sous deux

catégories : a) Les propriétés physiques, et b) les caractéristiques phasiques. Ces dernières sont définies comme étant les propriétés de l'amylose qui reposent soit sur la quantité relative de chaque phase (la composition phasique) soit sur l'interaction entre une ou plusieurs de ces phases.

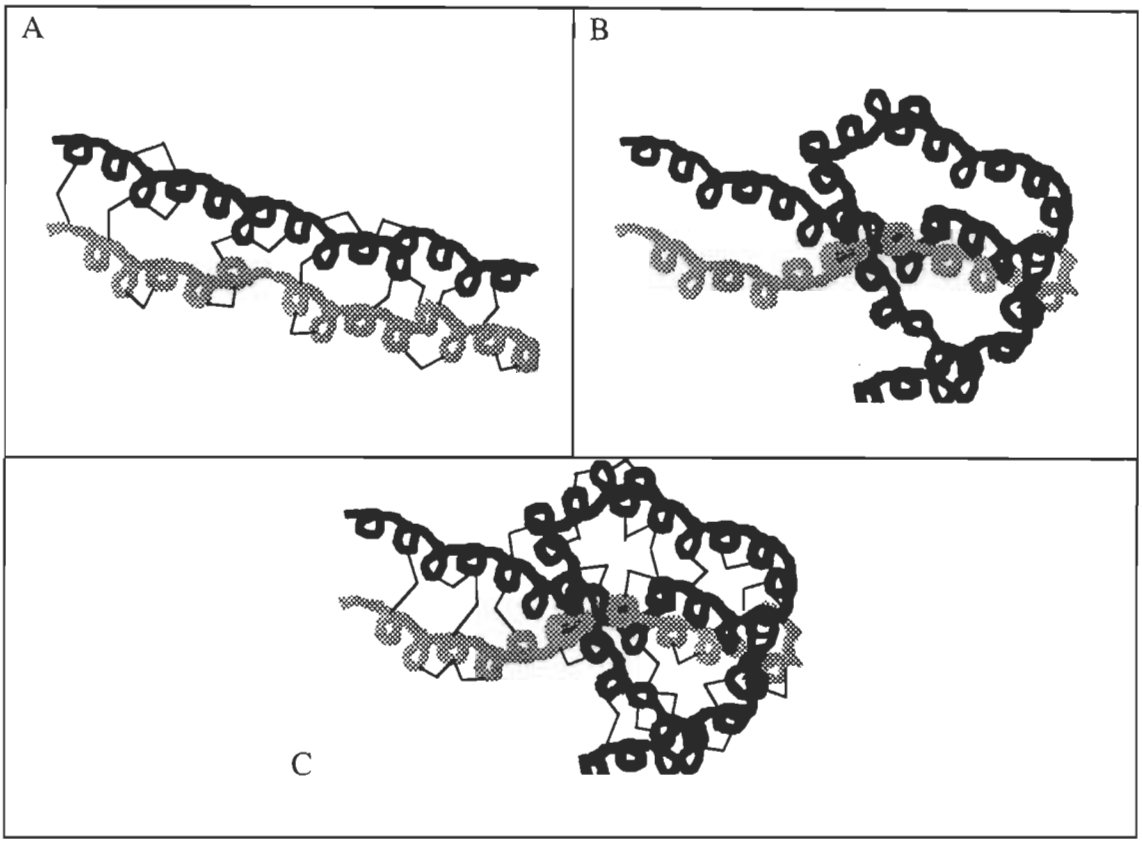

Figure 3. Schéma des réseaux non-ordonnés de liaisons hydrogène (A) et d'enchevêtrements (B) qui causent de la tension dans l'amylose. En (C) on retrouve la situation réelle où les deux types de réseaux existent simultanément.

Les interactions présentes dans le système amylose-eau sont nombreuses. La figure 3 présente de façon schématique, des exemples de deux interactions, soit les liaisons hydrogène (A) et les enchevêtrements entre les chaînes (B). Dû au fait que l'amylose possède de nombreux groupements OH, il a été observé que des ponts hydrogènes peuvent se former de façon soit intermoléculaire, soit intramoléculaire avec ou sans l'aide de molécules d'eau [17, 39]. La

complexité du système s'accroît lorsque les chaînes linéaires d'amylose s'enchevêtrent jusqu'à former des nœuds. La figure 3C montre la situation réelle où les enchevêtrements coexistent avec les ponts hydrogènes.

1.6.1 Structure de l'amylose

Quelques études récentes ont augmenté considérablement nos connaissances sur la structure de l'amylose. Nous mentionnerons tour à tour celles qui ont déterminé la structure cristalline de l'amylose et celles qui ont déterminé ses propriétés physiques. Il y a dans le système amylose–eau des états ordonnés et des états non-ordonnés.

1.6.1.1 États ordonnés de l'amylose

L'amylose peut être sous quatre formes cristallines différentes nommées A, B, C et V [9, 16]. Lorsqu'une complexation a lieu entre l'amylose et une petite molécule (acide aminé, alcool, etc.), il y a formation de la forme V qui est un cristal orthorhombique où les chaînes dans la maille cristalline sont des simples hélices. Dans les formes A B et C au contraire, les chaînes sont des doubles hélices. La forme A cristallise en cristaux hexagonaux. La forme B est une déformation des cristaux de types A. La forme C est rare et possède une structure cristalline intermédiaire entre les formes A et B. La forme cristalline d'un échantillon va être déterminée par sa provenance. Ainsi, la forme A est retrouvée dans les amyloses de céréales tandis que la forme B se retrouve dans les tubercules.

1.6.1.2 États non–ordonnés dans le système amylose–eau

La présence dans l'amylose de chaînes libres possédant une mobilité grande n'est pas contestée. Ces chaînes forment l'état amorphe. En plus de cet état, plusieurs chercheurs ont

supposé la présence d'une interphase dans le système amylose-eau [25, 40, 41]. Une de ces hypothèses est l'existence d'une interphase composée d'enchevêtrements dans les chaînes [42, 43]. De plus, Godet et ses collaborateurs, en utilisant la modélisation moléculaire, ont récemment noté qu'une forme de type simple hélice pouvait exister sans formation d'un complexe avec d'autres molécules [44, 45]. Nous parlons alors d'un type V amorphe.

1.6.2 Phénomènes physiques

Les études portant sur les changements de phase associés à l'amylose tels que la gélification et la rétrogradation, ont permis de comprendre et de contrôler ces phénomènes [4, 46]. La gélification est le processus menant à la formation irréversible d'un gel à partir d'un mélange concentré d'amylose–eau porté à une certaine température [4, 47]. Les chaînes gonflées formant le gel sont incrustées dans une matrice continue de chaînes enchevêtrées. La rétrogradation est le processus de l'augmentation de la cristallinité chez l'amylose avec séparation de phase. Elle implique la gélification préalable de l'amylose [20]. Ce phénomène se produit lorsque les gels sont entreposés pour un certain temps. Ils subissent la rétrogradation et leur fraction cristalline augmente.

1.6.2 Interaction avec l'eau

Les interactions de l'amylose avec l'eau sont très complexes: la présence d'eau est essentielle à la mobilité des chaînes et à la cristallisation de l'amylose hydraté. Par ailleurs, les solutions très diluées d'amylose ne sont pas stables et s'agrègent avec le temps. En effet, l'unique méthode pour obtenir une solution d'amylose est de faire une solution dans NaOH 1 N et de neutraliser par la suite. Ceci donne toutefois une solution métastable avec l'amylose qui rétrograde c'est-à-dire qui s'agglutine et précipite [4, 20, 31]. Plusieurs chercheurs se sont intéressés aux

interactions eau-amylose et eau-amidon. La plupart concluent que les liaisons hydrogènes stabilisent les formes en hélice et donc les arrangements cristallins [48, 49]. Cependant, l'apport des différents types de liaisons hydrogène par exemple les ponts inter- et intramoléculaires n'a pas encore été étudié.

Buléon *et al.* ont démontré en utilisant une combinaison de diffraction des rayons X et de modélisation moléculaire, que les doubles hélices qui forment les cristaux de type B, de structure cristalline hexagonale, pouvaient contenir trente six molécules d'eau tandis que les simples hélices qui forment les cristaux de type V, de structure cristalline orthorhombique ne peuvent en contenir que neuf [48]. La complexité de ces arrangements est telle que la compréhension du système amylose-eau est encore loin d'être complète.

1.6.3 Liaisons hydrogène

L'unité monomérique de l'amylose est un sucre qui possède plusieurs groupements OH (Fig. 1). Entre les chaînes et l'eau et entre les chaînes elles-mêmes, il peut se former des liaisons hydrogène intra- et intermoléculaires [46, 50, 51]. L'organisation de ce système est telle qu'elle provoque des changements dans la composition phasique et les propriétés mécaniques du composé.

L'agrégation de l'amylose dépend de la quantité d'eau présente dans le composé [28, 52, 53]. Biliaderis a démontré par des méthodes d'analyses thermiques, que les systèmes amylose-eau passent par plusieurs processus irréversibles [17]. La relaxation de ces processus est reliée aux différents ponts hydrogène tant inter– qu'intramoléculaires et peut être observée par des techniques calorimétriques.

La température de transition vitreuse de l'amylose est également reliée à la quantité d'eau

présente dans l'échantillon [28]. Le rôle de l'eau dans les transformations cristallines et morphologiques du composé n'est pas encore bien compris mais est essentiel dans la détermination des propriétés physiques de l'amylose. La possibilité d'une interphase entre la phase cristalline et la phase amorphe doit être envisagée.

1.6.4 Enchevêtrements

La présence d'enchevêtrements dans les polymères est un phénomène connu depuis plusieurs années [54, 55]. Dû à la difficulté de quantifier les enchevêtrements, les chercheurs considèrent que leurs effets sur les propriétés des polymères semi-cristallins sont négligeables [56].

Récemment, Nguyen *et al.* ont développé une méthode calorimétrique pour caractériser les enchevêtrements dans les polyoléfines [57-59]. Ils ont montré que des tensions développées au cours du chauffage, modifiaient de façon non négligeable les propriétés des échantillons. En effet, la vitesse à laquelle les cristaux de polypropylène fondent provoque une modification de la tension dans le polymère qui a pour conséquence de varier la quantité et la qualité des cristaux après une cristallisation lente. Les auteurs de cette étude ont évoqué l'hypothèse que le resserrement des enchevêtrements provoque des tensions entre les chaînes qui nuisent à la cristallisation. Plus la vitesse de chauffe est grande, plus grande est la tension.

Il est raisonnable de penser que le développement de la tension ne dépend pas de la nature des jonctions (enchevêtrements ou liaisons hydrogène). En effet, une étude a montré que la stabilité morphologique de l'amylose, par example la stabilité des hélices, est influencée par les liaisons hydrogène ou par des enchevêtrements [60].

1.7 Problématique pour l'étude structurale de l'amylose

1.7.1 État de la situation

La littérature sur l'amylose est unanime pour admettre que le détail des interactions amylose-eau et leurs changements dans des cycles de chauffage et de refroidissement (gélification, cristallisation) sont mal compris. Ceci est dû, d'une part à la complexité de l'amylose, et d'autre part au nombre limités de techniques pour éclaircir les interactions. Depuis quelques années, la RMN de l'état solide a été appliquée à l'analyse de phase et a permis d'identifier trois phases contenant de l'ordre: ordre à grande distance, ordre moléculaire et sans ordre. [25, 27]. Dans cette thèse, nous proposons la présence de deux morphologies dans l'amylose qui ont jusqu'ici été largement ignorées : 1) un réseau causé par les enchevêtrements entre les chaînes; 2) un réseau causé par les liaisons hydrogène. Ces deux réseaux sont appelés phases intermédiaires puisqu'elles possèdent une mobilité intermédiaire entre celles des phases cristalline et amorphe.

La présence de ces réseaux dits semi–ordonnés augmente la tension dans le système dans des conditions décrites ci-dessous. L'augmentation de tension se produit après le resserrement des nœuds lors d'une augmentation de volume provoquée par une immersion dans un solvant ou par une rampe de température. En présence de liaisons hydrogène, la tension pourrait croître dans les mêmes conditions que pour le réseau d'enchevêtrement mais aussi à la suite d'une transformation dans l'organisation des liaisons hydrogène qui peut avoir une autre origine. Quoiqu'en soit la cause, l'augmentation de la tension est liée à une diminution de la mobilité des chaînes. Cette diminution peut expliquer des phénomènes tels que la biréfringence ou la gélification. Ces deux phases ajoutent à la complexité de la morphologie de l'amylose dont les

phases cristallines (A ou B et V) ont été bien étudiées.

Notre avons basé notre approche sur l'importance des phases non–cristallines. Les phases non–cristallines incluent autant les chaînes libres que celles qui forment les réseaux. Les structures plus mobiles seront étudiées puisque celles-ci ont un lien étroit avec les propriétés physiques de l'amylose (gélification, formation de complexes). Les chaînes devenues mobiles après un traitement à haute température sont des précurseurs pour la préparation des gels cohésifs obtenus au refroidissement [29] ou pour la formation de complexes avec des petites molécules comme l'iode et le butanol.

La complexité de l'amylose est telle qu'une méthode simple d'analyse des réseaux n'a pas encore été développée. Nous croyons cependant que la méthodologie que nous avons développée pour l'étude des phases des polyoléfines peut servir d'étape à la compréhension de ce biopolymère.

1.7.2 Objet de l'étude

L'objet de cette étude est d'obtenir des informations de nature fondamentale sur la structure de l'amylose en étudiant plus spécifiquement ses phases non cristallines. Nous voulons également trouver la façon de contrôler les propriétés physico-chimiques de ce biopolymère.

Nous avons étudié le polyéthylène (PE), polymère linéaire comme l'amylose, utilisé systématiquement comme polymère modèle. Cette recherche nous permettra de développer une méthodologie d'analyse des polymères qui servira à comprendre le problème des enchevêtrements en absence de liaisons hydrogène. Par la suite, nous appliquerons cette méthodologie au système amylose–eau avec son réseau d'enchevêtrements et de liaisons hydrogène.

1.8 Les études antérieures sur le polyéthylène (PE)

1.8.1 Modèle à deux phases du PE

La détermination de la cristallinité du polyéthylène par différentes techniques a fait l'objet de nombreux travaux [61-64]. Le modèle classique des polymères semi–cristallins, est un modèle à deux phases, l'une cristalline, où les chaînes se replient sur elles-mêmes selon un arrangement ordonné, et l'autre amorphe, où les chaînes sont indépendantes les unes des autres et possèdent une mobilité élevée. Certaines propriétés du solide ou du liquide (biréfringence, temps de relaxation) sont incompatibles avec ce modèle [59, 63-65]. Dans la section suivante, nous développons un modèle plus complexe qui contient trois phases.

1.8.2 Modèle à trois phases du PE

La troisième phase, dont la mobilité est intermédiaire aux deux autres, [63-66] est selon les auteurs, appelée interlamellaire ou interstitielle. Elle a été caractérisée surtout par des méthodes telles la ^{13}C RMN et la spectroscopie Raman [65-66] qui recourent à des simulations spectrales. Ces simulations sont nécessaires car les pics représentant les trois phases se superposent. Une seule méthode, développée sur les gels de PE, permet d'identifier la troisième phase sans simulation [59]: lorsqu'un échantillon est soumis à une augmentation constante de tension, un fractionnement en fonction de la réponse à la tension va se produire. Cette propriété est utilisée dans la technique de calorimétrie lente qui détecte les effets thermiques associés aux changements de phase sous tension. Cet accroissement de tension indique la présence d'enchevêtrements dans l'échantillon. L'explication est la suivante: les enchevêtrements contenus dans le polymère forment des nœuds plus ou moins tendus. Lorsque on gonfle les chaînes, soit par l'ajout d'un solvant soit par l'augmentation de la

température, l'on tire sur les chaînes ce qui a pour effet de resserrer les nœuds et d'accroître la tension dans l'échantillon. L'existence d'enchevêtrements dans les polymères est un phénomène généralement reconnu mais ses effets sur les propriétés thermiques ont toujours été négligés parce que mal compris.

1.9 Méthodes analytiques

Il y a deux catégories de méthodes analytiques qui ont été utilisées pour l'étude de l'amylose. Dans la première catégorie nous plaçons les méthodes qui donnent de l'information globale sur l'état de l'échantillon. Ce sont les méthodes calorimétriques. Dans la deuxième catégorie nous plaçons les méthodes qui ont pour objet la détermination de la structure de l'échantillon. Ce sont la diffraction des rayons X, la RMN et les spectroscopies de vibration.

1.9.1 DSC (calorimétrie différentielle à balayage ou Differential Scanning Calorimetry)

Il y a deux types de calorimétrie qui peuvent être utilisés pour étudier l'amylose : la calorimétrie différentielle à balayage rapide (DSC_{Rapide}) et la calorimétrie différentielle à balayage lent (DSC_{Lent}).

1.9.1.1 DSC_{Rapide}

Les appareils commerciaux usuels sont du type calorimétrie différentielle à balayage rapide. La vitesse de la rampe de température est de l'ordre de 60 à 2400 K/min. Cette méthode a été utilisée pour étudier l'amylose et l'amidon [67-70] puisqu'elle donne de l'information sur la température à laquelle certains phénomènes se produisent. Ainsi le phénomène de gélification [71-76] et la température de fusion [77] ont été suivis en fonction du taux d'humidité dans l'amidon et de la température de gélification. D'autres analyses par DSC_{Rapide} tentent de

déterminer les changements de phase se produisant dans l'échantillon en fonction de la température. Des études ont suivi l'augmentation avec le temps de la cristallinité du système amylose-eau [78, 79]. Kim *et al.* ont comparé les résultats de DSC_{Rapide} avec des mesures de diffraction de rayons X et des méthodes de mesure de cristallinité par digestion enzymatique. Leurs conclusions stipulent que la méthode par diffraction des rayons X est la moins sensible et que la digestion enzymatique est la plus sensible [28]. Silverio *et al.* de même que Shogren *et al.* ont observé par diffraction des rayons X, l'augmentation de la cristallinité de l'amylose en fonction du temps [78, 79]. L'augmentation de la cristallinité due à la complexation de l'amylose a également été suivie par les mêmes auteurs en utilisant la DSC_{Rapide} [43, 80, 81]. Leurs résultats montrent qu'une chaleur exothermique se développait rapidement dans une solution d'amylose en fonction du temps d'attente. La cinétique de la recristallisation est donc rapide. Cependant, la chaleur exothermique mesurée en fonction du temps ne correspond pas à la chaleur endothermique de fusion mesurée après l'expérience. En d'autres termes, la quantité de cristaux formés (exo) n'est pas égale à la quantité de cristaux fondus (endo). Cette méthode n'est donc pas assez sensible pour mesurer précisément la cristallinité. De plus, la chauffe rapide peut transformer l'échantillon. Par exemple, la chauffe peut causer d'une part, une augmentation subite du volume libre ce qui entraîne une augmentation de la tension, et d'autre part, une augmentation de la quantité d'agrégats ce qui peut entraîner une transformation [29].

Ces études montrent que l'utilisation de la DSC_{Rapide} comme méthode d'analyse quantitative de la cristallinité n'est pas entièrement satisfaisante.

1.9.1.2 DSC_{Lent}

La technique de DSC_{Lent} à permis d'observer certains phénomènes que la DSC_{Rapide} n'a pas permis de voir [82-84]. La caractéristique principale de la calorimétrie différentielle à balayage lent, réside dans la faible vitesse de chauffe utilisée. Celle–ci est plus petite que 12 K/h. Les désavantages d'utiliser une telle vitesse de chauffe sont que la technique requiert beaucoup plus de temps et requiert l'utilisation d'échantillons de masse environ 10 fois plus élevée qu'en DSC traditionnelle pour compenser la perte de sensibilité. L'avantage d'utiliser une telle rampe réside dans la possibilité d'observer des transformations dont la cinétique est très lente comme les transformations d'un état métastable à un autre. Ainsi, des changements tels la fusion–recristallisation et la seconde fusion à plus haute température seront observables par DSC_{Lent}. La figure 4A montre une trace de fusion du polyéthylène utilisant une rampe de température rapide (600 K/h) et sur la figure 4B, une trace avec une rampe très lente (3 K/h). En comparant les deux traces, nous observons que ces dernières montrent toutes deux un endotherme relativement étroit vers 115°C, caractéristique de la fusion des cristaux. Cependant, à haute température, nous observons dans la trace utilisant la rampe lente de température, un second endotherme qui s'étale sur une large gamme de température et qui n'est pas observé en DSC_{Rapide}. Ce second endotherme correspond à la fusion sous tension des cristaux rendus fusibles par l'abaissement de la tension dans la rampe lente de température.

1.9.2 Méthodes pour déterminer la structure moléculaire des polymères

Les méthodes qui peuvent servir à déterminer la structure moléculaire des polymères sont la diffraction des rayons X et les méthodes spectroscopiques. Ces dernières comprennent la

spectroscopie à résonance magnétique nucléaire (RMN) et la spectroscopie vibrationnelle infrarouge.

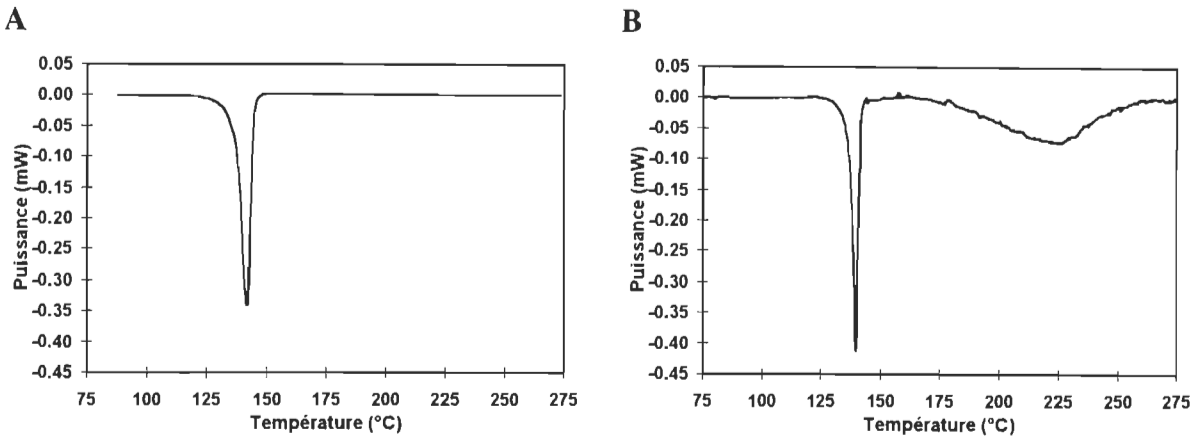

Figure 4. Traces de DSC_{Rapide} (A) et DSC_{Lent} du PE. Notons que la position endothermique est orientée vers le bas

1.9.2.1 Diffraction des rayons X

La diffraction des rayons X est une des méthodes les plus utilisées pour déterminer l'état ordonné dans l'amylose [52, 53, 85-91]. Son utilisation est avantageuse dû au fait qu'elle permet d'obtenir la quantité relative de cristaux dans l'échantillon [19, 89, 92], le type d'arrangement cristallin contenu dans l'échantillon [93, 94] de même que l'arrangement spatial des chaînes [45, 91, 95]. La diffraction des rayons X possède cependant deux désavantages marqués : celui de ne mesurer que les arrangements ordonnés dans les échantillons et celui d'être moins sensible que d'autres méthodes pour suivre les variations des phases cristallines dans l'amylose [28]. En effet la ^{13}C RMN et la DSC_{Lent} ont identifié un ordre qui contribue aux propriétés mécaniques de l'échantillon [27, 29]. L'amylose possède donc deux types d'ordres, un à grande distance perçu par la diffraction à rayons X, et un ordre à plus courte distance non

détectable aux rayons X.

1.9.2.2 ^{13}C RMN de l'état solide à l'Angle Magique en Polarisation Croisée (CP/MAS)

La spectroscopie à résonance magnétique nucléaire de l'état solide à l'angle magique en polarisation croisée (CP/MAS) (RMN), possède la capacité de distinguer les phases dans des systèmes polymériques parce qu'elle est sensible à l'environnement autour de l'atome étudié. Ainsi, un carbone situé dans une chaîne libre, amorphe, dans une maille cristalline ou dans une chaîne sous tension n'aura pas la même position dans le spectre RMN puisque son champ magnétique propre va varié selon son emplacement. La RMN a déjà été utilisée pour caractériser les différents types d'amidon et d'amylose [49, 92, 96-99]. De plus, les spectres RMN de glucides qui sont des molécules modèles ont permis d'attribuer les bandes [100] et à établir la présence d'hélices dans l'amylose [92, 101, 102].

De plus, des études par RMN sur la cellulose, un glucide similaire à l'amylose, ont démontré la présence d'une phase intermédiaire entres les phases cristallines et la phase amorphe [103]. L'amylose n'a pas fait l'objet d'une étude semblable quoique la technique de RMN semble prometteuse pour l'évaluation de la composition phasique des glucides. L'analyse par RMN est donc utilisée avec succès pour des polymères naturels ou synthétiques mais demande une expertise et un équipement qui ne sont pas actuellement disponibles à l'UQAM ou à l'UQTR.

Nous avons été amenés à considérer la spectroscopie IR pour l'étude du système amylose-eau. Cette méthode d'analyse permet l'observation de groupements fonctionnels dans des environnements différents qui peuvent être contrôlés.

1.9.2.3 Spectroscopie vibrationnelle

La spectroscopie vibrationnelle, (FTIR et Raman), a déjà été utilisée pour étudier l'amidon et l'amylose [41, 104-114]. La spectroscopie IR a premièrement été utilisée pour identifier l'amylose et l'amidon en les comparant à des monoglucides [107-110]. D'autres études faites par spectroscopie IR, ont permis de déterminer l'influence de divers traitements physiques et thermiques sur l'amylose [41, 60, 104, 105, 111, 112]. Parmi ces travaux, mentionnons ceux de Goodfellow [41] sur la gélification et ceux de van Soest [104] sur la rétrogradation. Ces auteurs montrent que l'intensité de certaines bandes IR reliées aux vibrations d'élongation C-O et C-C (1200-900 cm^{-1}) peut être corrélée avec la quantité d'ordre dans l'amylose. La complexation de l'amylose avec le glycérol a également été étudiée par spectroscopie IR [105]. Ces travaux ont permis de montrer que l'IR pouvait suivre l'augmentation des cristaux de types V lors de la complexation de l'amylose avec le glycérol [106]. Une autre étude sur les structures hélicoïdales B et V de l'amylose par IR montre que ces structures sont stabilisées par la formation de liaisons hydrogène intramoléculaires et que les structures B et V forment la totalité de l'ordre retrouvé dans l'amylose [110-111].

Dans les études précédentes, l'attribution des bandes de l'amylose diffère d'un auteur à un autre [23, 60]. Cette situation est due au fait que l'amylose existe sous plusieurs états métastables. Une étude IR des transformations cristallines de l'amidon en fonction du temps a été faite par van Soest *et al.* [104]. Ces auteurs montrent que des transformations d'une forme cristalline à une autre s'effectuent avec le temps.

Les interprétations divergentes des mesures IR de l'amylose viennent de ce que les auteurs recherchent dans les spectres une bande qui peut être attribuée à l'ordre donc à la phase

cristalline. Trois différents types d'ordre peuvent être trouvés dans l'amylose [115, 116]: 1) l'ordre à grande distance observable par rayons X; 2) la somme des ordres à grande et à courte distance, observable par IR et 3) l'ordre dû à la tension entre les chaînes. Dans les études présentées dans les références 115 et 116 il y a peu de renseignements sur les deux derniers ordres. De plus, puisque la phase amorphe est également difficile à étudier, les études sur l'amylose ont jusqu'ici porté sur les formes ordonnées.

1.9.3 Méthodes hybrides

Une seule méthode analytique ne peut donner toute l'information sur un système complexe comme l'amylose. Aussi faut-il évaluer la pertinence d'utiliser des méthodes hybrides. Plusieurs paires de méthodes ont déjà été employés. Gidley *et al.* de même que Nuessli *et al.* [27, 81] ont utilisé une combinaison de DSC_{Rapide} et de diffraction des rayons X. Ces deux méthodes observent sensiblement la même chose, l'ordre à grande distance. Elles ne se complètent donc pas. D'autres méthodes hybrides impliquent la RMN de l'état solide avec la DSC_{Rapide} ou la diffraction des rayons X [53]. Une étude utilise même une combinaison des trois techniques [27]. Les études RMN utilisent une méthodologie capable d'observer les enchevêtrements de même que l'effet des variations dans les liaisons hydrogène. Gidley utilisant ces hybrides a observé la présence d'une interphase sans toutefois pousser l'analyse plus loin.

La DSC_{Lent} met en évidence certaines transformations dans les systèmes amylose-eau que les autres techniques ne décèlent pas. Cependant, cette technique ne permet pas de savoir quels groupes fonctionnels sont impliqués dans la transformation. La DSC_{Lent} montre simplement l'existence d'une transformation à une température donnée. Il est donc important d'allier à

cette technique une technique moléculaire. Une méthode permettant l'obtention de valeurs relatives de la tension et de la composition phasique doit être corrélée avec la DSC_{Lent}. Comme méthode complémentaire pour étudier l'amylose dans différents états d'organisation nous avons choisi la spectroscopie IR parce qu'elle permet d'observer l'ordre à courte portée et l'état amorphe.

1.10 Traitement thermique des polymères

L'objet de la présente étude est, dans un premier temps, de déterminer la composition phasique de l'amylose en incluant les phases de réseaux semi-ordonnés et, dans un second temps, de contrôler la composition phasique d'un échantillon. Pour réaliser nos objectifs, nous devons développer une méthode simple qui permet de modifier les fractions des diverses phases. Plusieurs méthodes sont mentionnées dans la littérature :

a) Gidley *et al.* utilisent des échantillons d'origines différentes [31].

Cette méthode possède l'avantage d'être facile à utiliser. Le désavantage de cette méthode est que les échantillons obtenus sont tellement différents entre eux qu'il est possible que d'autres modifications se superposent aux changements de composition phasique (poids moléculaire, nombres de branchements, présence de lipides).

b) Godet *et al.* utilisent des amyloses de poids moléculaires différents (réalisés en hydrolysant des amyloses obtenus d'une seule source) [50, 52].

L'avantage d'utiliser une source unique d'amylose réside dans le fait qu'un seul paramètre varie. Le désavantage de cette méthode est que le degré d'enchevêtrements et les interactions amylose-eau dépendent du poids moléculaire. Nous ne pouvons donc utiliser cette méthode.

c) L'utilisation de traitements thermiques est la méthode que nous avons retenu pour ce projet.

Cette méthode est avantageuse dû au fait qu'elle permet d'utiliser un échantillon d'une seule et même origine et, puisqu'elle nous permet d'utiliser une amylose de haut poids moléculaire, qu'elle maximise les probabilités que nous avons d'observer les enchevêtrement entre les chaînes.

1.11 Présentation des articles

Dans cette thèse nous nous proposons de développer une méthode d'analyse de la composition phasique du système amylose–eau principalement basée sur deux techniques soit la calorimétrie différentielle à balayage lent (DSC_{Lent}) et la spectroscopie infrarouge à transformée de Fourrier (FTIR). L'objet de cette étude fondamentale est d'obtenir des informations sur la structure de l'amylose afin d'en contrôler les propriétés physiques et chimiques.

Ce projet a également pour but de déterminer l'effet de la tension sur la composition phasique de l'amylose de façon à expliquer certaines propriétés physiques, telle la résistance à l'amylase. En effet, Sievert et Pomeranz ont montré qu'un traitement thermique effectué de façon cyclique augmentait cette résistance [66].

Cette thèse comprend deux articles publiés et deux articles qui ont été soumis à des revues scientifiques. Les deux premiers traitent du développement de la technique hybride IR-DSC_{Lent} appliquée à une molécule modèle, le PE, tandis que les deux derniers traitent de la détermination de la composition phasique de l'amylose en utilisant la même méthodologie.

1.11.1 Présentation de l'article 1 : **« Analysis of physical and chemical networks by slow DSC and turbidimetry » : «Analyse des réseaux physiques et chimiques du polyéthylène par calorimétrie lente et turbidimétrie»** *P. Bernazzani et G. Delmas, Journal of Thermal Analysis, 1997, 49, 449-454.*

Les travaux de cette publication ont été faits par P. Bernazzani. Cet article a été rédigé par P. Bernazzani et fut corrigé par Mme G. Delmas-Patterson.

Dans cet article, nous voulons répondre à trois questions: a) est-ce que la tension existe dans les chaînes de PE? b) si cette tension existe, serait-elle produite par des enchevêtrements? c) la calorimétrie en rampe lente de T (DSC_{Lent}) est-elle une méthode efficace pour discerner la valeur de la tension causée par les enchevêtrements dans le PE?

Notre étude de gels physiques de PE nous a porté à croire que des changements de phase, indiscernables par DSC en rampe rapide de température, pouvaient être observés en utilisant une rampe de température très lente. Ces changements de phase ont également été observés sur un PE réticulé chimiquement. Une comparaison entre le polymère original et celui réticulé a été effectuée en utilisant les données obtenues en calorimétrie lente.

La trace de calorimétrie montre qu'un endotherme très large, de cinétique très lente, est trouvé à haute température sur le PE réticulé chimiquement. Cet endotherme est associé à la réticulation et donc au réseau chimique. Un endotherme similaire de moindre importance est trouvé dans le PE non réticulé et est attribué à la réticulation physique. La quantité de points de réticulation et donc d'enchevêtrements peut alors être mesurée en utilisant la DSC_{Lent}. La présence, dans le polyéthylène, d'une troisième phase qui a des effets sur les propriétés thermiques de l'échantillon, remet en question le modèle à deux phases. Dans certains cas où

la fraction d'enchevêtrements est faible ou que les nœuds entre les chaînes ne sont pas resserrés c'est-à-dire des chaînes non tendue, le modèle à deux phases peut être utilisé.

1.11.2 Présentation de l'article 2 : « **FTIR analysis of the phase content in low-density polyethylene» : «Analyse de la composition phasique du polyéthylène de basse densité par spectroscopie IR»** *P. Bernazzani, V. T. Bich, H. P. Nguyen, A. Haine, C. Chapados, L.H. Dao et G. Delmas, Canadian Journal of Chemistry, 1998, 76, 1674-1687.*

La grande partie du travail de cet article a été faite par P. Bernazzani. L'article fut rédigé à part égale par P. Bernazzani et G. Delmas-Patterson.

Dans cet article, nous développons la méthodologie de la technique hybride de DSC_{Lent} et de spectroscopie IR. Nous traitons des possibilités qu'offre la spectroscopie IR d'observer et de quantifier la tension due aux enchevêtrements dans le PE. L'utilisation de simulations spectrales sur les spectres permet de déterminer les fractions molaires des phases cristallines, amorphe et d'enchevêtrements. Nous avons comparé les valeurs des fractions cristallines avec celles mesurées par DSC_{Lent} pour déterminer, d'une part l'efficacité des méthodes à observer les trois phases et, d'autre part, pour associer une structure physique avec les changements observés par DSC_{Lent}. Il fut possible de quantifier les enchevêtrements par cette technique.

1.11.3 Présentation de l'article 3 : « **Phase change in amylose-water mixtures as seen by FTIR » : «Changements de phase dans les mélanges amylose-eau tels qu'observés par spectroscopie IR»** *P. Bernazzani, C. Chapados et G. Delmas, Biopolymers, accepté avec corrections 36 pages environ.*

Les travaux de cet article ont été faits par P .Bernazzani. La rédaction de l'article a été faite à

part égale par P. Bernazzani et G. Delmas-Patterson.. C. Chapados a corrigé la version finale.

Cet article sert à évaluer l'utilité de la spectroscopie IR pour la détermination de la composition phasique du système complexe amylose-eau.

La composition phasique de mélanges amylose–eau a été analysée par spectroscopie IR dans la région 1175-950 cm^{-1}. Cette région qui contient les bandes d'élongation C–O et C–C a été choisie parce que l'eau absorbe faiblement dans cette région. Les spectres ont été obtenus dans trois situations différentes: i) en fonction de la température; ii) à la température de la pièce après une chauffe lente suivie d'un refroidissement lent; iii) à la température de la pièce après une chauffe lente suivie d'un refroidissement rapide. La température maximale atteinte après la chauffe, T_{max}, varie entre 50 et 120 °C.

Le troisième article utilise la technique IR développée dans l'article deux et l'applique au système amylose-eau. Il montre qu'à l'aide de traitements thermiques il est possible de modifier l'échantillon. L'attribution de certaines bandes à différentes phases de ce système a été rendue possible grace aux modifications reliées aux variations de tension et de cristallinité. Cependant, pour obtenir plus d'informations sur les modifications dans l'échantillon, il est nécessaire de comparer les spectres IR avec les résultats de la DSC_{Lent}.

1.11.4 *Présentation de l'article 4 :* **« Double helical network in amylose as seen by slow calorimetry and FTIR » : «Réseau de double hélice dans l'amylose tels qu'observé par calorimétrie différentielle à balayage lent et spectroscopie IR »** *P. Bernazzani, C. Chapados et G. Delmas, Journal of Polymer Science, Part B, 2000, 38, 0000.*

Les travaux de cet article ont été faits par P. Bernazzani. La rédaction de l'article a été faite à part égale par P. Bernazzani et G. Delmas-Patterson. C. Chapados a corrigé la version finale.

Cet article est basé sur l'utilisation de la méthode hybride de DSC_{Lent} et de spectroscopie IR pour déterminer la composition phasique de l'amylose. Cette étude suit la relaxation de la tension et ses effets sur la cristallinité de l'échantillon.

La composition phasique de mélanges amylose–eau a été modifiée par des cycles lents de dissolution et recristallisation à partir de T_{max}. Les changements obtenus par ces traitements thermiques ont été suivis par la diffraction des rayons X, la DSC_{Rapide}, la DSC_{Lent} et la FTIR. L'ordre retrouvé dans les systèmes polymère–solvant refroidis lentement n'est pas dissociable lors d'une rampe de température rapide dû à la tension développée lors de la rampe. En utilisant le PE comme système modèle, nous avons pu établir la présence de phénomènes de tension et d'enchevêtrements dans l'amylose. La tension existe donc bien dans l'amylose tout comme dans le PE. Un modèle à plus de deux phases doit donc être utilisé pour interpréter les résultats. D'autre part, la technique hybride a permis de mesurer l'ordre à grande et à petite distance.

CHAPITRE 2

ANALYSIS OF PHYSICAL AND CHEMICAL NETWORKS BY SLOW DSC AND TURBIDIMETRY

Paul Bernazzani, Geneviève Delmas

Chemistry department, University of Quebec in Montreal

CP 8888 succ centre-ville, Montreal, Canada

H3C 3P8

Journal of Thermal Analysis, 1997, 49, 449-454.

ABSTRACT

Semi-crystalline polymers are made of a crystalline phase and of an amorphous phase. Recently, NMR, Raman and FTIR experiments have identified a third phase comprised of defects such as tie-molecules, in the organization of chains. Our investigation of physical gels has led us to believe that by following the heat flow in a very slow temperature ramp (0.05 K/min), phase-changes, unnoticed in the usual fast ramp, could be detected. These are associated to a physical network strained in the temperature ramp. In order to obtain more information on the network phase, the polymer has been crosslinked. The characteristics obtained by slow calorimetry and turbidimetry at a lower critical solution temperature, of the original and modified materials are compared.

Keywords: DSC, network, polyethylene, turbidimetry

INTRODUCTION

Polymers are traditionally thought to be two phase materials: a rigid crystalline phase and a liquid-like amorphous phase. Recent papers on the morphology of polyethylene (PE) have investigated the possibility of the existence of a third semimobile phase[1,2]. Although many hypotheses have been proposed to explain the existence of such a phase, they all seem tend to point to the presence of order in the amorphous phase. Further calorimetric (DSC) studies have noted the presence of a high temperature endotherm due to strain melting[3,4]. As the temperature was increased at a very slow rate, the tension in polyethylene and polypropylene increased. This increase suggests the presence of entanglements present mainly in the amorphous phase. The presence of entanglements in polymers has been widely accepted, but their overall effect on thermal properties being usually neglected. However, the results from DSC in a slow temperature ramp show that theses entanglements account for the presence of a third semimobile phase in polyethylene which we will now call the physical network phase.

In order to investigate the validity of the relation between entanglements and the third phase in polymers, we will apply the new technique of slow calorimetry (DSC in a slow temperature ramp) to crosslinked polymers. We will therefore attempt to quantify by calorimetry the network content of polyethylene.

Crosslinked PE has been used extensively in industrial applications. The strength increase and swelling abilities of these polymers have been the driving force of this industrial interest as a variation in the crosslinked content will have non-negligible effects on the physical properties of the polymer. It is therefore of interest to obtain an efficient

quantification method of measuring the network fraction. However, few characterization studies of crosslinked PE are found in the literature, and the only quantitative methods of determining the crosslinked fraction involves indirect measurements. These methods consist mainly in the extraction of the non-crosslinked fraction followed by its analysis by varying techniques. The main drawback of these methods resides in the faith that one must have in the ability of the solvent to extract all of the loose chains contained in the polymer. In the ASTM method, the recommended time for allowing this soluble fraction to separate is 12 h in xylene. Some authors[5] have found that a minimum of 48 h was necessary to reproducibly accomplish this task, making the experimental time very large. The new techniques of slow calorimetry[3,4] and turbidimetry[6,7] seemed appropriate for the analysis of the chemical networks since they have been known to measure physical networks.

Variation in the enthalpy of the network disordering

Based on previous experimental data[3, 4], we developed the hypothesis that slow differential scanning calorimetry represents an ideal solution. A high temperature endotherm assigned to the disordering of the network can be found using this method.

EXPERIMENTAL

Materials

The samples are linear low density polyethylenes from Dupont D(7) and D(12) and from long chain branched polyethylene from Union Carbide, U(18). The figure in parenthesis correspond to their methyl content per 1000 carbons and is indicative of the amount of branching in the samples. Their molecular weight is between 10^5 and $2x10^5$ g $mole^{-1}$. The branched sample U(18) was chemically crosslinked by peroxide addition (U(18C)) while linear

and branched Dupont samples were crosslinked using the same dose of gamma irradiation and noted D(7C), D(12C). Both these types are designated by the term chemical network.

Range of temperature

Previous analysis in slow DSC showed the presence of an endotherm after the melt of the crystalline phase of PE[3, 4]. Consequently, we measured the enthalpy variations up to 100 K after the fusion temperature.

Apparatus

The C80 calorimeter from Setaram is a sensitive DSC capable of accommodating large size cells (8 cm^3). Quantitative enthalpy measurements can be obtained at heating rates of 0.1 K/h however, for this study, we have limited ourselves to 3 and 12 K/h ramps.

The turbidity at the lower critical solubility temperature (LCST) measurements were made following the method described in previous works[6], using hexane as the volatile solvent. In this technique the amount of polymer phase separated on a given temperature interval is obtained through the turbidity, h_i, developed during the phase change. The sum of h_i (Σh_i) values over the complete interval of phase separation (typically 120 K), is proportional to the overall volume fraction of the polymer in solution. For a crosslinked sample, only the polymer molecules extracted from the network contribute to Σh_i. The ratio of Σh_i(crosslinked)/Σh_i(non crosslinked) gives the fraction of soluble material. The amount of material that is nonsoluble is considered to be the network fraction.

The ASTM F876-99a method of quantifying the network fraction has also been followed.

RESULTS AND DISCUSSION

Variation in the melting enthalpy of the orthorhombic crystals

Table 1 shows the calorimetric data for both the untreated and crosslinked PE samples. The different columns show respectively the sample identification, the melting temperature (T_m), the enthalpy of fusion of the orthorhombic crystals, ΔH_{ortho}, the enthalpy of disordering of the network, ΔH_{net}, the total enthalpy, ΔH_{tot}, and the network fraction f_{net}. The figures in parenthesis below the values of ΔH_{net} give the temperature interval used for the integration of the network fraction. In this table one observes that the T_m and ΔH_{ortho} diminish as the samples are crosslinked, as found in the literature[8]. Column 3 shows the enthalpy variations of the orthorhombic fraction, ΔH_{ortho}. For all of the uncrosslinked polymers, we find that this value is around 170 J/g confirming the values found in the literature[9].

Crosslinked samples give a lower enthalpy variation and therefore contain about one half less orthorhombic fraction. This can be explained by comparing the formed network to the branching of a linear polymer. Impeded by these defects, the polymer will crystallize with more of less difficulty depending on the length of these branches, and reducing the overall crystallinity.

Figure 1a shows a typical calorimetric curve of irradiated D(7) from which the baseline was subtracted. The sharp endotherm corresponds to the melting of the orthorhombic fraction (T_m = 130 °C). The flatter endotherm at higher temperatures (160-245 °C) is associated with the melt of the network. In this study, we have attributed this endotherm to the disordering of the region between the crosslinked chains. We therefore formulate the hypothesis that this new method can be used as a direct measurement of the crosslinked fraction in the samples.

The percentage of network fraction, f_{net} was calculated to be ($\Delta H_{net}/\Delta H_{tot}$) and is shown in column 6 of table I. From these values we note three points: a) the non-crosslinked samples have a small network fraction, b) the low density PE (LDPE) possess a higher content of network then the D(7), c) the chemically crosslinked PE contains a higher network fraction than the irradiated samples. We will now explain further these points individually.

Uncrosslinked

The value of T_m reflects the amount of methyl content in PE's. Higher values of CH_3 correspond to greather amorphous content. The value of ΔH_{ortho} is seen to decrease with increasing branch content in D(7), D(12) and U(18) as expected[8]. ΔH_{net} of these uncrosslinked PE's have values between quarter and two thirds of the total enthalpy (ΔH_{tot}).

Table 1 : Calorimetric data of varying crosslinked and non-crosslinked samples using a very slow temperature ramp.

Polyethylene Samples	T_m/°C	ΔH_{ortho}/J g^{-1}	ΔH_{net}/J g^{-1}	ΔH_{tot}/J g^{-1}	F_{net}/J g^{-1}
D(7)	130.4	184	66 (160-245)	250	0.25
D(7C)	129.8	152	142 (140-245)	294	0.49
D(12)	118.9	169	68 (160-250)	238	0.37
D(12C)	109.1	105	204 (150-250)	309	0.66
U(18)	112.8	147	53 (150-250)	200	0.27
U(18C)	107.7	108	217 (145-250)	325	0.66

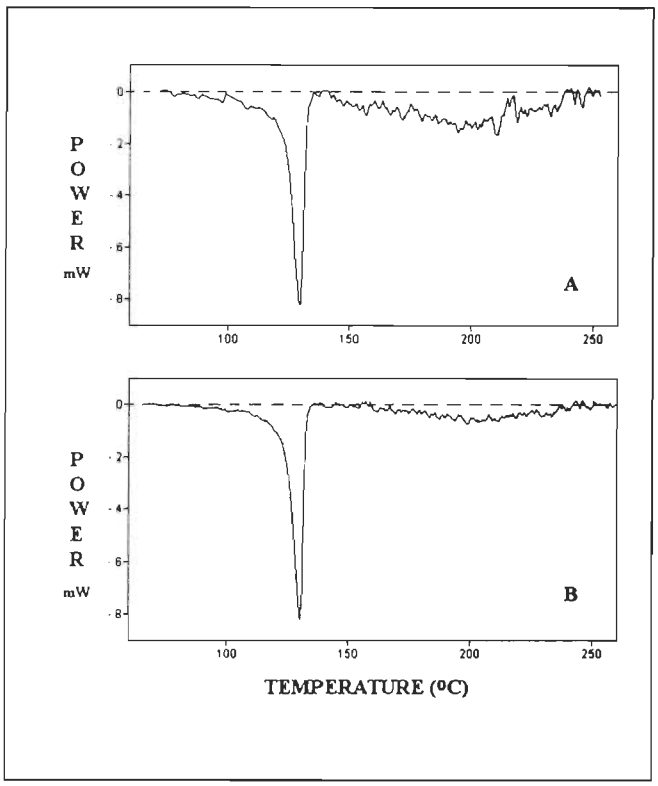

Figure 1: Slow DSC traces comparing (A) D(7C) crosslinked and (B) D(7) unmodified samples. Both sample mass are equal. Note that the orientation of endotherms is down.

Figure 1b gives the trace of slow melting of the D(7) sample before irradiation. The similarity of both traces is clear, the two curves differ only by the magnitude of ΔH_{net}. The present work supports the identification of the high temperature endotherm associated in a previous work to a network. The network endotherm for the non-crosslinked samples is weak from the slow DSC traces. There is a reason for its presence: in irradiated samples, D(7) is compression moulded and quenched from the melt, which increases the chances of entanglements in the sample. At a certain point, the number of these entanglements is so great that a physical network appears. Further evidence of this was found when we observed a smaller high temperature endotherm in a D(7) sample that was slowly cooled. This physical network will be found in all polymers that contain entanglements but is usually neglected in phase composition measurements.

Chemically crosslinked samples

The value of T_m and ΔH_{ortho} is seen to diminish as predicted by the thermodynamics of copolymers[8]. The lowering of T_m and ΔH_{ortho} is larger for the more amorphous polymer D(12), which experienced the same irradiation dose as D(7). ΔH_{net} increases in D(7), D(12) and U(18) after crosslinking are 76, 136 and 160 J/h respectively. Crosslinking has the effect of increasing the amount of meltable network content as expected. The later increase for D(12) compared to D(7) has the same origin as suggested above. The temperature interval on which the network fraction melt, depends on the size of ΔH_{net}. The high temperature endotherm has been explained as a consequence of strain melting. Expansion during the temperature ramp and also at T_m, lead to strain in the melted crystals. Strain can be sufficient to stop the melting which resumes at high temperature. The hindering of mobility which lead to strain must not be very different in origin, if the hindrance is an entanglement or a crosslink.

Chemically crosslinked PE has a higher network fraction than all other polymers studied. This can be attributed to the fact that this sample is a low density slightly branched polymer as can be demonstrated by the low molecular weight. However, we believe that the main reason for this high fraction is the crosslinking method. The network content in a polymer has been linearly related to the amount of peroxide added. This method can therefore produce very high levels of crosslinks. It should be noted that a certain peroxide content was found after the chemical treatment is over which had to be removed by successive washes.

Comparison of network fraction

In order to confirm the quantitative nature of the calorimetric results, network fraction was obtained by two other methods: 1) The ASTM method of measuring the amount of

product dissolved in xylene, and 2) by LCST measuring of the amount phase separating from a hexane solution. The results are compared with those of slow DSC in table 2. This table shows that for both irradiated samples, a high network fraction is found (55% for D(7) and 65% for D(12)), which agrees well with the calorimetric data. In fact the small difference between the two techniques is comparable to the standard errors of both techniques. However, the values found using the ASTM method are significantly higher for all the analyzed samples. We surmise that this is due to the extraction time being to short (12 h) to fully extract all the non-network chains. We conclude that the new slow DSC method to characterize the network fraction in a polymer is more precise and advantageous in that manipulations are kept to a minimum.

Table 2 : Comparison of the fraction of network phase in different samples as measured by three methods, ASTM (in xylene), LCST (in n-hexane) and DSC (slow)

Polyethylene samples	F_{net} ASTM	F_{net} LCST	F_{net} DSC
D(7)		0.22	0.25
D(7C)	0.65	0.54	0.49
D(12)		0.39	0.37
D(12C)		0.66	0.66
U(18)			0.27
U(18C)	0.75		0.66

CONCLUSION

In this study, our goals were twofold to validate the hypothesis that a third semi-rigid fraction in polyethylene was composed of a physical network caused by chain entanglements, and to demonstrate that DSC using a slow temperature ramp was capable of accurately quantifying the physical or chemical network fraction in polyethylene.

REFERENCES

1- R. Kitamaru, F. Horii, K. Murayama, Macromolecules, 19 (1986) 636.

2- R. Mutter, W. Stille, G. Strobl, J. Polym. Sci.: Polym. Physics, 31 (1993) 99.

3- H. P. Nguyen and G. Delmas, Thermochimica Acta 238 (1994) 257.

4- H. P. Nguyen and G. Delmas, Macromolecules, 30 (1992) 408.

5- Y. H. Kao and P. J. Phillips, Polymer, 27 (1986) 1669.

6- A. Barbalata, T. Bohossian, K. Prochazka, G. Delmas, Macromolecules, 21 (1988) 3286.

7- A. Barbalata, T. Bohossian, G. Delmas, J. Appl. Polym. Sci., 46 (1992) 411.

8- A. P. de Boer and A. P. Pennings, Farad. Discuss. Royal Soc. Chem., 68 (1979) 345.

9- B. Wunderlich, Macromol. Phys., Vol. 2, Academic Press, New York, 1976.

CHAPITRE 3

FTIR ANALYSIS OF THE PHASE CONTENT IN LOW DENSITY POLYETHYLENE

P. Bernazzani[1], V. T. Bich[1,2], H. Phuong-Nguyen[1], A. Haine[1], C. Chapados[3], Lê H. Dao[4] and G. Delmas[1]

Canadian Journal of Chemistry, 1998, 76, 1674-1687

[1]Chemistry Department, University of Quebec in Montreal,C.P. 8888 succ. A, Montreal, Canada, H3C 3P8.

[2] IMS, CNSNT , Hanoi ,Vietnam

[3] Département de chimie-biologie, Université du Québec à Trois-Rivières, Canada, G9A 5H7

[4] INRS-Energy and Materials, CP 1020 Varennes, Canada J3X 1S2

ABSTRACT

The phase content of a low density polyethylene was studied by analysis of the CH_2 rocking vibrations in non oriented films prepared from the press (P-films) or from solution (S-films). Spectral simulations of the transmission spectra give the mass fractions of the orthorhombic phase α_{ortho} and of two non-crystalline phases (monoclinic-like and amorphous). The values of α_{ortho}(IR) are compared to α_{ortho} (i) where (i) stands for the X-ray diffraction, density and DSC techniques. New results are obtained concerning the orthorhombic order and the change of phase content with aging. A two-phase analysis is justified for non-aged films containing a small amount of the monoclinic-like phase.

The values of α_{ortho} (IR) are larger than α_{ortho} (i), the difference ranging between 0.12 and 0.43. The difference is a measure of the short-range order. α_{ortho} (IR) can reach 0.73 for the S-films. The stability of the short-range order phase is investigated. The sample is also analyzed from the trace of slow calorimetry. The difference between α_{ortho} by DSC and slow calorimetry is a measure of strainable order.

During aging, the variation in the phase content is large for the non-crystalline phases (in content and frequency) and small for the orthorhombic. The increase of the monoclinic-like phase during aging suggests that it is a precursor of the more stable orthorhombic organization. The quantification of two non-crystalline phases on fresh and aged films clarifies some ambiguity found in the literature about the monoclinic-like phase and the localization of bands in the rocking region for sample characterization. The analysis of other regions of the spectrum is needed to confirm the present results.

Key-words : Low-density PE, Phase-content, FTIR, network phase, slow calorimetry

INTRODUCTION

In the two-phase model of semi-crystalline polymers, the fraction of the long-range order phase is obtained by X-ray scattering or calorimetry and the other phase is assumed to be liquid-like. In polyethylene, (PE), the presence of a third phase with mobility and order intermediate to that of the crystalline and amorphous phases, has been supported by a variety of techniques. The name and the characteristics of this third phase depends on the type of crystal growth (bulk, solution or fiber crystals) and also on the technique used to analyze it. The chains of the third phase may be entangled chains inside the crystallites or connecting them. In consequence, this phase is heterogeneous with a range of order and tension determined by the polymerization conditions and the sample history. In NMR (1) and Raman (2-4) studies, the third phase in PE has been called interlamellar, interfacial or interzonal, in reference to its links to the crystalline and amorphous phases. The presence of more than two phases in a semi-crystalline polymer is supported by analysis of the melt. In this state, two relaxation times (5) were found by ^{13}C NMR. Rudin *et al* (6) identified three phases by the same technique. An heterogeneous melt suggests that the solid melts in a complex mode and incompletely. From measurements such as birefringence, electron microscopy or small angle neutron scattering it is clear that, at the end of the endotherm of melting, a sizable amount of ordered domains remains in the melt for a long period of time. The order in the melt decreases by shear and recovers by annealing (7). The presence of a non-meltable order is consistent with the presence of at least three phases in semi-crystalline samples.

In recent works, we have analyzed the non-crystalline phases in polyolefins (8-15). Using a sensitive calorimeter, the heat flow was analyzed in the melt. It was found that

disordering of the melt can be followed if a very slow heating rate (T-ramp) is used. The usual fast T-ramp creates strain in the sample and prevents melting. The slow melting phase was called the network phase because the physical junctions in the network prevent normal expansion in the T-ramp and induce strain in the ordered regions. Another name for the network phase is the short-range order phase since the ordered CH_2 sequences are usually too short to give sharp peaks in the X-ray diffraction pattern. With samples having a large concentration of entanglements and junctions such as chemically cross-linked PE, non-orthorhombic X-ray diffraction patterns have been found in the melt.

PHASE CONTENT BY IR ANALYSIS

After having identified short-range order in a variety of polyolefins by slow calorimetry, we were interested in finding it by FTIR (16-17). The advantage of the IR technique compared to calorimetry is to analyze the sample as it is at room temperature (RT). The disadvantage is that the vibration of the CH_2 groups with different conformation overlap, a situation which requires spectral simulation. On the other hand, less superposition occurs in slow calorimetry because the strain generated by the expansion leads to the separation of the regions with different tension i.e. between the different phases. An exemple of the range of melting typical of a semi-crystalline polymer is given in figure 1A. Another drawback of the transmission FTIR is the preparation of the film itself (press or solution) which brings modifications difficult to control in the morphology of the sample to be analyzed.

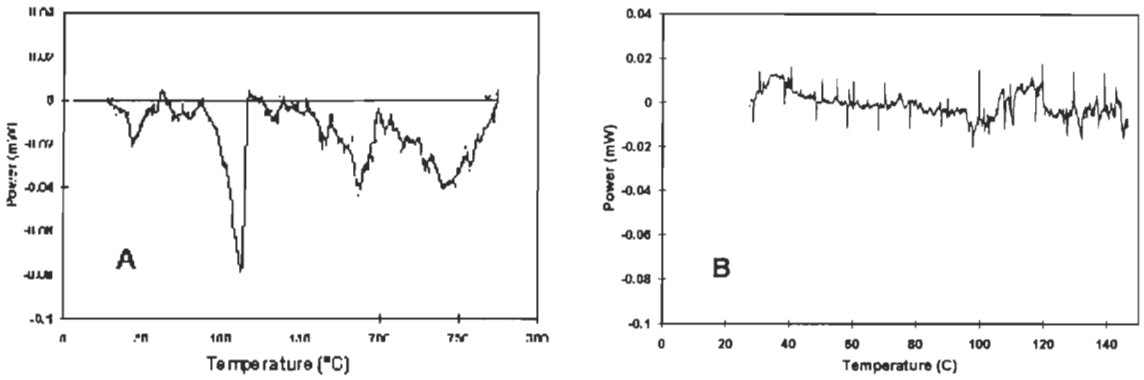

Fig. 1. (A) Melting trace of the as-received sample in a low scanning rate (1K/h). See table 2 for the values of ΔH. (B) Baseline of the calorimeter in the same conditions. Note that the orientation of endotherms is down.

The elucidation of the molecular structure of PE by IR has been the subject of many articles (18-27). The assignment of the trans-trans and gauche conformations has lead to the identification of ordered and less ordered regions. The ordered regions in the orthorhombic modification give a doublet in the rocking (730-720 cm^{-1}) and bending regions (1500-1400 cm^{-1}) due to the interaction between two chains in the unit cell. By analyzing the spectra of liquid, linear and cyclic alkanes and of molten PE, information on the less ordered regions of a semi-crystalline polymers have been obtained (21). The amorphous regions have been associated with peaks at 725, 720, 1078 and 1300-1368 cm^{-1}. To help resolve the active debate of the 1970's, concerning how a chain folds on itself to reenter the lamella, the conformation of the folds have been analyzed extensively, mainly on solution grown crystals with different crystal habits. Mixtures of PE and deuterated polyethylene gave information on two and three-dimensional order between the chains (18-20).

The characterization of the deformed crystals has also been studied extensively (18-20, 23-27). The bands associated with a monoclinic-like organization have been studied on fibers and modified samples where the orthorhombic crystals had been deformed by shaking or

drawing. A singulet at 715-718 cm^{-1}, appears and eventually replaces the doublet in these samples (19-20, 26). This band can also be detected in solution-grown crystals and on annealed melt-crystallized samples by spectral subtraction. It could be detected in samples where the X-ray scattering spectra could not detect the monoclinic organization (19). In an analysis of the rocking region of linear PE, the term monoclinic-like was proposed (26). It was to take account of the fact that some samples could present monoclinic IR bands without monoclinic X-ray diffraction peaks. The range of frequency at which the monoclinic-like peak appears in the present work is another reason for using this term in the description made below of the phase content. If reference is made of large absorbance at 716-717 cm^{-1} on a drawn sample, the term monoclinic is suitable.

Evaluation of crystallinity

Analysis of the bands in the bending region has been used early on to relate the X-ray or density crystallinity to the IR spectra of semi-crystalline samples (22). Wedgewood and Seferis (23) have analyzed the absorbance of crystalline and non-crystalline bands of well characterized films. They found a good correlation between the absorbance of the bands mentionned above and the crystallinity by density. Quantitative measurements of crystalline and non-crystalline phase orientation were also obtained. Using the multiple internal reflection spectroscopy, the ratio of the absorbances of the 730 and 720 cm^{-1} has been recently determined (25) in the characterization of the amorphous content of a commercial film and its heterogeneity as a function of penetration depth.

Several papers have remarked upon the objective difficulty of comparing the crystallinity of semi-crystalline PE by different techniques. In spite of the knowledge that the

vibrations are sensitive to near neighbors, i.e. to short-range order as well as long-range order, efforts were made to match the crystallinity obtained by IR and by X-rays or density. The information on short-range order as seen by FTIR should complement well the short-range order seen by slow calorimetry.

In the present work, we report the evaluation of the phase content of a low density PE. The spectacular improvement in the IR techniques during the last 10-15 years (FTIR and software) which allows for calculate integrated absorbance rather than the maximum absorbance leads to quantitative and reproducible results. During the investigation that we have pursued for several years on a variety of linear PE samples with different histories, we have developed confidence in the validity of the method (16-17). The results on low density PE seem suited to be published first since the more difficult phases to characterize, the non-crystalline phases are the main constituents of the overall material. The first results on films made with the press showed that the fraction of orthorhombic order by IR was higher than that obtained by the other techniques. It was decided then to prepare more ordered films from solution to evaluate the limit of orthorhombic crystallinity of the sample.

To evaluate the phase content, two regions of the spectra have been analyzed namely those corresponding to the wagging and rocking vibrations of the CH_2 groups. However, only the results for the rocking modes will be given here because the peaks of absorbance were simpler and the spectral simulation was straightforward in this region.

EXPERIMENTAL

Sample

Low density PE (Union Carbide) polymerized with the high pressure process was

received already extruded and stored at RT for several years. Table 1 lists the characteristics of the sample. The columns respectively give the density, Mw, Mw/Mn, the intrinsic viscosity in decalin, [η] at 130 °C, the number of methyls for 1000 carbon atoms and the melt index. The last three columns show the values of α_{ortho} calculated by standard methods using X-ray diffraction, density and heats of fusion from DSC in a fast T-ramp measurements. In the text below, the fraction of crystallinity by FTIR will be designated as an orthorhombic crystallinity, α_{ortho}(IR). The term α_{ortho} (i) is the value obtained with the other techniques. Note that α_{ortho}(DSC) is considered as orthorhombic and comparable to the others even if it may include some non-orthorhombic order. The molecular weight distribution has been obtained by the Lower Critical Solution Temperature (LCST) technique (28).

Table 1. Characteristics of the as-received sample.

							α_{ortho} [d]		
Sample	d g/cm^3	Mw[a] x 10^{-3}	M_w/M_n[b]	[η][c] dL/g	CH_3/ 1000C	MI g/10min	d	X-ray	DSC_{fast}
UC8	0.9132	260	2	1.80	30	0.08	0.418	0.44	0.38

Wide angle X-ray scattering

Diffraction diagrams were recorded using an Inel X-ray equipment operating at 40 KV and 30 mA. CuK_α1 radiation (λ = 0.15405 nm) was selected using a quartz monochromator. The values of α_{ortho} (X-rays) was determined from the ratio of the sum of the areas of all the crystalline peaks to the area of the large amorphous halo in the diffractogram.

Density measurements

The density of a liquid solution of tricholobenzene and toluene in which the solids (film or small pellet) were equilibrated was obtained using an Anton Paar quartz densitometer. The quantity α_{ortho} (d) was calculated from the density, d, and eq.1.

[1] $$1/d = \alpha_{ortho} / 1.008 + (1- \alpha_{ortho}) / 0.856$$

where 1.008 g/cm^3 is the density of the orthorhombic crystal and 0.856 g/cm^3 is the density of a fully amorphous CH_2 chain.

Calorimetry

Two significantly different calorimeters where used. In the standard DSC, a Perkin Elmer DSC7, 2-5 mg of the sample were placed in aluminum cupolas under nitrogen flow. A heating ramp of 20 K/min was used. In a special calorimeter, a C80 from Setaram, (Lyon, France), 20-35 mg of the polymer were placed over 1 cm^3 Hg, in a glass tube sealed under nitrogen. The heating ramp here was extremely slow (1 K/hour). The Setaram calorimeter is a very stable calorimeter used previously (9-12).

The absence of oxidative degradation in the slow heating have been checked as reported in previous publications. Furthermore, the high-T endotherms are seen as exotherms in cooling slowly the melt. Successive runs on the same samples confirm the findings of the first melting (9).

FTIR

A Bomen MB-series spectrometer was used in transmission mode at a resolution of 1 cm^{-1} with 25 scans.

METHODS

Film preparation

Thin transparent films must be prepared for transmission measurements. Two methods have been used as reported in table 3 : (a) by pressing the pellets for 5 min at 130 °C in a Carver press under air and a 21 metric tons pressure (IV) and quenching and (b) from solution. The 1% solution in xylene was prepared at 50 °C and quenched at RT. The solvent was left to evaporate at either room temperature or 70 °C. The films can be used as such (I) or pressed at different temperatures namely 90 °C (II) and 130 °C (III). The difference in phase content between the films evaporated at RT and 70 °C being small, the results given have been averaged for these two treatments. The procedure was not aimed at the growth of single crystals so quenching at RT was used rather than isothermal crystallization. Probably the slower crystallization rate of this low density PE explains the lack of sensitivity of the content of long and short-range order of this sample to the exact conditions of crystallization. It is possible also that the two parameters which are different in these two treatments namely the temperature of growth of the crystals and the temperature of evaporation of the solvent compensate each other in the final amount of total orthorhombic order. We have indications that IR measurements cannot distinguish between short- and long-range order but refined X-ray measurements should be done to confirm this observation.

The term S-films is used in the text only for films prepared without press (I) and the term P-films for the films prepared without solvent (IV). The treatments II and III give results intermediate between I and IV as will be detailed in the text. The spectrum of a unaged film corresponds to that of a film whose residence time at room temperature is less than three days

after its preparation.

Spectral simulations

The spectra were baseline corrected and the absorbance zero was set at 800 cm^{-1}. Spectral simulations of the 775-675 cm^{-1} regions in the IR spectra were then performed using the software BGRAMS/386 by Galactic industries. The simulations were performed using a Gauss + Lorenz band shape with a band width at half height of 3.5 cm^{-1} for the orthorhombic peaks (730 and 720 cm^{-1}), 10-16 cm^{-1} for the single chain band or amorphous region (725 cm^{-1}) and 15-19 cm^{-1} for the monoclinic-like peak (717 cm^{-1}). The abbreviation FWHM (Full Width at Half Maximum) is sometimes used. When Fourier self-deconvolution was used, the location of the peaks was found quite constant for the orthorhombic phase. On the other hand, the frequency of the non-crystalline phase was changing with the history of the film i.e. the sample morphology. When three phases were introduced, the frequency of the amorphous phase was found constant. However, the frequency of the monoclinic-like phase was found to change with the treatment. The physical reason we think is the following : in a sample under stress during the IR measurements, a band is found at 715-717 cm^{-1}. The samples prepared at the press or in solution do not keep long the tension associated with preparation so the 717 cm^{-1} disappears to be replaced by another band described in the literature as a non-crystalline band (24). In the present work, this band is associated with the network phase. The area of the orthorhombic doublet is found easily without repeating the simulation. On the other hand, the decomposition of the non-orthorhombic phases into the amorphous and the monoclinic-like phase was more difficult until it became clear that the frequency of the monoclinic-like band was varying with the sample treatment. Details on the decomposition are given in the

Justification section below.

The phase fractions were calculated from the simulated spectra using eq. [2]. The integrated absorbance of each band was ratioed against the total area of the 775-675 cm^{-1} region. The integrated absorbance of the two peaks at 730 and 720 cm^{-1}, both representing the orthorhombic fraction, were summed.

[2] $$\alpha_{\text{phase (I)}} = \text{Integrated Area}_{\text{phase (I)}} / \text{Integrated Areas}_{\text{all the phase}}$$

Extinction coefficients

The calculation of the fraction of each phase from the area of the peaks is suitable if the extinction coefficient of the different phases are the same. The extinction coefficient ε is obtained by plotting the integrated absorbance of the entire rocking region versus the film thickness for films with the same history. The value of ε has been obtained for linear and branched PE films of different density. When the thickness is expressed in micrometers (μm), ε varies between 0.34 and 0.42 for $0.4 < \alpha_c (d) < 0.8$ When the value of ε is corrected by the density, the ratio ε/d is found to increase from 0.37 to 0.43 (17). This result indicates that the crystalline phase has a higher extinction coefficient than the non-crystalline phases. No correction was introduced in [2] to take into account of this difference. For two reasons: a) because raw data are useful to other laboratories and b) because more analysis was needed to make an adequate correction. The use of the simple eq. [2] will lead to a overestimation of α_{ortho} (IR). In the rocking region, the integrated absorbance is linear with the film thickness for thickness up to about 100 μm. Fig. 2 is such a plot for the P-films.

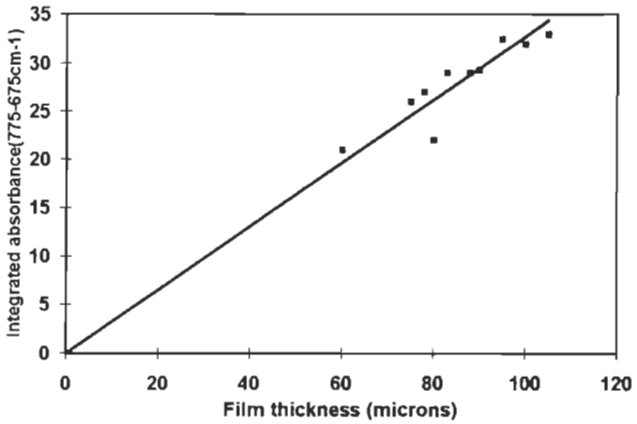

Fig. 2 Variation of the integrated absorbance in the rocking region as a function of sample thickness for P-films.

RESULTS AND DISCUSSION

1. Phase Content By Slow Calorimetry

Before presenting the FTIR results, the trace of melting of this sample using a very slow ramp will be given. As reported in previous work (8-12), slow calorimetry reveals endotherms not observed by fast DSC. The semi-ordered phase can melt when strain during the T-ramp is reduced. The rate of heating does not alter significantly the melting of the ordered chains which are not linked by entanglements. Slow calorimetry, on the other hand, allows the chains in a physical network to move during the T-ramp and avoid the level of strain which arrests melting in the usual rapid T-ramp. Fig. 1A is an example of a melting trace of the as-received sample. The first row of table 2 give the values of the enthalpies and the interval of T used for integration. The trace has been divided into three parts : the main sharp peak corresponds to the melting of long-range order, the medium size endotherm at low temperature is associated with crystals within the regions of the physical network which melt

at low T because they have few entanglements. The integrated heat flow between 30 and 125 °C is 142 J/g, i.e. about 60 J/g higher than in DSC. The next large endotherms have maxima at 180 and 250 °C. They correspond to the melting of order within an entanglement-rich network. The total enthalpy of disordering the chains between 30 and 280 °C is :

[3] $$\Delta H_{total} = \Delta H_{DSC} + \Delta H_{disor.network}$$

ΔH_{DSC} is the enthalpy measured in the fast T-ramp. The value of ΔH_{total} is now about 400 J/g i.e. larger than ΔH_o (293 J/g) the heat of fusion of perfect orthorhombic crystals. Discussion of this value is not suitable in the present paper on FTIR. It suffices to say here that the value of ΔH_o, obtained by different methods, corresponds to the change in enthalpy between 70 °C and 145 °C only. In the present technique, the change of enthalpy is followed over a larger T-interval and accounts for changes in enthalpy of the melt above Tm. The second row of table 2 give the analysis of a trace obtained at a more rapid rate of heating (12 K/h). The smaller value of ΔH_{total} is an indication that the strained network is not completely melted. Fig.1B is the signal of the calorimeter in the same conditions without the sample.

Table 2 Analysis of two traces in slow calorimetry.

v (K/h)	Mass (mg)	Tm (°C)	$\Delta H_{DSC\ long\text{-}range\ order}$ (J/g)	$\Delta H_{dis.net\ low\ strain}$ (J/g)	$\Delta H_{dis.net\ high\ strain}$ (J/g)	ΔH_{total} (J/g)
1	29.56	112.8	100 (87-120 °C)	40 (30-87 °C)	240 (120-273 °C)	380
12	37.24	113.1	100 (87-127 °C)	10 (48-87 °C)	40 (127-237 °C)	150

2. Phase Content By FTIR

This part has five sections. In parts A and B the phases of fresh films (A1 and A2) and of aged films (B1 and B2) are analyzed. In part C, the justification of a three-phase decomposition is given. In part D, we compare the information on a sample provided by FTIR and by the standard techniques of analysis and, in part E, an attempt is made to relate the meltable order of a sample as given by the slow melting trace presented in Fig.1A with the phase composition found by FTIR.

A. Un-aged films

A1. The orthorhombic phases

Figure 3A shows the IR spectra of a S-film aged at RT less than three days. The spectral simulation results in four bands. The two narrow bands correspond to the well known orthorhombic organization. The two wide bands of lower absorbance correspond to the amorphous and monoclinic-like phases. In fig.3A, the fraction of the orthorhombic phase, α_{ortho}, is 0.642, the monoclinic-like phase, α_{mono} is 0.100 and the amorphous phase, α_{amor} is 0.258.

Table 3 gives the values of α_{ortho} by the different techniques, for the films prepared with the different histories (I-IV). The first row lists data for a short aging (three days or less) and the second and third for longer aging times (4 and 11 months). Analyses made on some films after 17 months did not differ significantly from those at 11 months so they have not been reported. The data of α_{ortho} in these tables are averages of several films (4-7) for slightly different preparations (where the parameters were the initial concentration and the temperature of evaporation of the solvent).

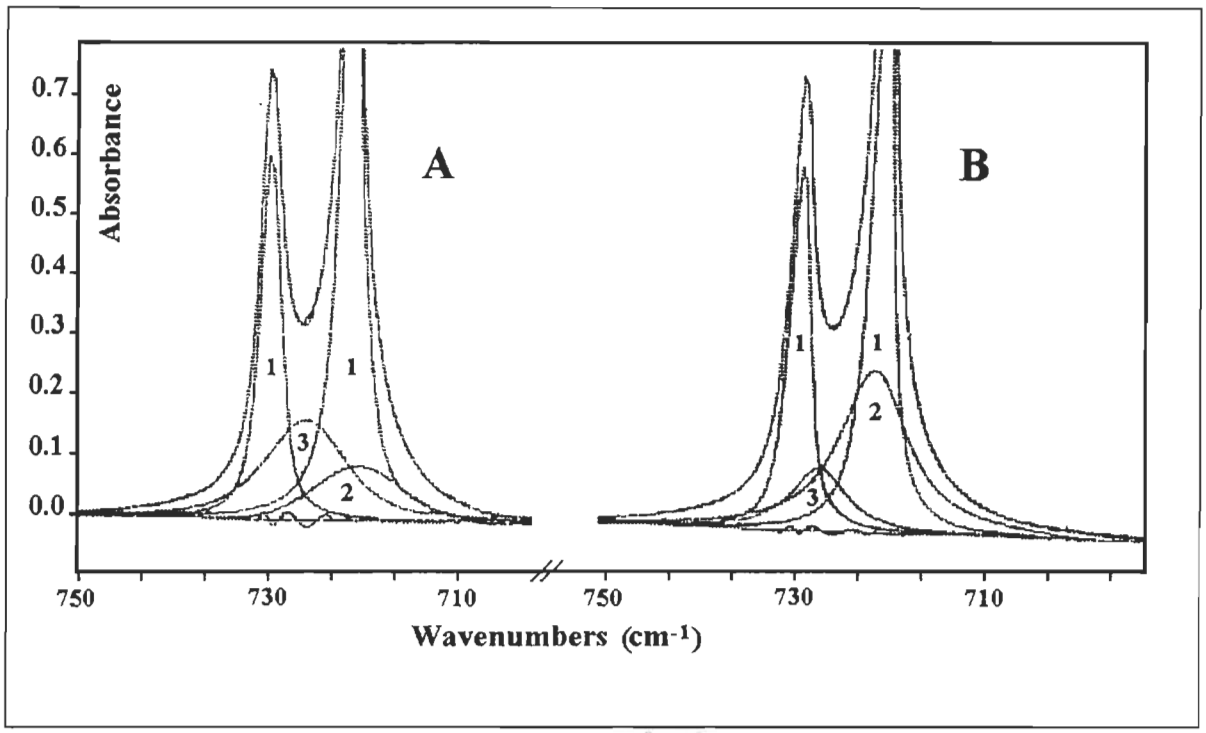

Fig. 3. (A) Spectrum in the rocking region of a S-film showing the three phases: 1. Orthorhombic 2. Monoclinic-like 3. Amorphous. (B) Same film as in A after a four month aging time showing an increase in the monoclinic-like phase.

The values by density and calorimetry of the P-samples are similar to those of the as-received sample (table 1). As expected, the value of α_{ortho} (IR) is higher for the S-films than for the P-films. The films made using solvent and press have, after aging values of α_{ortho} (IR) near those of the S- and P-films respectively. The overall result is that α_{ortho}(IR) - α_{ortho} (i), is positive, the difference increasing with α_{ortho}. Each value of α_{ortho} (IR) - α_{ortho}(i) will be commented separately.

Table 3. Values of α_{ortho} (IR), α_{ortho} (d) and α_{ortho} (X-ray) for treatments I-IV as a function of aging time.

Aging (months)		Sample preparation I, solution [a] No press	II, solution [a] Pressed : 90°C	III, solution [a] Pressed : 130°C	IV Pressed : 130°C
<0.1	α_{ortho} (IR)	0.64	0.60	0.54	0.58
4	α_{ortho} (IR)	0.59	0.51	0.46	
11	α_{ortho} (IR)	0.67	0.67	0.57	0.56
<0.1	α_{ortho} (d)	0.48	0.47	0.38	0.38
4	α_{ortho} (d)	0.5	0.47	0.40	0.40
11	α_{ortho} (d)	0.49	0.46	0.39	0.39
<0.1	α_{ortho} (X-ray)	0.34	___	___	0.45
4	α_{ortho} (X-ray)	___	___	___	0.45
11	α_{ortho} (X-ray)	0.50	___	0.43	0.48

[a] In Xylene (1%).

Note: the values above are averages of 4-7 films for each treatment. The range of data for the same treatment is the same: α_{ortho} (d): 0.001-0.01, with the lower values for aged samples. α_{ortho} (IR):0.01-0.04 with the lower values also for aged samples. α_{ortho} (X-ray): 0.04.

Difference between crystallinity determined by IR and X-rays

The difference for the non-aged films is large but larger for the S-films (0.30) than the

P-films (0.11). As the X-ray diffraction measures solely the long-range order, the origin of the difference resides in the short-range order :

[4] $\alpha_{ortho}(IR) = \alpha_{ortho}$ (long-range order) + α_{ortho} (short-range order)

Obviously, there is continuum of order in the sample but the simple separation in two types of order in [4] corresponds to the limit in size which gives a sharp X-ray diffraction pattern.

[5] α_{ortho} (short-range order) = α_{ortho} (IR) - α_{ortho} (X-ray)

Difference between crystallinity determined by IR and DSC

The value of α_{ortho} (DSC), obtained by dividing ΔH by 293 J/g is 0.32 ± 0.04 for all the samples. The figures for the different treatments and the effect of aging for the P-films and S-films have not been reported in detail because the trends are not clear. The value of α_{ortho} (DSC) is lower than $\alpha_{ortho}(IR)$ because the latter contains some order which cannot melt because it is strainable in the T-ramp.

[6] α_{ortho} (strainable order) = $\alpha_{ortho}(IR)$ - α_{ortho} (DSC)

In the low T-ramp of Fig.1A, 140 J/g is absorbed at low T, i.e. below 120 °C (instead of 85 J/g in DSC). The meltable order, in these special conditions, has increased from 0.32 to 0.48 but remains lower than α_{ortho} (IR).

Difference between crystallinity determined by IR and density

The difference varies as $\alpha_{ortho}(IR)$ since $\alpha_{ortho}(d)$ varies little. It is smaller (0.17) for the non-aged S and P-films. After aging, the similarity of the values of α_{ortho} (d) and α_{ortho} (X-rays) permits to evaluate α_{ortho} (short-range order) from the density :

[7] α_{ortho} (short-range order) = α_{ortho} (IR) - α_{ortho} (d)

An illustration of the difference between α_{ortho} (IR) and α_{ortho} (d) for the different treatments is given in fig.4 where α_{ortho} (d) and α_{ortho} (IR) are plotted in abcissa and ordinate. If the two estimations of α_{ortho} were the same, the data would be on the ligne x=y. The differences between the bar and the x-y line is seen to vary with the treatment (0.16-0.25). The range of α_{ortho} (IR) is seen very narrow for the P-films (IV) and large for the other treatments (I-III). The range of α_{ortho} (d) is narrow. This implies that movements of the chains which modify short-range order can be carried out without changing the overall density. A trace similar to fig.4 could have been done using the values of α_{ortho} (X-ray) in abcissa but with a lower precision than α_{ortho} (d).

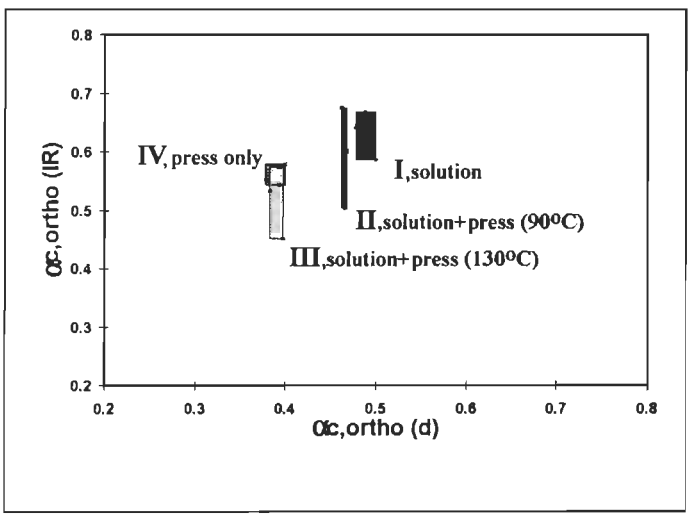

Fig. 4 Correlation between α_{ortho} (IR) and α_{ortho} (d) for treatments I-IV. The higher values within the same treatment is for aged samples.

Solvent and vapor stability

To verify that the solvent in which the densities were taken was inert towards this low density PE analyzed, the values of d, α_{ortho} (X-rays) and α_{ortho} (IR) were obtained after immersion in the usual solvent mixture used for density and in another mixture

(ethanol/water). They have been found the same. On the other hand, α_{ortho}(IR) can be made to increase by leaving the films to be swollen in the vapor of a solvent. After three days in the vapors of CCl_4 at 40 °C the value of α_{ortho} (IR) has increased to 0.72 for the S-films and to 0.60 for the P-films.

Order of the skin of the film

Some X-rays data have been recorded in a Siemens D-5000 reflection diffractometer the beam of which, in the actual settings, goes at a depth of a few dozen A across the sample surface. For the P-films and the aged S-films, α_{ortho} (X-ray) has the same value as for the transmission measurements. However, for the non-aged S-films the diffractogram is diffuse and the value of α_{ortho} (X-ray), is found to be around 0.1. This suggests that the first few layers of the surface seen by the beam have little long-range order. The time for recovery of the usual spectra has not been measured. A similar difference has been found on thin films of amylose (Hylon VII) made from solution whose crystallinity was also measured with the two X-ray techniques.

Resistance of the orthorhombic phase to mechanical deformation

When the films made in solution are pressed at 90 °C they do not melt completely but deformation occurs may be as a consequence of a temperature gradient between the surface and the interior. In consequence, the value of α_{ortho} (IR) is diminished from 0.64 to 0.60 (II in table 3) with an increase in the amorphous and monoclinic-like phases. It is interesting to note that the density is not changed with the deformation. With time, these films recover almost to the values of the S-films. The films made in solution and pressed at 130 °C have no memory of the preparation in solution with one exception. This is the diminution of α_{mono} (IR) aged 4

months which seems a feature of all the films made in solution (I-III) as illustrated in fig.5.

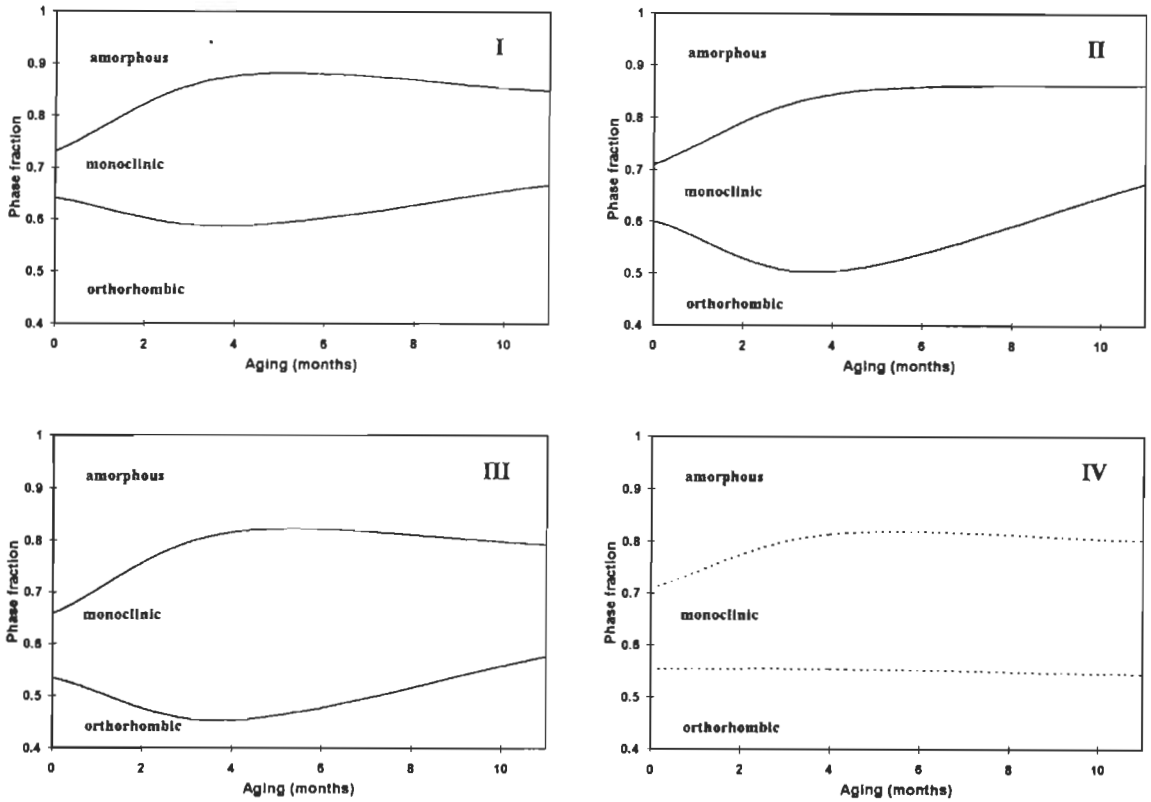

Fig. 5 Phase composition of films as a function of aging for I-IV. The lower and upper regions represent the orthorhombic phase and the amorphous phase respectively .The region in-between is the monoclinic-like phase. The scale starts at 0.4 not at 0. The dotted lines in IV represent extrapolation from incomplete data.

A2- The non-orthorhombic phases

Table 4 gives the fraction of the non-orthorhombic phases for the films whose orthorhombic content is given in table 3. The first two rows, labeled two-phase decomposition, give the results of decomposition which leads to such a small amount of the monoclinic-like phase (0.05) that a two-phase model would be almost sufficient. This occurs only for non-aged films. One sees on the next rows that the non-aged S-films have little monoclinic-like content. Further discussion will be made below in the part describing the effect of aging. The data of Tables 3 and 4 have been plotted in figs 4 and 5. Further details on

the two-and three-phase decomposition are given below under the title *Justification.*

Table 4. Values of α_{mono} (IR) and α_{amor} (IR)for treatments I-IV as a function of aging time.

		Sample preparation			
		I, solution [a]	II, solution [a]	III, solution [a]	IV
		No press	Pressed : 90°C	Pressed : 130°C	Pressed : 130°C
Two-phase decomposition[b]					
	α_{mono}	<0.05	0.05	0.04	0.05
	α_{amor}	0.31	0.35	0.40	0.42
Three-phase decomposition					
Aging (months)					
<0.1	α_{mono}	0.09	0.11	0.12	0.16
<0.1	α_{amor}	0.27	0.29	0.34	0.26
4	α_{mono}	0.29	0.34	0.36	
4	α_{amor}	0.12	0.15	0.18	
11	α_{mono}	0.18	0.19	0.22	0.26
11	α_{amor}	0.15	0.14	0.21	0.18

[a]In xylene (1%)

[b]The two- and three-phase decompositions are similar when α_{mono} is less than 0.05, see Table 6. The ranges of data are the same as in Table 3.

B. Films aged or in the process of aging

According to practice and thermodynamics theory, aging at room temperature enables the lowest free energy phase, the crystalline phase, to grow within the limits imposed by the kinetics of chain reorganization in the solid state. The usual techniques of crystallinity evaluation should show an increase in crystallinity during aging. If more refined probes are used such as small angle X-rays scattering (SAXS) or Raman spectroscopy (30), one notes that aging is a complex phenomena which involves exchange of the CH_2 segments between the phases, widening of the distribution of the lamellar thickness and a displacement of

Tm not towards the high temperature. (32) In consequence, one cannot expect that aging will take place only in the orthorhombic phase with short-range order becoming long-ranger order as aging time increases. The data of figs. 5 and 6 show that changes in the three phases occur with time.

B1. The orthorhombic phase

The change of α_{ortho} (IR) with time is reported in table 3 and also in fig.5. The ordinate of the bottom trace follows the variation of α_{ortho} (IR) with time for the different treatments. It is informative to remark that α_{ortho} (IR) diminishes by 0.06-0.1 in the first months of aging before increasing. This can be understood by the analysis made above where part of α_{ortho} (IR) does not belong to the stable long-range order but is associated with short-range orthorhombic order belonging to the network phase. The movements in these chains is subordinated to those in the non-orthorhombic phases.

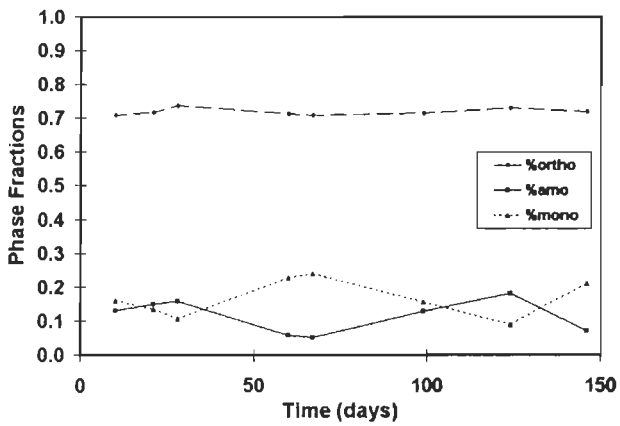

Fig.6 Phase content variation of a S-Film during an aging of 150 days.

Table 3 shows that the change of α_{ortho} (d) with aging is small and difficult to interpret since a two-phase model has been used to calculate it. It is somewhat surprising that α_{ortho} (d)

does not increase more. Linear PE, on the other hand, when submitted to a long gradual T-ramp up to a few degrees below Tm, reaches a value of α_{ortho} (d) = 0.92 (32). The authors succeeded to prove by this several year long experiment that regular PE could reach the same equilibrium state as high-pressure crystallized PE. Probably, the low value of α_{ortho} (d) in the present sample due to the branches could be increased by a specific annealing at higher temperature. The long annealing experiment showed also that no change in molecular weight occurs in the well-purged samples as a consequence of the high-T treatment.

Correction of α_{ortho} (d) in low density PE

The values of α_{ortho} (d) in the tables have been calculated with the data of eq.1. Recent X-rays scattering studies of linear low density PE give higher cell dimensions and lower values of d(orthorhombic), namely 0.9679 and 0.9820 g cm^{-3} (33-34) for samples having respectively 20 and 22.7 methyls for 1000 C atoms. If an intermediate value of d is used, for instance 0.975 instead of 1.008 g cm^{-3}, the α_{ortho} (d) values found from eq.[1] are higher than those given in table 3. As an example, α_{ortho} (d) for the films made from solution becomes 0.60, not too different from the value obtained by IR (0.64). The present X-ray measurements have not been analyzed with sufficient detail to spot an eventual difference in the peak position of the S- and P-films.

The results of slow DSC will not be commented upon since, as said above, we were not able to see a trend in α_{ortho} (DSC) with time. After a long aging, α_{ortho} (X-ray) reaches about 0.50 for the S- and P-films and the difference between them, found before aging (0.1), disappears.

B2. The non-orthorhombic phases and the overall composition

The spectrum of the S-film shown in fig. 3A is given in fig. 3B after it has aged during 4 months. The monoclinic-like phase (curve 2) increases for this sample from 0.10 to 0.28 while the amorphous phase (curve 3) diminishes from 0.26 to 0.12. This suggests that the monoclinic-like organization is a necessary step for increasing long-range order. This was reported qualitatively in the literature (18-20).

One can visualize the change in phase composition with time in figure 5 (I-IV) for the four treatments. The lower and upper regions represent the orthorhombic phase and the amorphous phase respectively, while the region in between is the monoclinic-like phase. The scale for the orthorhombic amount starts at 0.4 and not at 0.

As seen in the graphs (I-III) after four months, the concentration of the monoclinic-like phase increases significantly with time reaching 0.29-0.36 at an aging time of four months for the S-films. After eleven months, the concentrations of the two non-crystalline phases are similar, the monoclinic-like phase being reduced to about the amount of the amorphous phase. For the P-films (with the trace in dotted line because they were not analyzed after a 4 month aging), α_{mono} is still high after an 11 month aging time, an indication of incomplete aging in the non-orthorhombic phases. This interesting feature may be related to the state of the melt more thoroughly disordered by the solvent than by the fusion under the press. We intend to take the spectra of the sample crystallized from the melt which has undergone the slow T-ramp in the calorimer. It is likely that the slow melting has the same effect as the solvent for increasing chain mobility in the sample after recrystallization. It is noteworthy that the non-orthorhombic phases keep the memory of the solvent history (III)

even after pressing and a long aging at RT. The increase of α_{mono} with time has been observed on many samples of PE with different densities.

The change of phase content with time of one sample is reported on Fig.6. Eight spectra of the same film were analyzed over a period of 150 days. For that sample, the orthothombic content (top line) fluctuates little with time (0.04 at maximum) with a small decrease at around two-months of aging which follows the initial increase. The monoclinic-like fraction (bottom line) is seen to increase by more than a factor of 3 over some period, the amorphous content varying in a complementary way. The fact that a maximum in α_{mono} (IR) occurs after two months while it arrived after four months for the films made and averaged in table 3 may come from small differences in the film preparation such as film thickness and homogeneity.

Movements of methylene chains in the solid state

It was said above that α_{ortho} (IR) could decrease during aging because part of the chains in this phase are mobile since they do not belong to long-range order. Another information suggests chain mobility at RT : It was found quite late in the history of the orthorhombic morphology perhaps because it was counterintuitive, that chains packed in long-range order can move. The heat capacity of solid linear PE between RT and Tm has been found higher (35) than the value calculated, using a two phase model, from its crystallinity and the known vibrations of the methylene groups in the two phases. Through modelization (35), this feature was explained by recognizing that the ordered chains in the orthorhombic crystals rotate with a high frequency, a freedom of movement unexpected for chains so close to each other. One can expect that the non-orthorhombic phases will be even

more mobile, at least in the regions distant from the knots. In consequence, the change with time of the relative amount of the phases as seen by FTIR is not unexpected. The diminution of the α_{ortho} (IR) in the first months of aging comes in our opinion mostly from changes in the short range order as said above. However, it is likely that some unfolding of the chains takes place in the long-range order also to permit the growth of thicker lamellae.

Assuming that aging corresponds to a slow annealing, insight into aging can be obtained through studies of the change of morphology during annealing. Different techniques have been used to follow annealing, each viewing a different size or different order in the sample. One of this techniques which measures the straight-chain lengths in PE by Raman spectroscopy may give information relevant to the present analysis (30). The study reveals unexpected and drastic changes in straight-chain length distribution as a result of annealing. Since the frequency ν of the longitudinal acoustic mode (LAM) is related by a simple equation to L the straight-chain lengths, the distribution of frequency of the LAM band permits to calculate the distribution of straight-chain lengths in the sample. The authors find that the band half-width increases from 100 to 300 A upon annealing. They observe also that the shape of the band does not change regularly with time. Since some annealing temperatures for the LAM experiments were low (90 °C) i.e. well below the value of Tm, the physical phenomena underlying the movements of the chains in the crystalline phase as seen by LAM and FTIR are likely to be similar. Again, the variation observed in the high density phase by Raman during aging permits to accept that the large variations that we observe in the lower density phases by FTIR have a physical significance.

Change of frequency of the characteristic bands

The description of the phase change given in fig. 5 is incomplete since the frequency of the non-crystalline phases change with time. It has been observed that the frequency shift of the monoclinic-like phase is related to its concentration in the sample. Fig. 7 is a plot of the frequency of the monoclinic-like phase as a function of α_{mono} (IR). The lower frequency is found in freshly prepared samples and highly deformed material but the amount of this phase is different for these two histories. The regular shift of the frequency with α_{mono} (IR) seems to indicate that the deformed phase which is not abundant after the preparation is replaced by a phase with specific characteristics, not closely linked with the monoclinic structure which may have existed in the fresh film. This result clarifies some ambiguity in the literature where the monoclinic-like band had to be associated with monoclinic reflections in the X-ray pattern (18-20, 26). The points at the upper right of the graph correspond to films where the monoclinic-like phase and the amorphous phases are a single phase. The frequency of the amorphous band at 725 cm^{-1} is shifted also when α_{amor} (IR) diminishes. The chains in the monoclinic phase, are thought to belong to the physical network described to explain the slow calorimetry results. Phase separation between the network chains and the free chains which favors better interactions within the same phase, may be at the origin of the shift during aging.

The frequencies of the orthorhombic bands after decomposition have not been found to change with the treatment. The distance between the two peaks, 10.6 ± 0.2 cm^{-1}, is very similar to that found (10.5) for linear PE (18). The band-widths have not been found larger than for linear PE.

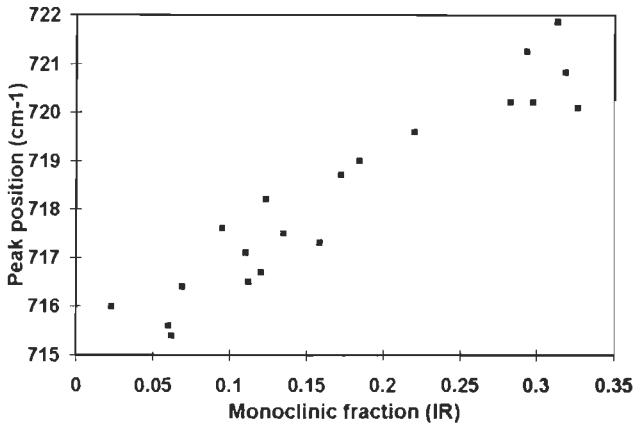

Fig. 7 Correlation between the peak position of the monoclinic-like phase and its amount in the samples. The points for $\alpha_{mono} > 0.30$ correspond to films with only two phases, the abcissa being for those α_{amor} instead of α_{mono}.

C. Justification of the decomposition of the aged films with a three-phase model

Tables 5 and 6 give for a S-film and a P-film the details of the decomposition using either two- or three- phase model. The corresponding spectra as given in Figs. 8 and 9. The columns give successively the type of simulation and the aging status of the films, the phase content, the frequencies of the bands, their width at mid height, their shape, and the χ^2 values. The number χ^2 corresponds to the difference between the experimental and calculated absorbances over the whole band. The rows (A) and (B) are for the un-aged films and (C) and (D) for the aged films. The data for a two- and three-phases decomposition of the un-aged film given in (A) and (B), present the following features : i. the orthorhombic phase content is the same in (A) and (B) i.e. it does not depend on the number of phases ii. Neither the frequency of the amorphous band nor its shape (completely Gaussian) vary when the decomposition introduces a small amount of monoclinic-like phase (<0.05). The data in (C) for an aged film gives a different picture : the frequency and amount of the orthorhombic phase are still independent on the number of phases but the characteristics of the amorphous

Table 5. Justification of the three phase model for an aged P-film : Characteristics of spectrum simulation with a two-phase and three-phase decomposition.

	Sample P-film	Fraction	Position (cm^{-1})	FWHM (cm^{-1})	Shape (%Lorentz)	χ^{2g}
	Unaged	0.60(α_{ortho})	730.1	3.56	85	
Fig. 8A	Two phase		719.4	4.14	100	10^{-5}
	Simulation	0.40(α_{amor})	725.4[a]	13.73[b]	0[c]	
	Unaged	0.58(α_{ortho})	730.3	3.56	85	
Fig. 8B	Three phase		719.0	4.14	100	10^{-5}
	Simulation	0.37(α_{amor})	725.2	13.73	0	
		0.05(α_{mono})	716.4	16.85	38	
	Aged	0.51(α_{ortho})	730.5	3.50	78	
Fig. 8C	Two phase		719.6	3.33	82	0.80
	Simulation	0.49(α_{amor})	720.8[a]	16.89[b]	40[c]	
	Aged	0.57(α_{ortho})	730.3	3.54	84	
Fig. 8D	Three phase		719.4	3.55	100	10^{-2}
	Simulation	0.17(α_{amor})	725.3[d]	13.49[e]	0[f]	
		0.26(α_{mono})	718.2	17.46	53	

Aging has three effects on the characteristics of the amorphous phase, as follows:
[a]A displacement of the frequency
[b]An increase in band width.
[c]A change in band shape
These effects are reduced by the introduction of a third monoclinic-like phase. The data with the superscripts *d, e, f* are similar to those with the superscripts a, b, c.
[g] χ^2 values of 10^{-5} indicate an excellent fit while 10^{-2} is acceptable and 0.80 is not

phase are different. The value of ν is shifted to 720.8 cm^{-1}, the band-width has increased by 3 cm^{-1} (13.7 to 16.9) and the band shape is changed from 100% to 60% Gaussian. With a three phase simulation (D), the characteristics of the amorphous phase (frequency, width and shape) are restored to the values obtained with the two-phase model (A). Note that the frequency of the monoclinic-like phase has increased between C and D as reported in fig.8.

The same results are obtained in table 6 on the S-film. The frequencies of the orthorhombic bands after decomposition have not been found to change with the treatment. The distance between the two peaks, 10.6 ± 0.2 cm^{-1}, is very similar to that found (10.5) for linear PE (18). The band-widths have not been found larger than for linear PE.

Table 6. Justification of the three phase model for an aged S-film : Characteristics of spectrum simulation with a two-phase and three-phase decomposition.

	Sample S-film	Fraction	Position (cm^{-1})	FWHM (cm^{-1})	Shape (%Lorentz)	χ^{2g}
	Unaged	0.65(α_{ortho})	730.1	3.65	80	
Fig. 9A	Two phase		719.6	3.54	100	10^{-5}
	Simulation	0.35(α_{amor})	724.0[a]	14.00[b]	0[c]	
	Unaged	0.64(α_{ortho})	730.2	3.65	80	
Fig. 9B	Three phase		719.5	3.54	100	10^{-5}
	Simulation	0.32(α_{amor})	723.4	14.00	0	
		0.04(α_{mono})	716.6	16.00	43	
	Aged	0.58(α_{ortho})	730.2	3.61	78	
Fig. 9C	Two phase		719.3	3.48	94	0.37
	Simulation	0.42(α_{amor})	719.7[a]	17.79[b]	37[c]	
	Aged	0.68(α_{ortho})	730.3	3.54	80	
Fig. 9D	Three phase		719.6	3.56	100	10^{-8}
	Simulation	0.11(α_{amor})	724.8[d]	14.05[e]	0[f]	
		0.21(α_{mono})	718.0	17.46	60	

Aging has three effects on the characteristics of the amorphous phase, as follows:

[a]A displacement of the frequency

[b]An increase in band width.

[c]A change in band shape

These effects are reduced by the introduction of a third monoclinic-like phase. The data with the superscripts *d, e, f* are similar to those with the superscripts a, b, c.

[g] χ^2 values of 10^{-5} indicate an excellent fit while 10^{-2} is acceptable and 0.80 is not

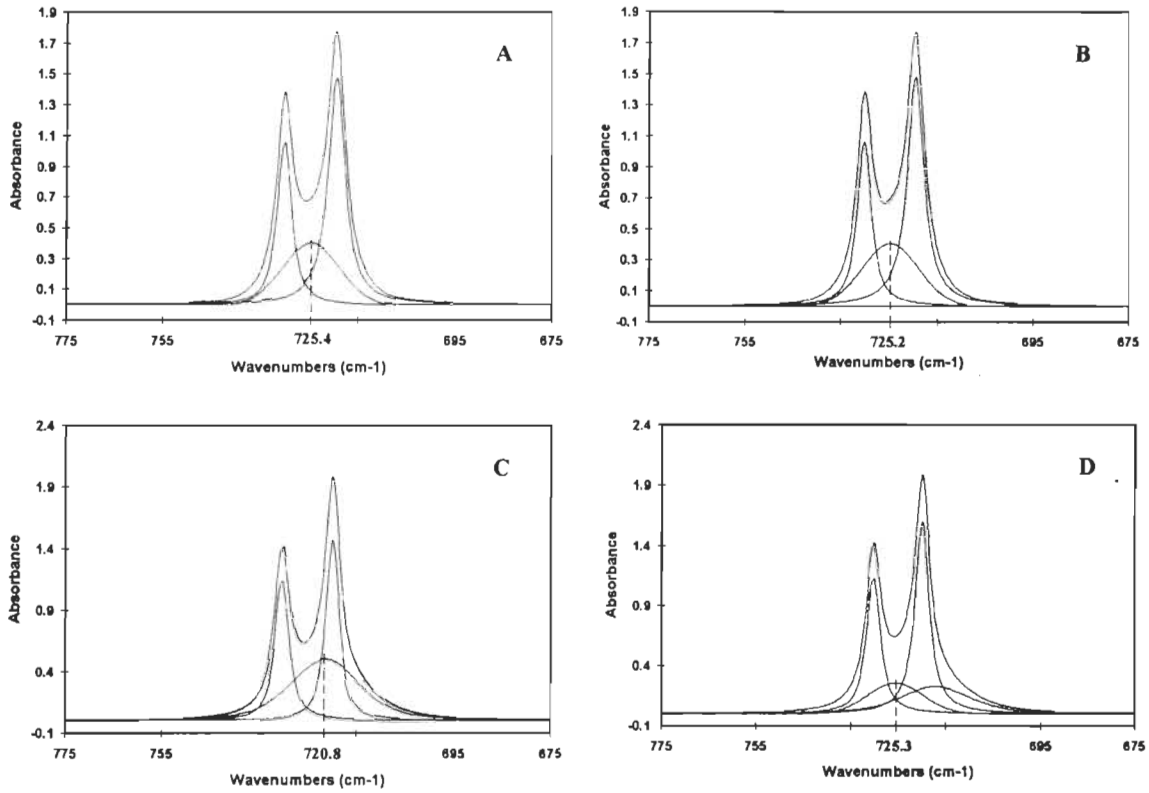

Fig. 8 Spectrum in the rocking region of a P-film with a two-phase decomposition (A,C) and a three phase decomposition (B,D). The spectra A,B are for non-aged films and the spectra C,D are after a four month aging time at RT . The dotted vertical line shows the frequency of the maximum of the amorphous phase in the two-and three-phase decompositions.

The information obtained through the spectral simulation for samples with different histories, the consistency between the results constitute, we believe, the worth of the decomposition at this stage. To our knowledge, a single technique, Raman spectroscopy, has lead to the definition of four phases for linear PE (2). The conditions of the experiment (geometry of the film, temperature of crystallization, time of aging), different from the present ones, do not permit to compare the phase content of this in-depth investigation with the present one. Combination of IR and Raman on the same sample should allow verification of the present results. We are also planning to explore other regions of the IR spectra that could confirm the change of the relative amount of the non-orthorhombic phases with sample history.

D. Information on the sample given by the phase content obtained by FTIR

Long-range order

When precise information on a sample having undergone a specific history is required, IR by transmission with its unavoidable stage of film preparation (press or solution/crystallization) may not be the best method because the film preparation may obscure the exact properties of the sample. To overcome this problem, reflectance techniques such as internal or attenuated reflectance have been used. An advantage of these techniques is, for instance, to probe at different depth into the sample and reveal heterogeneity or orientation of the material (24) However, they are more delicate to operate than Transmission IR as they require excellent physical contact between the crystal and the sample, a requirement which is sometimes difficult to address without changing the history of the sample. If the overall crystallinity of a sample is needed (i.e. the long-range order), the measurement of the density, of the X-ray pattern or of the heat of fusion of annealed films are, in most cases, capable of giving of good picture of the sample morphology. Data in table 3 indicate however, that the density is not too sensitive to sample history. The measurement of density gives another information since it can reveal unambiguously heterogeneity in large samples crystallized with an unwanted temperature gradient (insulating material for cables for instance).

In spite of the changes of morphology induced by film preparation, the measurement of the phase content by FTIR gives sound information. Analysis of the phase content of linear PE (16-17) gives α_{ortho} = 0.84 and 0.81 for the S and P-films. These values are, as expected, higher than for branched PE. Furthermore, in films stabilized by their history, a controlled melting under the press does not erase the film history. Samples of linear PE have

been cooled at 3 K/h to record for instance the different crystallization endotherms and analyze the monoclinic-like morphology induced by slow cooling. The material had to be pressed for IR measurements but it kept in this process a high amount (0.25) of monoclinic-like material. The evaluation of short-range order from spectral simulations and measurement of its density or X-ray diagram (eq. [4]) is a unique information drawn from FTIR.

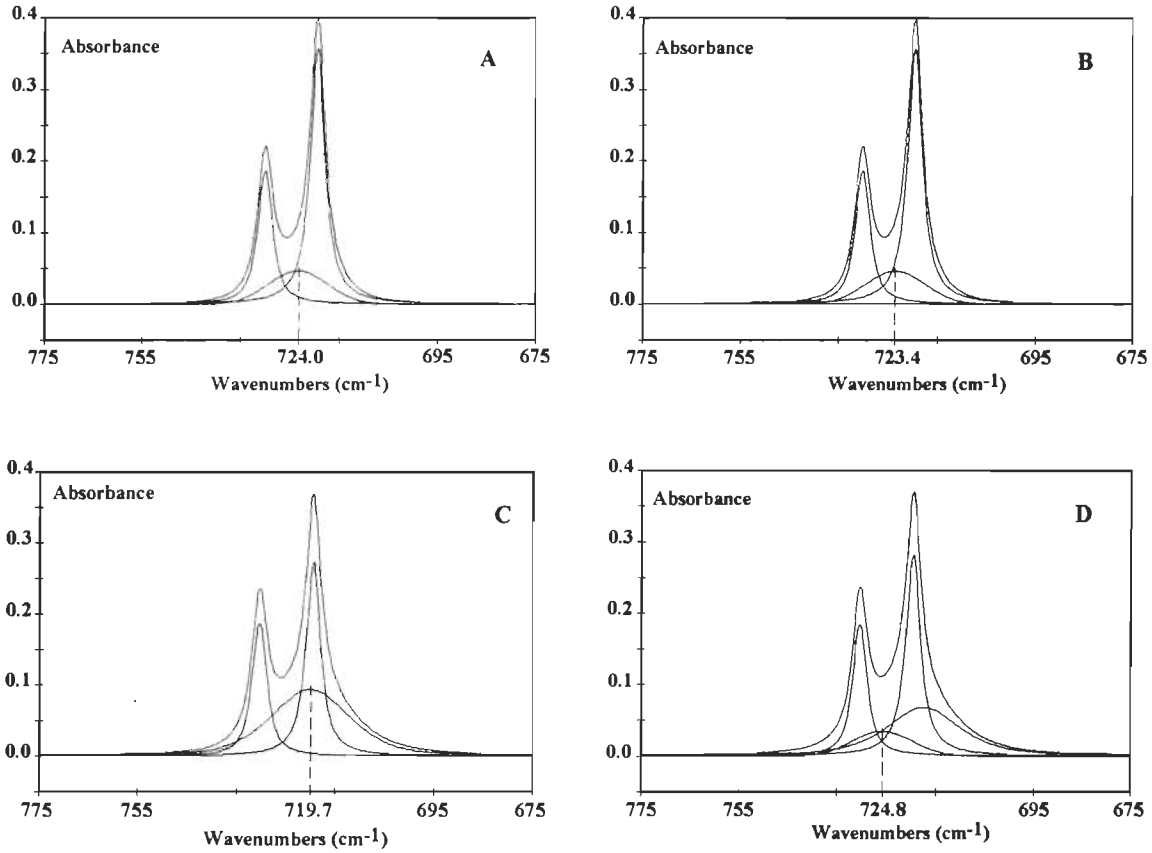

Fig. 9 Spectra in the rocking region of a S-film with a two-phase decomposition (A,C) and a three phase decomposition (B,D) .The spectra A,B are for non-aged films and the spectra C,D are after a four month aging time at RT .The dotted vertical line shows the frequency of the maximum of the amorphous phase in the two-and three-phase decompositions.

The non orthorhombic phases

The knowledge of the complexity of the non-orthorhombic phase obtained by our group or others (5-7) permits to integrate information in the literature related to the FTIR analysis and to other polymer techniques. The studies of the rocking bands made for instance

to evaluate the sample crystallinity locate two amorphous bands at 720 and 725 cm^{-1} (25, 26). But no quantitative treatment has been done using both bands. The merit of the present study is to have detached the monoclinic-like band of that observed in deformed samples and show that it exists in most samples and permits to characterize a distinct non-crystalline phase. This is an important result which was made possible through the previous phase content analysis by slow calorimetry.

The variation of the non-orthorhombic phases with preparation and aging is an unique information that the usual techniques measuring long-range order cannot give. The data given in figs. 5 and 8 show large amplitude in the phase content variations with a periodicity which must depend on many parameters. The equilibrium phase content of a S-film (0.70, 0.15, 0.15 for the orthorhombic, monoclinic-like and amorphous) is a useful information to obtain. It may be related not only to the methyl content of the sample but also to the catalyst used for the polymerization.

The network phase

If the query does not concern the last crystallization but rather the morphology of the polymer itself, the IR spectra can give important information concerning the amount of network phase and its localization in the different phases. Entanglements must be distributed in all the samples but their concentration is expected to be higher in the non-crystalline phase. It was interesting to discover that half of α_{ortho} (IR) of the S-film (data obtained from α_{ortho} (IR) - α_{ortho} (DSC) did not melt in a fast T-ramp. This points out to the fact that a fraction of short-range order is strainable due to its inclusion in a network. In a non-strained situation, the network content of the non-orthorhombic phases is difficult to evaluate quantitatively. An indication of the presence of the network phase in the monoclinic-like

phase is that its shape and peak position changes the most under strong deformation. Further work continues on the characterization of the network phase by FTIR

E. The sum of all meltable order

We have started this analysis to evaluate the phases which could correspond to those disordered in the trace of fig. 1. To account for large value of ΔH (table 1), we have searched for indications of phases which could be disordered and give the endotherms found at high temperature. With the reasonable assumptions that the orthorhombic and monoclinic-like fractions can be disordered in the T-ramp, the sum of these two phases is about 0.8 for the P-films. The as-received sample whose melting trace is given in Fig. 1 has a morphology similar to a aged P-films. The question to be asked now concerns the possibility of finding the complement (0.2) of meltable order in the third phase, i.e. the amorphous phase. It seems that the answer is positive. It has been reported in the literature that in melt-crystallized samples, some of the chains fold in the 200 plane rather than the 110 plane common to single crystals (18-20). These chains are too far apart to experience field splitting so they absorb as a singulet at 725 cm^{-1} instead of the usual doublet. Due to their high fraction of trans-trans, they have been called trans-planar chains (24). The trans-planar chains are more numerous in a low density PE or in a deformed sample (24) than in a high density PE. If this assumption is exact, the supplement of order needed to make consistent the slow calorimetry and FTIR analyses would be contained in the amorphous phase whose trans-planar chains would get disordered when the temperature is raised.

CONCLUSION

This investigation of the rocking regions of low density PE has permitted the detection of three phases in films made in solution or in pressed films associated respectively with the orthorhombic, monoclinic-like and amorphous morphologies. The quantitative measurement of two non-crystalline phases in non-strained samples is a new and probably general finding for semi-crystalline polymers. The orthorhombic content of aged films made in solution can reach 0.67 while it is 0.5 by X-ray and density. FTIR constitutes an unique way to detect short-range order orthorhombic (0.2) in this highly branched PE. The fraction of meltable order by DSC is low (0.32) due to the easily strainable entangled regions. The phase with short-range order and the monoclinic-like phase are associated with the network fraction whose melting can occur in melting conditions which diminish the strain (slow calorimetry).

During aging, the concentration of the three phases changes. The monoclinic-like structure increases in size and its frequency is displaced during aging, changes associated with phase separation of free and entangled chains. The monoclinic-like phase seems to be an intermediate step to increased crystallinity. The IR analysis confirms the findings of slow calorimetry but it uses a quicker and more widely available technique. The present report is not definitive however. We are currently analyzing other regions of the spectrum to confirm or complete the information given on this low density PE

ACKNOWLEDGEMENTS

The subvention of the National Research Council of Canada is gratefully acknowledged. We would also like to thank Dr. Patricia Le Bail (INRA, Nantes) for the X-ray measurements.

REFERENCES

1. R. Kitamura, F. Horii, K. Murayama. Macromolecules, **19**, 636 (1986).

2. R. Matter, W. Stille, G. R. Strobl. J. Polym. Sci. Polym. Phys. Ed., **31**, 99 (1993).

3. G. R. Strobl and W. Hagedorn J. Polym. Sci. Polym. Phys. Ed., **16**, 1181 (1978).

4. M. Glotin and L. Mandelkern. Colloid Polymer Sci., **260**, 182 (1982).

5. P-G. de Gennes. Macromolecules, **17**, 703 (1984).

6. T. Bremner and A. Rudin. J. Polym. Sci. Polym. Phys. Ed., **30**, 1247 (1992).

7. M. van Prooyen, T. Bremner and A. Rudin. Report of the Institute for Polymer Research, University of Waterloo, 1992.

8. G. Delmas. J. Polymer Sci. Polym. Phys. Ed., **31**, 2011 (1993).

9. H. Phuong-Nguyen and G. Delmas. Macromolecules, **25**, 408 (1992).

10. H. Phuong-Nguyen and G. Delmas. Macromolecules, **25**, 414 (1992).

11. H. Phuong-Nguyen, G. Charlet and G. Delmas. J. Therm. Anal., **46**, 809 (1996).

12. H. Phuong-Nguyen and G. Delmas. Collect. Czech. Chem. Commun., **60**, 1905 (1995).

13. F. G. Morin, G. Delmas, D.F. R. Gilson. Macromolecules, **28**, 3248 (1995).

14. P. Bernazzani and G. Delmas. J. Therm. Anal., **49**, 449 (1997).

15. X. Zhang, H. Phuong-Nguyen, P. Bernazzani, I. Lapes,and G. Delmas. Can. J. Chem., **75**, 1354 (1997).

16. P. Bernazzani. M. Sc. Thesis, University of Quebec in Montreal (1995).

17. A. Haine. M. Sc. Thesis, University of Quebec in Montreal (1996).

18. M. I. Bank and S. Krimm. J. Polym. Sci. Part A: **27**, 1809 (1969).

19. S. Krimm. Adv. Polym. Sci. **2**, 51 (1960).

20. K. Yoshikaru and S. Krimm. J. Macromol. Sci., Part B: **4** , 461 (1970).

21. M. Maroncelli, S. P. Qi, H. L. Strauss and R. G. Snyder. J. Am. Chem. Soc. **104**, 6237 (1982).

22. T. Okada and L. Mandelkern. J. Polym. Sci. Part A: **25,** 239 (1967).

23. A. R. Wedgewood and J. C. Seferis. IUPAC publication. *Edited by*. J. C. Seferis and P. S. Theocaris. 1983.

24. E. Agosti, G. Zerbi and I. Ward. Polymer, **34**, 4219 (1993).

25. G. Zerbi, G. Gallino, N. del Fanti and L. Baini. Polymer, **30**, 2324 (1989).

26. P. C. Painter, J. Havens, W. W. Hart and J. L. Koenig. J. Polym. Sci. Polym. Phys. Ed. 1237 (1977).

27. H. W. Siesler. Infrared Phys. **24**, 239, (1984).

28. T. Bohossian and G. Delmas. J. Appl. Polym. Sci. **46**, 411 (1992).

29. E. W. Fischer, H. Giddar and G. F. Schmidt. J. Polym. Sci. Part B: **5**, 619 (1967).

30. R. G. Snyder, J. R. Scherer, D. H. Reneker and J. P. Colson. Polymer, **23**, 1286 (1982).

31. D. A. Blackadder, and G. J. Poidevin. Polymer, **13**, 584 (1973).

32. A. Marigo, R. Zannetti and F. Milani. Eur. Polym. J., **33**, 595 (1997)

33. A. Marigo, G. Cingano, C. Marega, R. Zannetti, G. Ferrara, G. Paganetto. Macromol. Chem. Phys. **196,** 2537 (1995).

34. B. Wunderlich. Thermal Analysis, Academic Press, Toronto, 1990.

CHAPITRE 4

PHASE-CHANGE IN AMYLOSE-WATER MIXTURES AS SEEN BY FTIR

Biopolymers, accepté avec corrections

P. Bernazzani[1], C. Chapados[2] and G. Delmas[1]*

[1]Département de Chimie-Biochimie, Université du Québec à Montréal, C. P. 8888 succ. Centre-Ville, H3C 3P8, Montreal, Canada. [2]Département de Chimie-Biologie, Université du Québec à Trois-Rivières, G9A 5H7, Trois-Rivières, Canada.

ABSTRACT

The phase content of amylose-water mixtures (0.7 / 0.3 W/W) has been analyzed by transmission FTIR spectroscopy in the 1175-950 cm^{-1} region. Spectra are obtained under three different conditions: i) as a function of temperature (T) from 25 to 97°C, ii) at room temperature (RT), after slow cycles of T, and iii) at RT after quenching. Tmax, the maximum temperature in the cycle, ranges from 50 to 120°C. The quality of the seven-band spectra allows for an unambiguous determination of each band area. Unexpectedly, slow cooling after different Tmax brings about wide changes in the spectra while quenching does not. Two phase-changes are found: one at 70°C and the other above 105°C. They are associated respectively with the glass transition, Tg, of amylose-water mixtures and with the dissolution temperature of amylose in water. The spectra have two distinct regions, the low wavenumber region (1078-950 cm^{-1}) and the high wavenumber region (1175-1078 cm^{-1}). A distinct gain in the 1175-1078 cm^{-1} region at the expense of the 1078-950 cm^{-1} region when

Tmax increases is interpreted as a change from strained to unstrained environments. In light of the ^{13}C NMR evaluation of the change of molecular order with T, the observed changes of the IR spectra correspond to a transformation of a network of double helices into freer chains, possibly single helices. The present in-depth analysis of equilibrium or near equilibrium states by FTIR can serve to understand, through in-situ spectra, molecular mechanisms during the gelation / crystallization of amylose and other gel-forming polymers.

Keywords: Amylose, FTIR, phase-change, strain, glass transition, network dissolution.

INTRODUCTION

Starch is a polysaccharide containing both 1-4 α-D glucan links and side chains linked to the 6^{th} carbon. The physico-chemical properties of starch, an important storage material for higher plants have been extensively studied as well as those of amylose, a linear component of starch. Both have long-range order measurable by electron and X-ray diffraction[1, 2, 3, 4] but also short-range order followed by ^{13}C NMR[5, 6], IR[7] and slow calorimetry.[8] The presence of the single chain helices and double-chain helices in the solid has been established by X-ray diffraction and ^{13}C NMR.[9-11b] Single helices form a complex with small molecules (alcohol, organic solvents, iodine, fatty acids) and an ordered solid which yields a specific diffraction pattern (V-type). Molecular modeling has been used to understand the solvent-polymer organization of the complexes.[12] Amylose samples such as the material used in the present work can be prepared without long-range order.

Thermal analysis of semi-crystalline polymers

Bulk polymer

Phase-changes in semi-crystalline polymers have been observed in DSC traces obtained using rapid T-ramps. They show at low temperature (the glass transition temperature, Tg) a

change of Cp attributed to the increase of mobility of the amorphous phase and at higher T, an endotherm associated with the fusion of long-range order. This DSC technique is unable to detect short-range order at least of the type which is part of a network.[13] In consequence, short-range order has been largely ignored in the analysis of semi-crystalline polymers. However, several authors have reported evidence of partial melting and inhomogeneity in the melt suggesting that it contains at least two phases. Others have observed phase-changes in the melt[14] using different techniques including IR spectroscopy.[15] For instance, it was recently observed that the short-range order in polyolefins could be melted if the rise of temperature was made very slowly.[8, 16-18] However, thermal analysis of dry starch does not reveal phase-changes because the material is too cohesive to be transformed by heat before it decomposes.

Solutions

Dissolution traces have been obtained, though infrequently, for semi-crystalline polymers. They give information similar to melting traces on the sample's crystallinity but also some details of polymer-solvent interactions. The glass temperature is usually not observed because it is lowered by the solvent and is much below Td, the dissolution temperature of the crystals. The use of a slow T-ramp is also an effective method to dissolve the short-range order.[17]

Thermal analysis of amylose-water mixtures

Calorimetry has been used extensively for analyzing phase-changes in starch-water and amylose-water mixtures.[19-22] Crystalline and amorphous amylose in presence of water behave as does a crystalline or an amorphous synthetic polymer in a T-ramp. A dissolution endotherm (ΔH = 2-20 J/g) at Td, spread between about 55-75°C, is observed for the

crystalline samples and is absent for the amorphous material. However, amylose is different from semi-crystalline polymers because above Td the polymer is not completely in solution. The suspensions become transparent and relatively homogeneous only at higher temperature (110-160°C).[11a] The heat associated with this phase–change cannot be recorded in the DSC ramp. These characteristics suggest that starch and amylose contain a cohesive network whose short-range order is stable in the presence of water at elevated temperatures well above the disappearance of long-range order at Td. Using slow calorimetry, the dissolution of the network has been recorded on samples without long-range order.[8] Integration of the endotherm of dissolution of amorphous amylose between its limits (70 – 130°C) leads to an enthalpy of 60 J/g measurable only in a very low T-ramp (1-6 K/hour). Order in the amorphous phase of starch has been proposed to interpret the chemical shift range observed in the material.[11b]

Glass transition in amylose-water mixtures

Another difference between amylose-water mixtures and polyolefin-solvent mixtures rests in the position of Tg compared to Td. When measurements of Cp are made isothermally, in dilute solution, Tg is found to occur at about the same temperature as Td[22] instead of being lower as in polyolefin solutions. When measurements of Cp are made in a T-ramp, in more concentrated solutions, the expected change of Cp is often ambiguous or not observed at all.[19] On the other hand, Tg has been observed in starch-water mixtures as a sharp change in mechanical properties. This unusual behavior of starch and amylose comes from the fact that the phases are interdependent due to the strong cohesive forces between the glucan residues. In a T-ramp the endotherm of dissolution overlaps the change in Cp and obscures it.

The non-equilibrium character of the phase-changes observed by DSC has been recognized

in many papers. Investigation in equilibrium conditions, of properties likely to change at Tg, can bring a valuable contribution to the understanding of phase-changes in amylose-water mixtures such as those found in gelation and retrogradation processes. An investigation by FTIR techniques, seems appropriate because vibrations are sensitive to the environment at short distance. The aim of this paper is to trace the phase-change of amylose-water mixtures by using FTIR.

IR spectra of semi-crystalline polymers

FTIR spectra have been used mainly to identify chemical groups. The effect of the environment on the vibrations has dealt mainly with hydrogen bonding and the crystalline environment. In films, fibers or surfaces, IR spectroscopy has been used to follow orientation or deformation.[23]

The finding of a clear tracer for the orthorhombic crystal in polyethylene (PE)[24] and in-depth work on samples of different crystallinity[25] still has not made IR a standard technique for crystallinity evaluation. Two reasons may reverse this situation: the first is technical and associated with the improved performance of recent FTIR equipment combined with the use of spectral simulations. The second is the recent acceptance that the value of crystallinity obtained by IR has no reason to be identical to that found by X-ray diffraction. The IR crystallinity value is higher than that found by other techniques since it includes short-range crystals not accounted for by other measurements.[26] Furthermore, the simple two-phase model of a semi-crystalline polymers is no longer used exclusively for the correlation of structure properties. Analysis of PE with different histories by ^{13}C NMR[27] and Raman[28] where a three or even four-phase model is proposed to interpret the data, established a solid base for a comparative evaluation of non-crystalline order by IR.

IR spectra of carbohydrates

Structural informations have been obtained on native or treated cellulose from the well resolved IR spectra of samples with high crystallinity. The regions of the hydrogen bonds and of the CH and CH_2 stretching vibrations are sensitive to the cellulose morphology (either native or with a different crystalline modification).[29-32] Methylation of cellulose on the (C2, C3 or C6) carbons makes it possible to distinguish between intra and inter-molecular hydrogen bonding[33] in the 3500 cm^{-1} region. On the other hand, polysaccharides of different morphologies and also α-D-glucose, exhibit similar spectra in the 1175-950 cm^{-1} region.[34-36] This observation suggests that, in view of the relatively large size and cyclic structure of the glucose ring, most of the vibrational modes present in this region for amylose, can be assigned to vibrations occurring in the individual residue with little effect from the skeletal chains. Acknowledging this, we thought it worthwhile however, to investigate systematically how the concentration of the specific bands could change with the environment as defined by the sample history. Thermal history is used in the present work as an alternative to the strategy applied in a recent work where different spectra are obtained by analyzing mixtures of amorphous and crystalline amylose.[7]

Preparation of samples of different phase content

Semi-crystalline polyolefin samples of high crystallinity are prepared by cooling slowly a dilute solution. Samples of low crystallinity or gels are usually obtained by quenching a sample from the melt or from solution. The same strategy has been used here as described in the experimental section; amylose-water mixtures are either slowly cooled or quenched from a given temperature, Tmax, and then analyzed at RT. Slowly crystallized samples give better

defined IR or Raman spectra. The novelty here is to assume that preparation of equilibrium samples can also improve the resolution of bands associated with non-crystalline phases.

EXPERIMENTAL

Sample

Potato-starch amylose has been purchased from Sigma (St. Louis, Mo, USA). The powder was cold washed in ethanol to eliminate the fatty acid residues and left for at least 12 hours at room temperature in a vacuum dessicator containing P_2O_5. X-ray spectra of non-treated amylose-water mixtures revealed their almost fully amorphous nature.

FTIR

A Bomem MB-series spectrometer was used in transmission mode at a resolution of 1 cm^{-1} with 50 scans. Due to large water absorption elsewhere, the region of the CO and CC stretching vibrations (1300-800 cm^{-1}) was the only one investigated. The intensities are given in absorbance unit (a.u.).

For measurements between RT and 97°C (f(T) treatment), a custom-made Teflon/Aluminum oven, controlled by a temperature controller (Setaram, France) was used. Thermal equilibrium in the sample was assured by a low heating rate (3 K/hour). Spectra were taken every hour with 25 scans. A background was performed for each temperature to take into account the effect of thermal radiation. Using a Harrick polarizer, it was verified that the band intensities did not depend on the polarization of the incident light.

PREPARATION OF THE SAMPLES

Water was added to the dried amylose to have a 0.7 amylose fraction (W/W). The mixture was then thoroughly stirred using first a glass rod then a magnetic stirrer until a paste was formed.

Room temperature and f(T) measurements

A quantity of the paste was spread evenly between IR plates and the spectra taken at different temperatures ranging from RT to 97°C. The layer of the amylose / water mixture was 5-15 μm thick. The baseline intensity which was subtracted was smaller than 0.2 a.u. Degradation of the spectra due to the deterioration of the IR plates by water was found to be negligible.

Thermally treated samples: the f(Tmax, Crys) and f(Tmax, Q) treatments

The amylose paste was placed in a glass tube sealed under nitrogen and heated to Tmax, using a heating rate of 3 K/h, with 50 < Tmax < 120°C. The sample was maintained 10 h at this temperature and then cooled either slowly (3 K/h) or quenched to RT. In these two treatments, named the f(Tmax, Crys) and f(Tmax, Q), spectra are taken at RT.

ANALYSIS OF THE IR SPECTRA

The quantitative analysis of the effect of the treatment is not ambiguous in the present mixtures. However, it was thought useful to analyze the spectra by several methods which could be applied to the case of spectra with more overlapping bands. Of the three analysis described below, only the third one entails spectral simulations.

First analysis:

In the first analysis, the effect of the treatment on the left and right regions of the spectra is measured. The integrated intensities between 1175 and 1078 cm^{-1} and between 1078 and 950 cm^{-1} are compared. As the 1078 cm^{-1} band is unchanged by the treatments giving equilibrium mixtures, there is no ambiguity in dividing it by a vertical line to make the integration.

Second analysis:

A quantitative measurement of the phase content can be obtained by the fractional

maximum intensity of a given band. This is calculated by measuring the maximum intensity, A_i, for each band in the 1175-950 cm^{-1} region:

$$\text{Fractional maximum intensity } (\bar{\nu}_i) = \left(\frac{A_i (\bar{\nu}_i)}{\sum A_i (\bar{\nu}_i)} \right) \quad (1)$$

Third analysis

A quantitative measurement of the phase content can also be obtained after spectral simulation which gives the integrated intensity or area of each band:

$$\text{Fractional integrated intensity } (\bar{\nu}_i) = \left(\frac{\text{Integrated intensity } (\bar{\nu}_i)}{\sum \text{Integrated intensity } (\bar{\nu}_i)} \right) \quad (2)$$

In the figures below, the data are all called fractions independently of whether they are calculated from eqs. (1) or (2), the term second or third analysis being added to differentiate the mode of calculation. As will be seen, the second and third analysis give about the same results for equilibrium mixtures.

Spectral simulations

Fourier self deconvolution and second derivative traces have been used to find the peaks in spectra of materials such as polysaccharides[38, 39] or polyolefins.[37] In the actual spectra, most of the maxima could be observed visually. However, the second derivative was useful in some treatments where a band was very low and also in the 1175-1040 cm^{-1} region whose band position is sensitive to the treatment. The use of seven peaks was found to best fit the original spectra for equilibrium mixtures. For the quenched samples, decomposition used nine bands, but two pairs of bands were added together to calculate the fraction with seven bands.

Analysis of the well resolved peak observed at 1078 cm^{-1}, showed that it had a value of the

full width at half height (FWHH) equal to 18±3 cm^{-1} as well as a Gaussian shape. It was found that the Gaussian shape was satisfactory for the other bands in the region. However, the FWHH for the bands 1153, 1045, 1022 and 999 cm^{-1} was found to be larger (30 cm^{-1}) and up to 40 cm^{-1}, for the bands in the 1140-1080 cm^{-1} region. The FWHHs were found unchanged by the treatment.

In the simulations, we aimed at having the bands situated always at the same frequency for the different treatments which, on the other hand, do have an influence on the fraction of each band. This was quite possible for the 1153, 1078, 1045, 1022 and 999 cm^{-1} bands. In the non-equilibrium mixtures, the band frequencies could be shifted by 3-4 cm^{-1} in the treatment sensitive region (1140-1080 cm^{-1}).

To verify that there were no ring opening during the long T treatment, the band fractions found in amylose and in the α-D and β-D-glucose spectra are compared in table 3 of the appendix. The data for glucose have been obtained from the literature.[34-36] Looking at the table permits to conclude that the high T treatment does not lead to a mutarotation-like transformation of the amylose segments similar to that which occurs spontaneously in glucose solutions and that hydrolysis does not occur to form glucose.

RESULTS

In the present work, we used the spectra of amylose-water mixtures to establish the phase composition of amylose. The bands in the region 1200 to 950 cm-1 are assigned to C-C or C-O stretching vibrations. The parameters which characterize these vibrations are many, namely the vibrating group's place in a single or a double helix, or its vicinity to an intra- or intermolecular hydrogen bond, which neighbor the group has in the repeating unit, the place of the chain to which it belongs in the material organization (crystalline, network or

amorphous phases) and the internal strain to which the chains near the bond are submitted.

Equilibrium and non-equilibrium states

In order to reduce the number of environments and consequently of bands, we have aimed at keeping the sample in the most thermodynamically stable states for a given thermal treatment. By changing only the value of Tmax while retaining the same slow cooling ramp, it was hoped that the samples would all be in or near an equilibrium state. If so, one would expect that the spectra of the samples with different values of Tmax should have bands at the same frequency but with a different maximum intensity. On the other hand, when the sample is quenched from a high temperature to RT, the material is *in a non-equilibrium state* where more molecular states exist and overlap in the spectra. Non–equilibrium states also occur in mixtures for which the time of contact between water and amylose is insufficient. Some regions of the spectrum are more sensitive than others to the rate of cooling. One of these is the 1078 cm^{-1} band. In treated samples, this band is stable and has a good resolution while in non-treated samples and in quenched samples, it is split into several components (see Figs 13a, b). The term conformation will be used later in the text as an alternative to environment associated with a vibration. A conformation slow to form means that the environment does not reach its equilibrium value rapidly.

Reference band

Fig.1 is a plot of the maximum intensity at 1078 cm^{-1} versus the integrated intensity of the region (1175-950 cm^{-1}). There are five points for the different values of Tmax on different samples of different thickness and a cloud of points for the f(T) measurements made on the same sample. The quenched samples are not plotted on the graph due to the lack of resolution of the 1078 cm^{-1} band. This figure shows that a modest change of temperature (40-97°C) has

no large effect on the overall integrated intensity. It indicates also that the treatment (50°C < Tmax < 120°C) has either the same effect on the intensity of the 1078 cm^{-1} band as it has on all the bands or no effect at all. As will be discussed below, temperature or treatment changes have the effect of redistributing the intensity amongst the different peaks in the 1175–950 cm^{-1} region. The maximum intensity of the 1078 cm^{-1} band is used to normalize the spectra of treated samples. It is also used for the non-equilibrium samples but with less accuracy. The band at 1078 cm^{-1}, being insensitive to the treatments, is not commented upon.

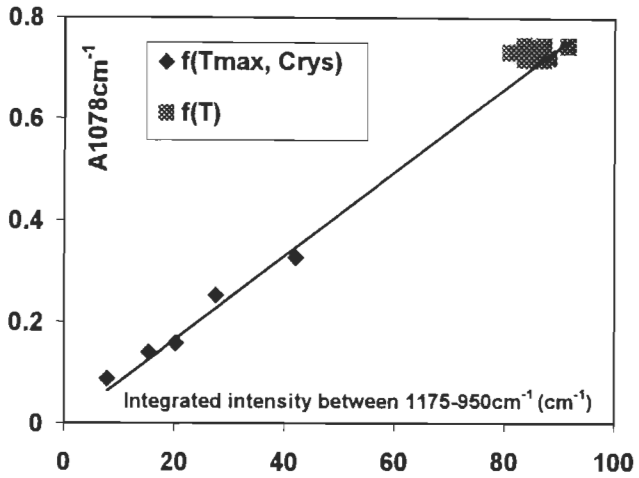

Figure 1 **Maximum intensity of the 1078 cm^{-1} band versus the integrated intensity (1175-950 cm^{-1}) for the two equilibrium treatments f(T) (squares) and f(Tmax, Crys) (lozenges) for amylose-water mixtures (0.7:0.3).**

Typical spectra for the different treatments

The results are presented in the following order f(T), f(Tmax, Crys), f(Tmax, Q). Two IR spectra taken as a function of T are given in Figs.2a, b for the lowest (T = 50°C) and highest (T = 97°C) temperatures measured. In Fig.2c, a few typical spectra taken between 50 and 97°C as f(T) have been overlapped. The spectra clearly show that when the temperature is raised, the intensity in the right-hand region of the spectra decreases at the expenses of the left-hand region, a change seen on either the maximum or the integrated intensity.

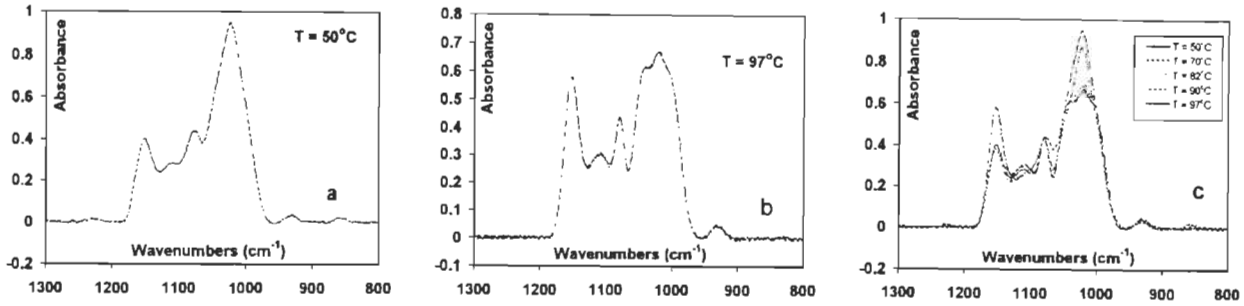

Figure 2 Spectra obtained in a T-ramp (v = 6K/h) of amylose-water mixture (0.7:0.3 W/W). 2a, at T = 50°C and 2b T = 97°C. 2c shows an overlaid of five spectra for T = 50, 70, 82, 90 and 97°C.

Fig.3d, the spectra for the five different values of Tmax are given. They have been normalized to a 0.1 a.u. for the 1078 cm^{-1} band. One sees that the high T treatment followed by slow cooling diminishes the massif at the right-hand region of the spectra (around 1022 cm^{-1}) and increases that at the left-hand (around 1153 cm^{-1}).

Observation of Fig.2a and 3a illustrates the effect of slow cooling from Tmax = 50°C: the slow cooling has reduced the 1153 cm^{-1} band drastically in Fig.3a compared to Fig.2a and increased the 1022 cm^{-1} band. Note that only the spectra in Fig. 3d have been normalized.

In Figs.3 a, b and c three typical spectra for Tmax = 50°C, 95°C and 105°C are shown.

The effect of quenching is demonstrated in Fig.4a, b, where typical spectra of mixtures after quenching from two values of Tmax are presented. The effect on the spectra of the time of contact between amylose and water is shown in Fig.5a, b. The 1078 cm^{-1} band is better defined in Fig.5b where the stirring time of amylose and water is longer (4h instead of 1h).

ANALYSIS OF THE SPECTRA

First analysis:

Effect of the treatment on the left and right regions of the spectra

Fig6a, b and c show the variation of the left and right regions of the spectra as a function of T for the f(T) and f(Tmax, Crys) and f(Tmax, Q) treatments. One sees a phase change at 70°C in

Fig.6a and another on Fig.6b which could be anywhere between the points for Tmax = 70°C and Tmax = 95°C. The line has been drawn with the phase change at 70°C taking into account the results in the T-ramp (Fig.6a). Between 105 and 125°C an abrupt change is noticeable in the left and right areas in Fig.6b. In Fig.6c, the areas of the left and right regions of the spectra plotted against Tmax for the quenched samples show that the treatment has no a sizeable effects on them.

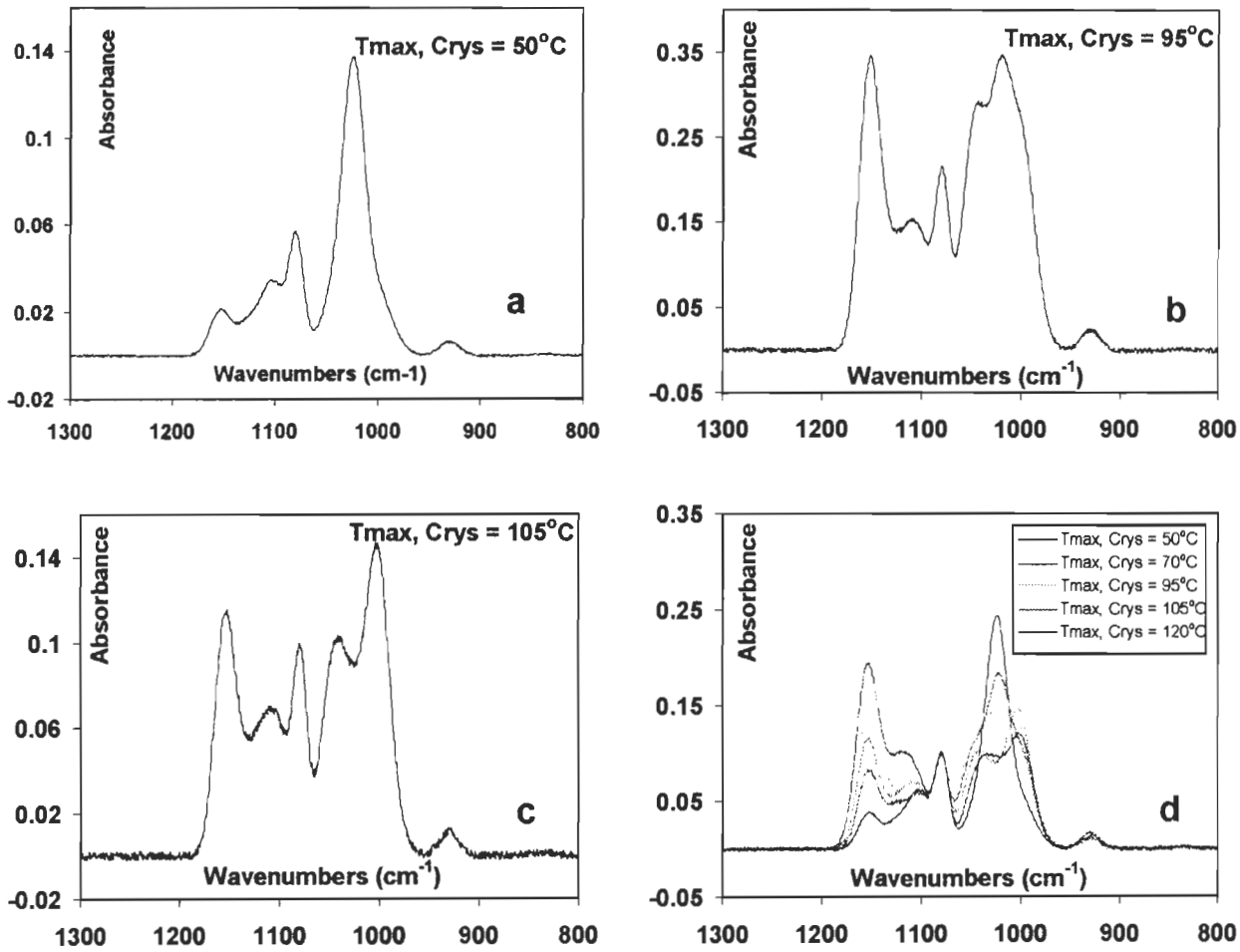

Figure 3. Spectra at RT of amylose-water mixtures (70/30 W/W), after the f(Tmax, Crys) treatment. a, b and c represent three spectra of the amylose-water mixture treated respectively at Tmax = 50, 95 and 105°C. d is a cumulative figure showing all the treated amylose spectra overlapped. They have been normalized by the intensity at 1078 cm^{-1}.

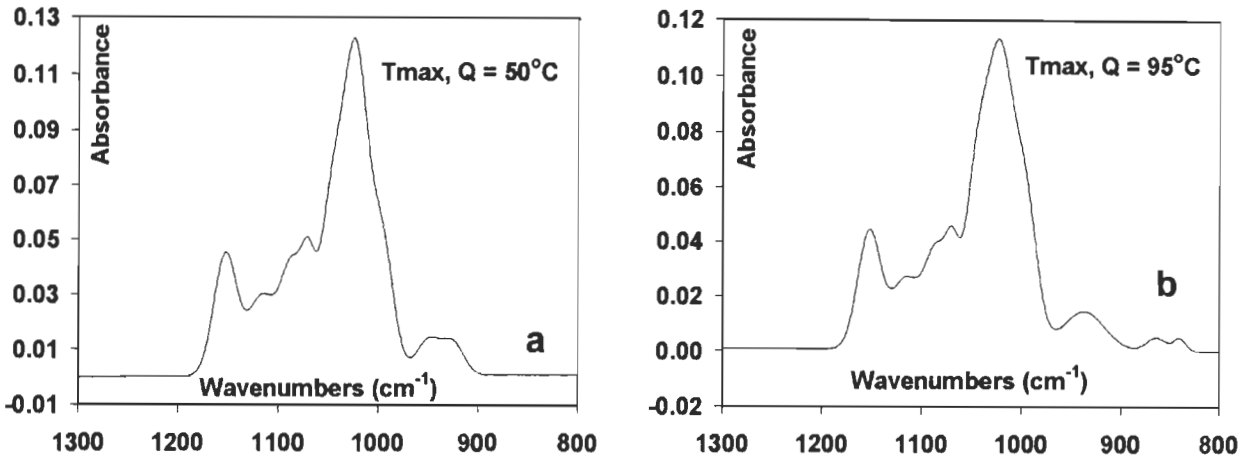

Figure 4 Spectra at RT of amylose-water mixtures (0.7:0.3 W/W) after the f(Tmax, Q) treatment. These non-equilibrium spectra have not been normalized. 4a, b for Tmax = 50 and 95°C.

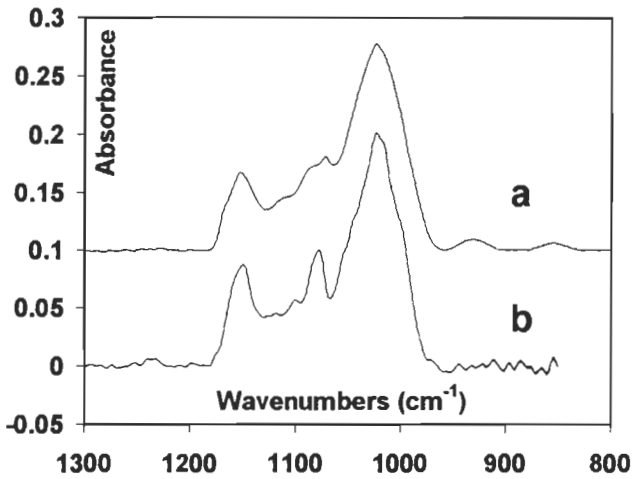

Figure 5 Spectra at RT of amylose-water mixtures (0.7:0.3 W/W) without treatment. Differences between the spectra A and B (intensities at 1078 cm^{-1} and 1165 cm^{-1}) are due to the time of homogenization in water at RT, where B was homogenized for 2h while A was not.

Second analysis:

Maximum intensity as a quantitative measurement of the phase content (eq.1)

In Figs. 7-10, the fraction of each band is represented as a function of treatment temperature. There is a certain amount of repetition in the presentation of the results with the following intent: Fig.7 a-e is an easy-to-visualize display to better see the changes due to the treatments of the five

bands using the maximum intensity. Figs 8-10 give the fraction of two bands, 1153 and 1022 cm^{-1}, using the maximum intensity of the original spectra.

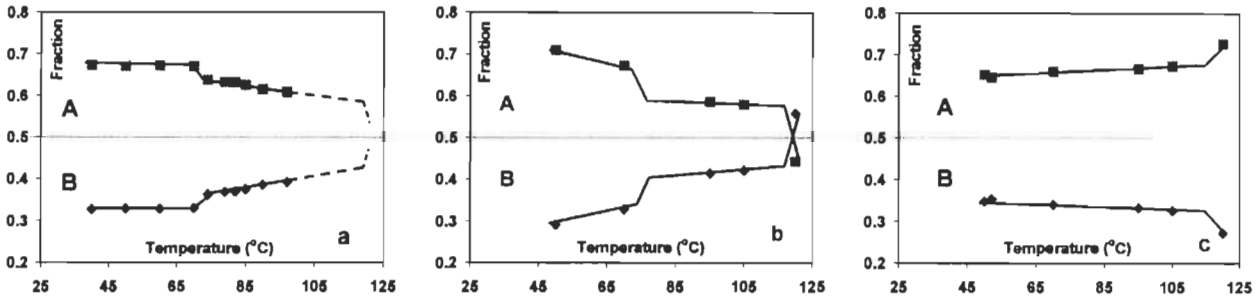

Figure 6 Variation of the fraction of the integrated intensity in the right (A) and left (B) regions of the spectra, noted as first analysis. The intensity at 1078 cm^{-1} separated the two regions. 6a, 6b, 6c correspond to the three treatments: f(T), f(Tmax, Crys) and f(Tmax, Q). The phase change at low T is seen in Figs. 6a and 6b, the phase change at high T is seen on Fig. 6b and to a smaller extent in 6c. The abscissa is T for 6a and Tmax for 6b and 6c.

Third analysis:

Fractional integrated intensity as a quantitative measurement of the phase content (eq.2)

Figs. 11-13 are examples of spectral simulation for the three treatments. Figs.14-16 uses the data of Figs. 11-13 for six bands and the three treatments. They show about the same changes observed using the second analysis.

DISCUSSION

Strain in long-chain morphology

Variations in band intensity with treatment will mainly be explained in terms of change in amount of strain in the sample. Strain can develop in different conditions, as the result of an external force or as a consequence of either hindered expansion in a T-ramp or of rapid polymerization/crystallization during synthesis. Strain is reduced when mobility is increased by solvent or temperature. But strain reduction is going to be durable only if the solvent/temperature treatment is followed by a slow return to the non-expanded state i.e. by slow cooling. It is

counter intuitive and contrary to the usual practice, that a slow cooling enables us to obtain a better image of the state of a polymer at high T than would quenching the sample. Therefore, slow crystallization constitutes a better tracer of events at Tmax than is quenching.

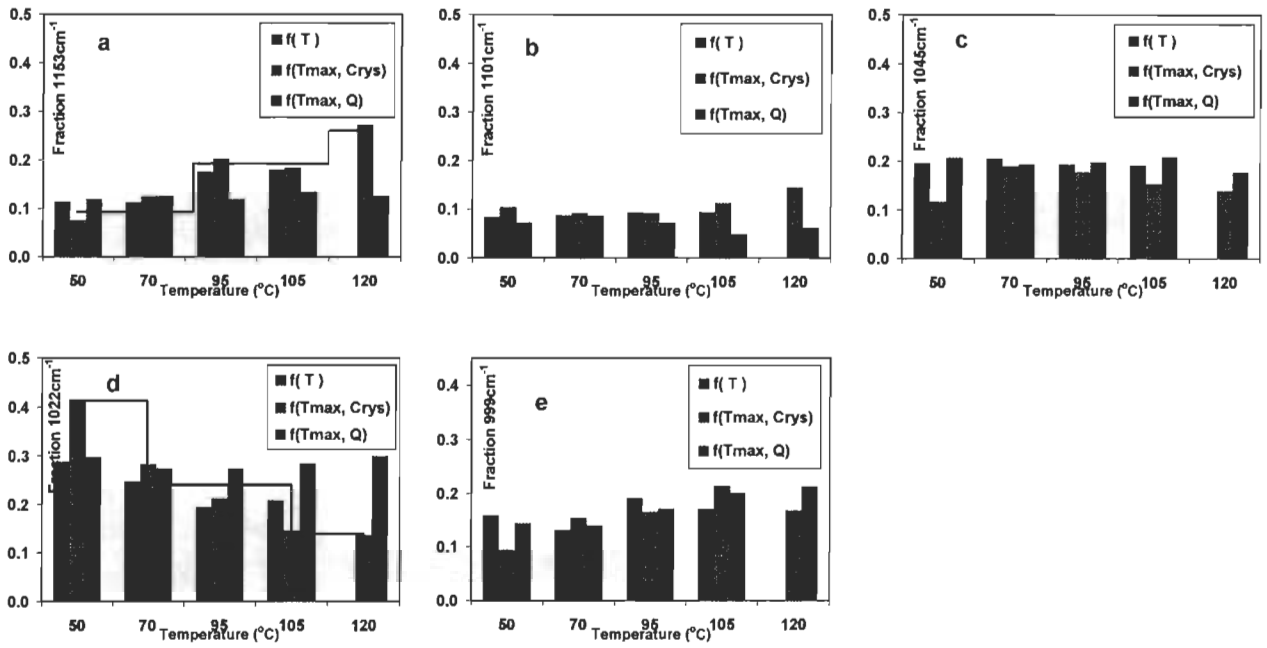

Figure 7 Variation with treatment of the fractional intensity of each band for the three treatments, noted as second analysis. Figs. 7a-e correspond respectively to the 1153, 1101, 1045, 1022 and 999 cm^{-1} bands. Larger changes are observed for the 1153 and 1022 cm^{-1} bands. The values in the f(T) treatment at 97°C has been placed as a data point at 105°C. The lines in Figs. 7a and 7d illustrate the phase changes for the f(Tmax, Crys) treatment.

Studies have investigated the effects on IR band positions of strain generated by an external force. Since deformation, such as uniaxial stretching, displaces the bands towards lower wavenumbers[23], one can expect that strain generated from other sources will have the same effect on the frequency shift.

In polyolefins, a source of these strain comes from chains entangled during polymerization/ rapid-crystallization. In amylose, entanglements, cooperative hydrogen bonds and segments of chains which belong in part to double and single chain helices contribute to the formation of strain. In consequence, it seems reasonable to link strain relaxation to a chain being released

from a knot or a double helix in order to become either a single helix or statistical coil. Liberation from entanglements promotes crystallization.

The IR characterization of the two crystalline organizations (B and V) of potato amylose will not be considered in detail because IR spectroscopy is not the best technique to investigate this long-range order.

The present discussion will focus on a reference band, then on the two regions of the spectra and finally on the different bands in the left and right region of the spectra.

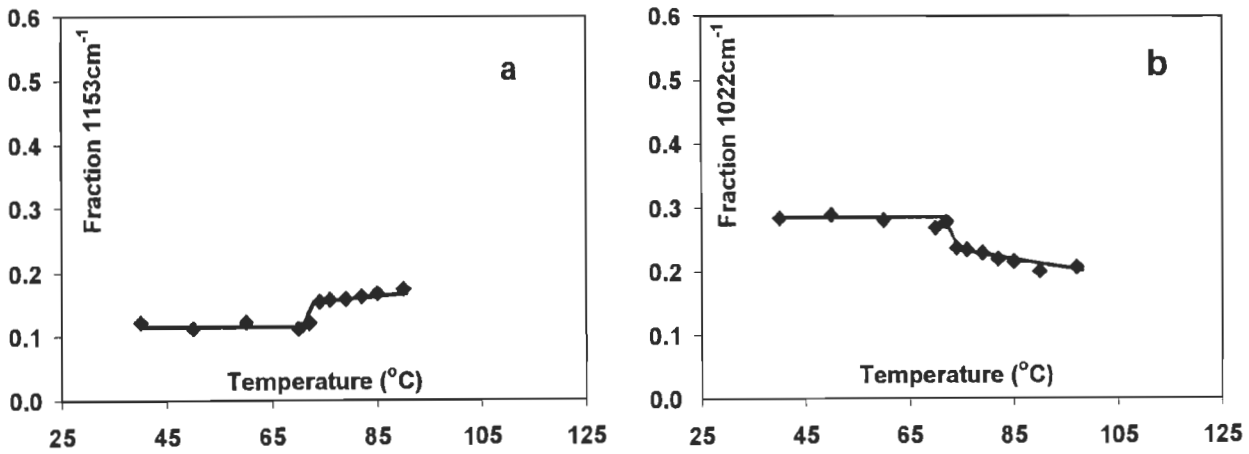

Figure 8 Phase change at low T noted as Second analysis. Fraction of the 1153 cm^{-1} (8a) and 1022 cm^{-1} (8b) bands as a function of T, in the f(T) treatment.

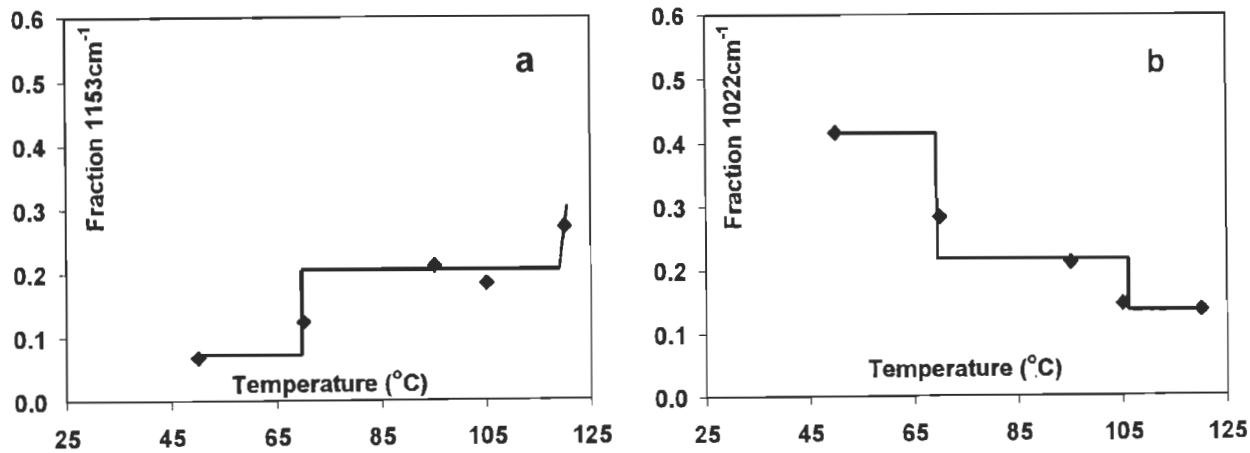

Figure 9 Fraction of the 1153 cm^{-1} (9a) and 1022 cm^{-1} (9b) bands as a function of Tmax (Tmax, Crys). Note the large value of the fraction of the 1022 cm^{-1} band after the treatment at 50°C. More values of Tmax would be needed to define the exact temperatures of the phase changes.

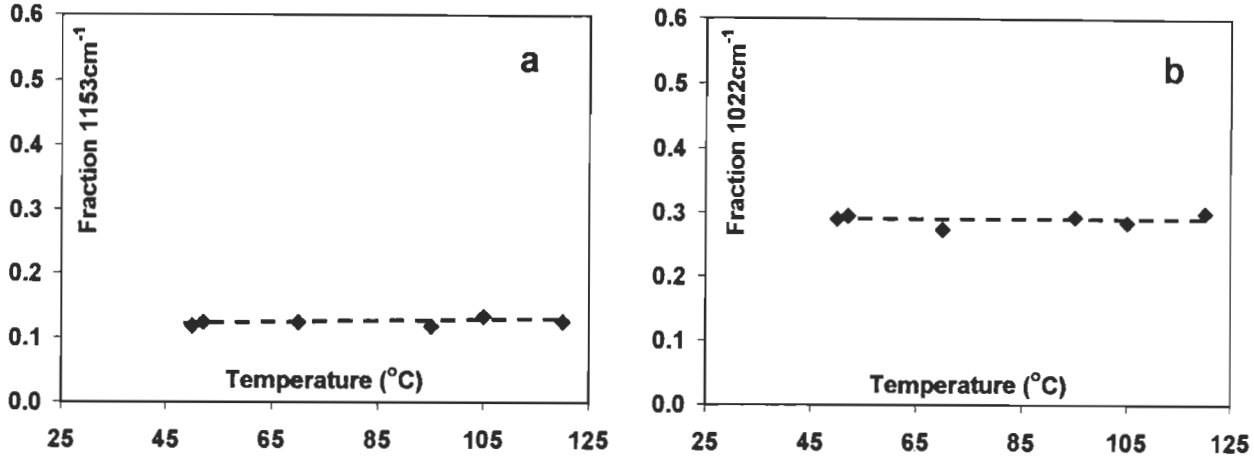

Figure 10 Phase change at low and high T noted as Second analysis are absent in the f(Tmax, Q) treatment. Fraction of the 1153 cm^{-1} (10a) and 1022 cm^{-1} (10b) bands as a function of Tmax.

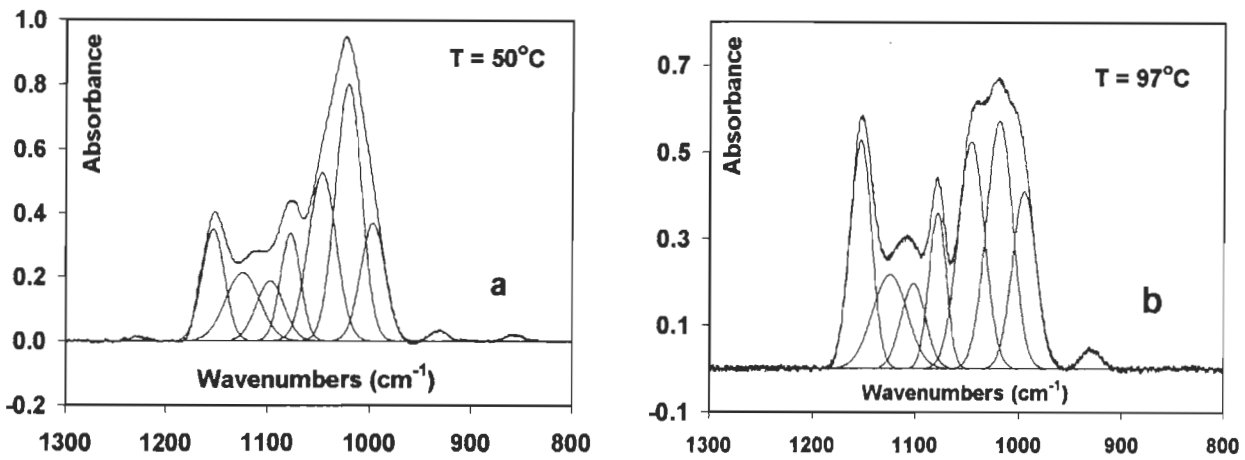

Figure 11 Spectra showing the seven bands after decomposition for the f(T) treatment noted as Third analysis. 11a, T = 50°C, 11b, T = 97°C.

Reference band

Fig.1 indicates that the 1078 cm^{-1} band is not affected by strain in samples in an equilibrium state. Since α-D-glucose and amylose have the same fraction of this band (0.09-0.10), one can speculate that this low fraction is associated with the C_1 carbon and hence is linked with the α bridge. On the other hand, β-D-glucose and cellulose[33] which have a β linkage have a large fraction of this band (see table 3 in the Appendix). However, this conformation may be slow to

form in water since it is not well defined in the quenched samples or in the non-treated spectra at RT (Fig. 5).

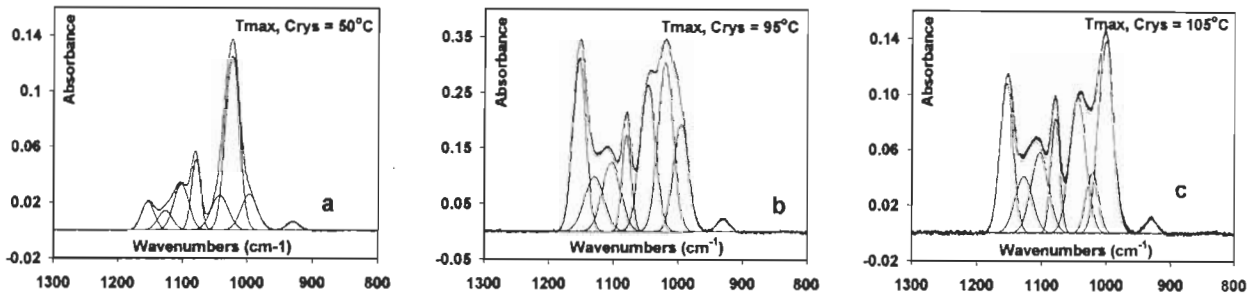

Figure 12 Spectra showing the seven bands after decomposition for the f(Tmax, Crys) treatment noted as Third analysis. 12a, Tmax = 50°C, 12b, Tmax = 95°C, 12c, Tmax = 105°C

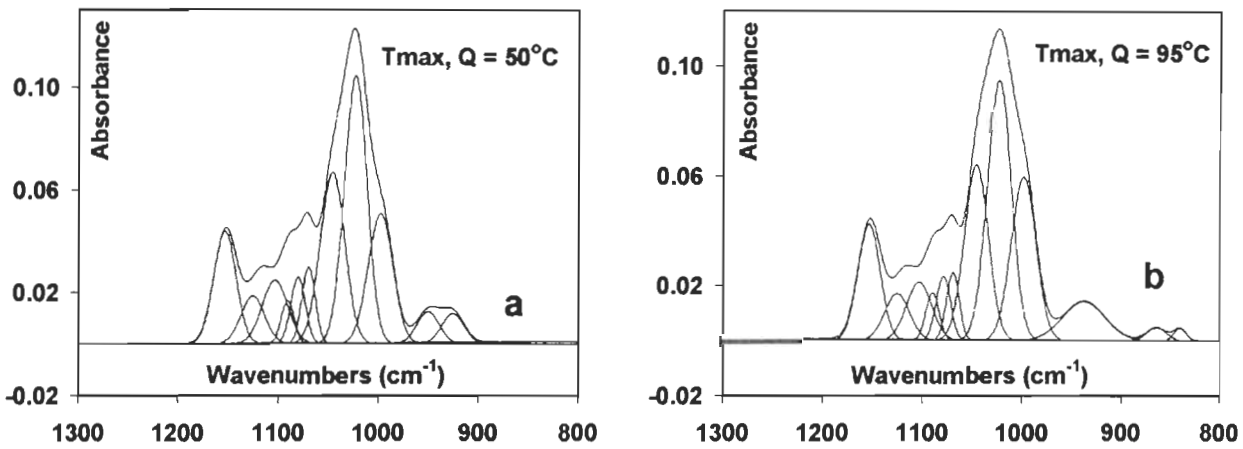

Figure 13 Spectra showing the seven bands after decomposition for the f(Tmax, Q) treatment noted as Third analysis. 13a, Tmax = 50°C, 13b, Tmax = 95°C. For these non-equilibrium treatments, two extra bands are necessary to fit the spectra in 1175-1050 cm^{-1} region.

Integrated intensity in the right and left regions

According to the first analysis (Fig. 6), reduction of the right region takes place when the temperature increases in the f(T) and f(Tmax, Crys) treatments. Since the tension is reduced by increasing T and by using high T treatments followed by slow cooling, it is reasonable to associate the right region to vibrations under tension or in a network phase and the left region to

relaxed vibrations. The shift in position (~ 100 cm^{-1}) due to the release of strain is larger for the C-O stretching vibrations than that found in polyolefins for the CH_2 rocking vibration (~10 cm^{-1}) due to the higher polarizability of the former. The lack of response of the quenched samples to Tmax (Fig. 6c) implies that strain is recovered easily on cooling in these concentrated mixtures. This result is consistent with the common practice to prepare gels i. e. network-rich samples by quenching.

Phase-changes at Tg and high T

The phase-changes can be seen on the individual bands (Fig. 8-10) or on the integrated intensity (Figs. 14-16). Tables 1 and 2 give the fraction of the different bands across the low and high T phase-changes. In these tables, some data are given for values of Tmax which do not correspond to an experiment data point. For these, the values of the fractions are interpolated from Figs. 14-16. The figures in bold character correspond to the bands most sensitive to the phase changes.

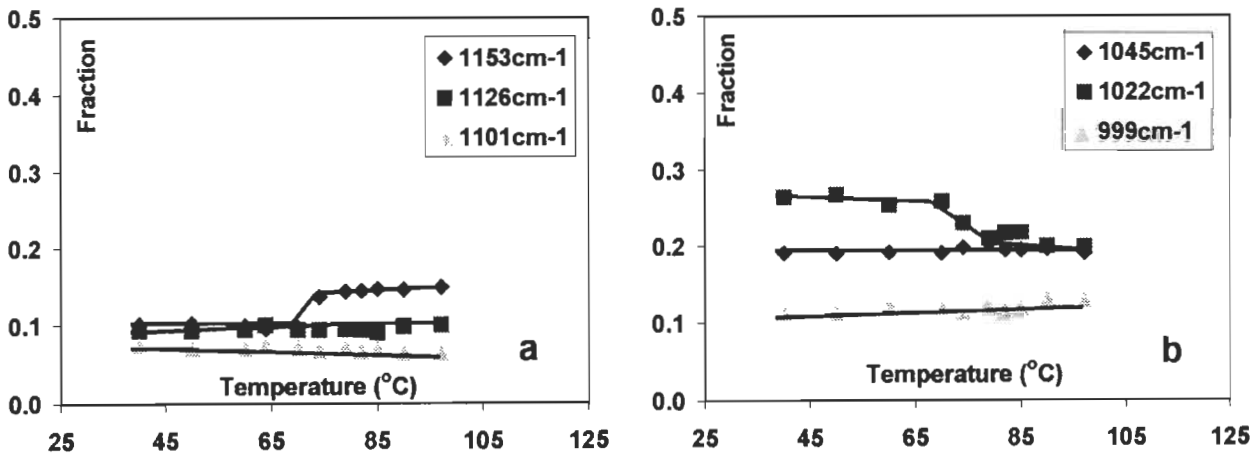

Figure 14 Phase-change at low T noted as Third analysis. Fraction of the 1153, 1126 and 1001 cm^{-1} bands (14a) and 1045, 1022 and 999 cm^{-1} bands (14b) in the f(T) treatment.

In non-crystalline amylose-water mixtures, the changes in the fractions of the 1153 and 1022 cm^{-1} bands, in the vicinity of 70°C, is linked with the passage through Tg. The increase in mobility of the chains at Tg suggests the following attribution: the band which diminishes most

(1022 cm^{-1}) corresponds to vibrations in an environment consisting of a rigid phase while the band which increases (1153 cm^{-1}) is associated with an environment consisting of a mobile phase. Then, among the strained vibrations, states in this environment which are associated with the 1022 cm^{-1} band are stable and easy to form. *We would like to qualify this band as the network band* without supposing that this is the only conformation present in the network.

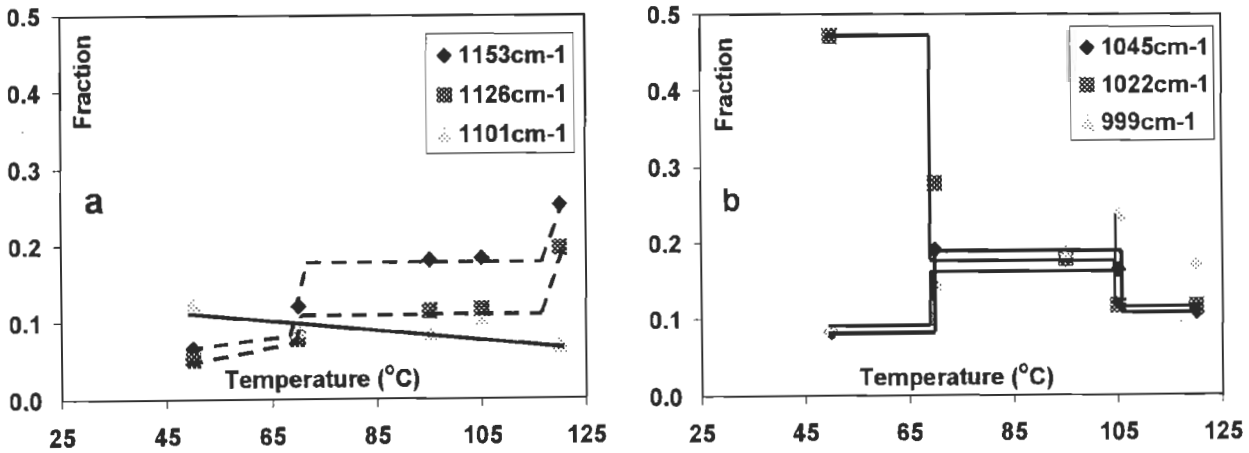

Figure 15 Phase-change at low and high T noted as Third analysis. Fraction of the 1153, 1126 and 1001 cm^{-1} bands (15a) and 1045, 1022 and 999 cm^{-1} bands (15b) in the f(Tmax, Crys) treatment. More values of Tmax would be needed to define the exact temperatures of the phase changes.

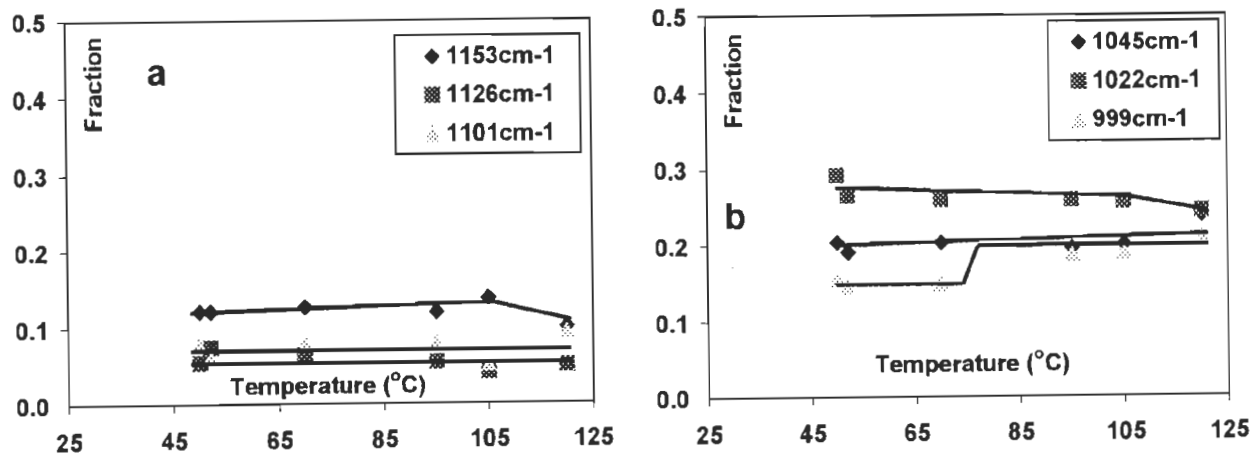

Figure 16 Phase-change at low and high T noted as Third analysis are absent for the f(Tmax, Q) treatment. Fraction of the 1153, 1126 and 1001 cm^{-1} bands (16a) and 1045, 1022 and 999 cm^{-1} bands (16b) as a function of Tmax.

It is noteworthy that a second-order phase change, hardly detectable by DSC as previously stated[19], is clearly observed in the IR spectra either in the T-ramp or after the f(Tmax, Crys) treatment.

The high T jump in the intensity of several bands observed in the f(Tmax, Crys) treatment is associated with further dissolution of amylose chains.

The slow calorimetry result on amylose/water mixtures mentioned earlier suggests that these two apparent phase-changes belong to the same molecular phenomena, a non first order transition interpreted as the dissolution of the network. The dissolution of the less strained short-range order takes place at Tg with a cooperative effect when mobility begins. At higher temperature, dissolution of the more strained regions occurs up to the temperature where the amylose-water mixture is clear. A continuous dissolution takes places between these two temperatures. In the IR analysis, at the higher temperatures, strain is reduced but not eliminated as can be observed on Fig. 6b where the fraction of the strained (or right) region is still 0.4 at 120°C. The fraction of the strained region is higher and almost constant (0.65-0.67) with the f(Tmax, Q) treatment. Dissolution must take place in that treatment during the slow T-ramp but the chains on quenching come back to the state they had before heating.

The different bands in the right and–left regions

Bands in the right or strained region

The partition of the intensity between the bands which is different at low and high Tmax points to the chain mobility and the slow crystallization as factors which determine this distribution.

Entangled mixtures with low mobility

Below Tg at 65°C, the two equilibrium treatments do not lead to the same partition of intensity. In the f(Tmax, Crys) treatment, the intensity is unequally distributed among the three bands

(0.09, 0.47, 0.09 as reported in the third row of Table 1) while it is more evenly distributed in the f(T) treatment (0.20, 0.26, 0.13). The fact that the composition of the quenched mixture (5^{th} row) is similar to that of the f(T) treatment points to an important step to increase to 0.47 the fraction of the 1022 cm^{-1} band, namely the slow crystallization.

To understand the growth of the "network band" during the slow crystallization at the expense of the 1045 and 999 cm^{-1} bands, it is useful to remember the increase of the strength of the hydrogen bonds when the temperature is lowered. The free energy of the system will be lowered more successfully at low T than at higher T as more bonds are formed due to the change in the enthalpy of the system. A morphology richer in short-range order, with many cohesive junctions, is going to have a lower free energy than another with less junctions and possibly even low amounts of long-range order. The short-range order which has grown in the 1022 cm^{-1} band during annealing/recrystallization is easily meltable at Tg as illustrated in Figs. 7d, 9b and 15b.

Table 1: Fraction of the seven bands of amylose-water mixture (0.7:0.3 W/W) at two temperatures As a function of treatment showing a phase change at Tg

T(measure)	Treatment	**1153**	1126	1101	1078	1045	**1022**	999
65°C	f(T)	**0.11**	0.10	0.09	0.11	0.20	**0.26**	0.13
85°C	f(T)	**0.16**	0.10	0.09	0.10	0.21	**0.21**	0.13
RT	f(Tmax=65°C)[a]	**0.09**	0.06	0.11	0.09	0.09	**0.47**	0.09
RT	f(Tmax=85°C)	**0.18**	0.11	0.09	0.08	0.19	**0.18**	0.17
RT	f(Tmax, Q=65°C)[a, b]	**0.12**	0.07	0.08	0.10	0.20	**0.28**	0.15
RT	f(Tmax, Q=85°C)[b]	**0.12**	0.06	0.08	0.08	0.20	**0.27**	0.19

[a] Tmax = 65 has not been done but as said in the text the values of the fractions of each band are read on fig. 15

[b] In the quenched samples, the 1126 and 1101cm^{-1} bands includes two bands

Less-entangled mixtures with higher mobility

Figure 15 shows that above the dissolution temperature at 120°C, the intensities of the 1045, 1022, and 999 cm^{-1} is small but about equally distributed amongst these three bands. The values

given in the 2nd and 4th rows of Table 2 for the f(Tmax, Crys) (0.11, 0.11, 0.18) and the f(Tmax, Q) (0.23, 0.24, 0.20) treatments show the efficiency of the f(Tmax, Crys) treatment in reducing the strained bands.

Mixtures in transition at T= 85–95°C

The intensity is about equally distributed amongst the three bands (1045, 1022, 999 cm^{-1}). The exact values (0.13-0.21) are given in the 2nd and 4th row of Table 1 for the f(T) and f(Tmax, Crys) treatments. The sample after quenching from Tmax = 85°C has a higher fraction of the 1022 cm^{-1} band (0.27 instead of 0.18).

Table 2: Fraction of the seven bands of amylose-water mixture (0.7:0.3 W/W) at two temperatures As a function of treatment showing a phase change at the dissolution[a]

	T(°C)	**1153**	1126	1101	1078	1045	**1022**	999
f(Tmax, Crys)	100	**0.18**	0.11	0.09	0.08	0.19	**0.18**	0.17
f(Tmax, Crys)	120	**0.25**	0.20	0.07	0.08	0.11	**0.11**	0.18
f(Tmax, Q)[b]	100	**0.12**	0.06	0.08	0.08	0.20	**0.27**	0.19
f(Tmax, Q)[b]	120	**0.10**	0.04	0.10	0.09	0.23	**0.24**	0.20

[a] Spectra taken at 25°C

[b] In the quenched samples, the 1126 and 1101 cm^{-1} bands include two bands each

However, slow crystallization in half disentangled samples increases the 999 cm^{-1} band. At the higher range of this region, such as 105°C, the 999 cm^{-1} band increases to its highest value 0.20 while the 1022 cm^{-1} band is reduced to 0.11 (Fig. 15b).

Bands in the left or non- strained region

When Tmax is low or in quenched samples, the intensity fractions are small (about 0.1) and equally divided between the three bands (1153, 1126, 1101 cm^{-1}). On the other hand, when tension is reduced, the 1153 cm^{-1} increases, followed by the 1126 cm^{-1} in the f(Tmax, Crys) treatment.

As a simplified account of the effect of slow crystallization, one can state the following: in

disentangled mixtures, the 1153 and 1126 cm^{-1} bands are increased, while in moderately disentangled mixtures, the 999 cm^{-1} and to a smaller extent the 1045 cm^{-1} band, are reinforced. In entangled mixtures (below Tg), the dominant environment is represented by the 1022 cm^{-1} band. As a consequence of the link between slow crystallization and long-range order and of the change in the IR spectra, one may conclude that if long-range order is present in the sample, it may be associated with the 999 cm^{-1} and the 1045 cm^{-1} bands and with the 1153 and 1126 cm^{-1} bands respectively in the strained and less strained regions. A comparative analysis of the X-ray patterns and of the IR spectra may show a difference between long-range order of the two types. However, as strain has various effects on the X-ray diffraction spectra (variations in both relative intensity and diffraction angle) distinction between the strained and non-strained crystals may be difficult.

Molecular order and short-range order

By comparing the effect of T on the ^{13}C NMR spectra and the DSC traces, several authors[6, 7] have been able to characterize an order in amylose-water mixtures, called molecular order. They found that molecular order is disrupted at about the same temperature (60-70°C) as long-range order. This result is independent of the starch concentration (up to c = 0.25 W/W) or of the crystallinity.[6] The loss of molecular order has been associated with the transformation of double helices into single helices.[12] In the IR spectra, changes in band intensities only occur for two peaks located at 1022 and 1153 cm^{-1} at $T \equiv 70°C$. These two bands could then be associated with double and single helices respectively. The single helices grow at Tg after being liberated from the network phase without necessarily involving crystalline order. The decrease of the 1020 cm^{-1} band parallels the increase of the 1153 cm^{-1} band. A clear correlation exists for these two bands (not reported here). The two other bands in the strained region (1045 and 999 cm^{-1}) are also

associated with double helices but possibly possess different packing. The better packing of the chain segments which correspond to the 1045 and 999 cm^{-1} bands is possibly the origin of their stability to heat which is better than that of the 1022 cm^{-1} band seen in the f(T) treatment for instance. The remaining bands in the less strained region (1126, 1101 cm^{-1}) correspond to single helices also in different packing morphologies. ^{13}C analysis of amylose mixtures in dilute solutions or in gels permit to distinguish rigid double helical junctions and mobile amorphous single chains.[10] The distinction corresponds to the present strained and relaxed regions.

Starch mixtures treated at high temperatures contain a fraction of amylase-resistant amylose whose content can be increased by repeated heating-cooling cycles. Comparison between the phase composition of amylase-resistant amylose and the present treated samples is relevant because the heating part of the treatment is similar between the two techniques of modification of amylose morphology[8]. The strained fraction in samples quenched from Tmax = 120°C is equal to 0.67 (table 2) by IR, a value which compares well with that found in enzyme resistant starch for ^{13}C NMR double helical order (0.70).[41] By slow cooling from Tmax = 120°C, the double helices or strained fraction is reduced to 0.40.

Long-range order and IR spectra

One expects few changes in the spectra when long-range order grows after a high Tmax and slow crystallization.[40] X-ray measurements have been performed on the f(Tmax, Crys) samples. They show an increase of the diffraction peaks corresponding to the B and V crystals when Tmax is raised. When the X-ray diagram reveals crystallinity, the concentration of one or of several IR bands increases. Quantitative measurement of each crystalline form seem hazardous since the two forms may have different specific diffraction due to their different packing. The data will be published later along with the slow calorimetry traces.

CONCLUSION

Thermal treatments are used to modify the phase content of amylose in water (0.7/0.3 W/W) while IR measurements in the 1175-950 cm^{-1} region follow the changes. The fractions of two of the seven bands present vary during a T-ramp (limited to 97°C) while the fractions of six bands are greatly altered by a treatment which involve slow cycles of temperature between RT and 120°C. Slow cooling is known to reduce entanglements and strain.

Interpretation of the spectra is made in terms of strain which shift the position of the IR bands. The strained region (three bands) is large in samples treated at low T or quenched while the relaxed region (three bands) increases in disentangled samples treated at high temperature and cooled slowly. A tracer of the gel or network phase is found in the 1022 cm^{-1} band. The fact that this band increases when the mixture is annealed below Tg and diminishes when it is heated, points to this assignment. Using the molecular information obtained by the change of ^{13}C NMR traces with temperature, the strained region is associated with double helices and the unstrained region with single helices.

The present work makes a bridge between information on amylose/water-mixtures found in the literature and our own in slow calorimetry. We could then trace an endotherm of dissolution of short-range or molecular order between 60 and 130°C. The presence of network order resistant to high T but meltable in some conditions explains the need to autoclave starch and amylose mixtures to obtain a homogeneous mixture. The fact that the order belongs to a network and is short-range explains the inability of DSC and X-ray measurements to detect it. In IR, the two phase-changes observed on samples treated at different values of Tmax correspond to the beginning and the end of the dissolution of the network.

It is important to have in mind that systems with little strain and few double helices are not

obtained after the usual treatments which one could call mild (in term of time rather than temperature). More radical treatments like those used in the present work to obtain relaxed non-entangled chains still leave a sizeable amount of the strained chains. The abrupt change observed in the parameters measured after a mild treatment, corresponds only to the beginning of chain disentanglements or changes in environments. To treat the data otherwise is not satisfactory for quantitative evaluation of the amylose phase content.[8] The IR spectra show that slow cooling from Tmax should be added to the usual strategy of quenching from Tmax to extract more information on the phase changes in amylose/water systems. Further work where the f(T) treatment would be pursued to higher T (120-130°C) and analysis of dilute or semi-dilute mixtures would permit to confirm or infirm some of the assumptions of the present work.

ACKNOWLEDGEMENTS

The financial support of the National Science and Engineering Research Council of Canada is gratefully acknowledged.

REFERENCES

(1) Sarko, A.; Zugenmaier, P. (1980) *Fiber Diffraction Methods*, Eds. French, A. D. Gardner, K. C., ACS Symposium series, 141, 459.

(2) Bader, H. G.; Goritz, D. (1994) *Starch*, 46, 229.

(3) Muller, J. J.; Germar, C.; Muller, E. V.; Vorwerg, W.; Damaschun, G. (1995) *Biopolymers*, 35, 271.

(4) Brisson, J.; Chanzy, H.; Winter, W. T. (1991) *Int. J. Biol. Macromol.*, 123, 31.

(5) Horii, F.; Yamamoto, H.; Hirai, A.; Kitamaru, R. (1987) *Carbohydrate Research*, 169, 29.

(6) Cooke, D.; Gidley, M. J. (1992) *Carbohydrate Res.*, 22, 105.

(7) Van Soest, J. J. G.; Tournois, H.; de Wit, D.; Vliegenthart, J. F. G. (1995) *Carbohydrate Research,* 279, 201.

(8) Le Lay, P.; Delmas, G. (1998) *Carbohydrate Polymers*, 37, 49.

(9) Veregin, P. P.; Fyfe, C. A.; Marchessault, R. H.; Taylor, M. G. (1984) *Macromolecules*, 19, 1030.

(10) Gidley, M. J. (1989) *Macromolecules*, 22, 351.

(11) Welsh, E. J.; Bailey, J.; Cahandarana, R.; Noris, W. E. (1992) *Progr. Nutr. Sci.*, 6, 45.

(11a) Gidley, M. J.; Bulpin, P. V. (1989) *Macromolecules*, 22, 34.

(11b) Gidley, M. J.; Bociek, S. M. (1985) *J. Am. Chem. Soc.*, 107, 7040.

(12) Godet, M. C.; Tran, V.; Delage, M. M.; Buleon, A. (1993) *Int. J. Biol. Macromol.*, 15, 11.

(13) A fast T-ramp has two effects which almost balance each other: it displaces the equilibrium towards the liquid (or solution phase) but also increases the strain on the crystals an effect which displaces the equilibrium towards the solid phase. The end of the dissolution endotherms does not means that there is no more order in the system but is a reflection of the

fact that there is no more meltable order in the conditions of the dissolution.

(14) Mitchell, G. R. (1987) Order in the amorphous state of polymers, Keinath, S. E.; Miller, R. L.; Rieke, J. K. Eds., Plenum Press, New York, 1.

(15) Bubeck R.A. Smith P.B.; Bales S.E., (1987) Order in the amorphous state of polymers, Keinath, S. E.; Miller, R. L.; Rieke, J. K. Eds., Plenum Press, New York, 347.

(16) Nguyen, P.; Delmas, G. (1992) *Macromolecules*, 25, 408.

(17) Nguyen, P.; Delmas, G. (1992) *Macromolecules*, 25, 414.

(18) Delmas, G. (1993) *J. Polym. Sci., Polym Phys Ed.*, 31, 2011.

(19) Biliaderis, C. B.; Page, C. M.; Maurice, T. J.; Juliano, B. O. (1986) *J. Agric. Food Chem.*, 34, 6.

(20) Krueger, B. R.; Knitson, C. A.; Inglett, G. E.; Walker, C. E. (1987) *J. Food science*, 52, 715.

(21) Billiaderis, C. G. (1991) Water relationship in Food, Levine, H.; Slade, L., Eds., Plenum Press, New York, 251.

(22) Jasra, R. V.; Ahluwalia, J. C. (1982) *J. Sol. Chem.*, 11, 325.

(23) Siesler, H.W. (1984) *Infrared Phys.*, 24, 239.

(24) Maroncelli, M.; Qi, S. P.; Strauss, H. L.; Schnyder, L. (1982) J. *Am. Chem. Soc.*, 104, 6237.

(25) Wedgewood, A. R.; Seferis, J. C., Ed. Seferis J. C.; Theocaris, P.S. (1983) IUPAC.

(26) Bernazzani, P.; Bich, V. T.; Nguyen, P.; Haine, A.; Chapados, C.; Dao, L. H.; Delmas, G. (1998) *Can. J. Chem.*, 76, 1674.

(27) Kuwabara, K.; Kaji, H.; Horii, F.; Bassett, D. C.; Olley, R. H. (1997) *Macromolecules*, 30, 7516.

(28) Matter, R.;.Still, W.; Strobl, G. (1993) *J. Polym. Sci. Phys. Ed.*, 31, 99.

(29) Higgins, H. G.; Steward, C. M.; Harrington, K. J. (1961) *J. Polym. Sci.*, 51, 59.

(30) Vasko, P. D.; Blackwell, J.; Koenig, J. L. (1972) *Carb. Res.*, 23, 407.

(31) Cael, J. J.; Koenig, J. L.; Balckwell, J. (1975) *Biopolymers*, 14, 1885.

(32) Liang, C. L.; Marchessault, R. H. (1959) *J. Polym. Sci.*, 39, 269.

(33) Kondo, T.; Sawatari, C. (1996) *Polymer*, *37*, 393.

(34) Cadet, F. (1999) *Talanta*, 48, 867.

(35) Kodad, H.; Mokhlisse, R.; Davin, E.; Mille, G. (1994) *Can. J. Appl. Spectros.*, 39, 107.

(36) Libnau, F. O.; Christy, A.; Kvalheim, O. M. (1994) *Vibrational Spectroscopy*, 7, 139.

(37) Chapados, C.; Trudel, M.; Miletic, J. (1994) *Chemometrics and Intelligent Laboratory*, 22, 209.

(38) Doublier, J. L.; Coté, I.; Llamas, G.; Charlet, G. (1992) *Progress in Colloid and Polymer Science*, 90, 1.

(39) Béliveau, J.. (1987) Séparation par traitement informatique des bandes infrarouges de la chlorophylle A en monocouche et en multicouche" Thèse de Maîtrise, *Université du Québec à Trois-Rivières,* Canada

(40) Polyethylene is an almost unique case to the contrary. Because of the small distances between the chains in the orthorhombic cell, a band splitting occurs in the IR spectra which constitutes a tracer of the orthorhombic cell even when not much long-range order is present in the sample.

(41) Gidley, M. J.; Cooke, D.; Darke, A. H.; Hoffman, R. A.; Russell, A. R.; Greenwell, P. (1995) *Carbohydrate Polymers*, 28, 23.

APPENDIX

The first two rows of table 3 below, give the fractions of each band in the 1175-950 cm^{-1} region for the pure α-D and β-D-glucose isomers. The next three rows give the fractions for an amylose/water mixture in three conditions namely, at RT and after the f(Tmax, Crys) treatment for Tmax = 50°C and 105°C as reported above.

Table 3 Fractions of the different bands in the 1175-950 cm^{-1} region for α–D and β–D glucose solutions (0.9/0.1) and amylose–water mixtures (0.7/0.3 W/W)

	Position (cm^{-1})														
Sample	1158	1153	1149	-	1126	-	1108	1105	1101	1080	1078	1053	1045	1039	1032	1022	999	993
glucose																		
α			0.09					0.14		0.09		0.14			0.26			0.28
β	0.15						0.14			0.16				0.26				0.29
amylose																		
RT		0.10			0.30				0.06		0.07		0.16			0.18	0.13	
Tmax 50		0.07			0.05				0.13		0.11		0.08			0.47	0.09	
Tmax105		0.17			0.12				0.11		0.09		0.16			0.12	0.24	

The spectrum of glucose/water mixtures changes due to the mutarotation of glucose and reaches an equilibrium state which corresponds to a sizeable fraction of the two isomers (33(α)/67(β)). The values are in agreement with that found by other measurements such as calorimetry or rotatory power. The data presented in recent papers[35-36] have been used to obtain, after an approximate band decomposition, the values in the table. One observes that a significant difference in the spectra of α and β glucose resides in that the band found at 1080 cm^{-1} is significantly greater for β-glucose than for α-glucose. The authors also find that as one anomer transforms into the other, this band increases or decreases proportionally to the amount of β-glucose in the sample. Therefore, as we have found that this band in amylose is not affected by the treatment, it is clear that the IR spectra of amylose does not correspond to the spectrum of

pure β-D glucose, so the high T treatment does not induce hydrolysis of the polymer, a transformation of the a-conformer to the B-conformer, or an opening of the ring. Also, one should note that the spectra of glucose found in recent papers [34-35] present significant difference from the present work to show that glucose is not formed and is not present in our samples.

CHAPITRE 5

DOUBLE-HELICAL NETWORK IN AMYLOSE AS SEEN BY SLOW CALORIMETRY AND FTIR

by P. Bernazzani[1], C. Chapados[2] and G. Delmas[1]

[1]Département de Chimie-Biochimie, Université du Québec à Montréal, C. P. 8888 succ. Centre-Ville, H3C 3P8, Montréal, Canada. [2]Département de Chimie-Biologie, Université du Québec à Trois-Rivières, G9A 5H7, Trois-Rivières, Canada.

Journal of Polymer Science, Part B, 2000, 38, 0000

Key-words: amylose-water, X-rays, fast T-ramp DSC, slow calorimetry, FTIR, strain, B and V crystals.

ABSTRACT

The phase content and crystallinity of initially amorphous amylose-water mixtures (70/30 W/W) have been changed by slow cycles of dissolution and recrystallization from Tmax with 50°C < Tmax < 120°C. Analysis of the treatment-induced changes is made by X-ray diffraction, FTIR, fast T-ramp DSC and slow calorimetry. Our interest was to follow the relaxation of the network phase and its consequence on the growth of crystallinity. The main point of this work is that the fast T-ramp DSC technique is unable to follow the growth of crystallinity achieved by treating the samples. In highly interactive polymer-solvent systems, order is unmeltable in a fast T-ramp due to strain developed during the ramp. In a 6 K/h T-ramp, the order becomes meltable and grows from 21 J/g to 147 J/g when Tmax increases. The other conclusion is that strain-melting and the network phase, characterized first in polyolefins has a more prominent role in the characterization of H-bonded polysaccharide–water mixtures. Correlation is achieved between the concentration of bands in the C-O stretching region, the fraction of single and double helices and the three endotherms found on the slow T-ramp dissolution traces. FTIR spectra show that chains in the network cannot be disentangled by quenching but can be organized during a slow cooling. The B and V crystalline modifications are observed in the treated samples. Quenched treated amylose and enzyme-resistant amylose seem to contain a comparable amount of double-helical/strainable fraction.

INTRODUCTION

Amylose and amylopectin are components of starch. Both are polysaccharides, their difference residing in the content of branched chains which is small for amylose and sizeable for amylopectin. Amylose can crystallize in three usual forms denominated type A, B and V.

Types A and B consist of double helix packing in an orthorhombic form with the A form being slightly deformed. Type A is found mainly in tuber while type B is mostly found in potato starch. Finally, type V is a single helix crystal form that occurs only when amylose forms a complex with a suitable ligand such as n-butanol, iodine or fatty acids. The aim of the present work is to complete the general knowledge of the morphology of amylose by measuring its non-crystalline components.

Physico-chemical characteristics of polyolefins and amylose solutions

Polyolefin solutions

Polyolefins such as linear polyethylene (PE) or polypropylene (PP) dissolve in non-polar solvents at their dissolution temperature Td, usually located 40 K below their melting temperature, Tm in dilute solutions. Samples of high crystallinity can grow over a period of weeks by isothermal crystallization at Tc situated a few K below Td. The increase in crystallinity after isothermal crystallization is measured on the dry polymer by X-rays, fast T-ramp DSC or density. A crystallinity parameter α, characterizing long-range order has been found to increase from 0.5 to 0.7 by a careful choice of conditions. A crystallinity index is defined by the relation:

$$\alpha\ (\Delta H_{crys}) = \Delta H_m / \Delta H_o \qquad \text{eq. 1}$$

where ΔH_m and ΔH_o are respectively the heat of fusion of the sample and that of a perfect crystal[1]. For instance, the 0.2 increase in α (calorimetric) obtained by isothermal crystallization for PE corresponds to a raise in ΔH_m from 150 J/g to 210 J/g. For highly entangled solutions, typical of ultra high molecular weight PE, polymers with branches and copolymers, the same conditions lead to an increase of short-range i.e. an order the size of which is not large enough to lead to well-resolved X-ray patterns. The lack of quantitative

techniques to evaluate short-range order has led scientists to ignore it. Increasing long-range order in gel-forming polymers such as poly 4 methyl pentene-1[2] is a harder task than in PE. It is probably linked to the chains retaining in solution the helical conformation present in the solid state. With simple or double helices, the kinetics of network formation is faster than that of thick lamellae leading to a low to medium value of α, the crystallinity obtained by the methods mentioned above.

The helical conformation of amylose and other polysaccharides has been investigated by ^{13}C NMR[3-5] and fluorescent polarization.[6] Amylose presents some features of synthetic polymers in solution but also some differences. One cannot measure a value of Tm due to the high cohesion of the polymer but the dissolution temperature of crystalline amylose, Td, is found around 70°C in water.[7-16] The Td values vary with chain length according to the Flory-Huggins equation for the chemical potential of the solvent[7-8, 13], an indication of true solution as are the light-scattering or intrinsic-viscosity measurements.[6] The dilute solutions of amylose are not stable however but form on standing aggregates rather than single crystals. The difference between Tm and Td gives an information on the solution. Based on the fact that amylose contains several properties similar to glucose and that, contrary to cellulose, amylose easily hydrolises to glucose, we assume that Tm (amylose) is of the same order of magnitude as Tm (glucose) i.e. 190°C. By assuming this, one finds Tm-Td = 120°C, a large value characteristic of favorable solvent-water interactions. The exothermic heat of wetting of amorphous amylose (-57 J/g) at room temperature (RT) is typical of a favorable amylose-water interchange energy.[17] The heat of wetting of the more crystalline starch is -17 J/g.[18-19] In spite of this favorable interaction with water, only a fraction of amylose or starch dissolves at Td. One has to reach 120-130°C to obtain a translucid solution which may not be

homogeneous since observation under the microscope of amylose-water mixtures shows undissolved granules up to 160-180°C.[20] Conditions to have an equilibrium phase-change at Td have been approached by measurements of heat capacity. [8, 18-19]

The difference between polyolefin solutions and amylose-water mixtures above Td has been explained[13] in terms of a network phase whose dissolution is impeded due to strain as explained below. The difference is quantitative rather than qualitative since strained dissolution has been found in solutions of ultra-high molecular weight polyethylene[21] but partial solubility above Td does not lead in polyolefin solutions to turbidity while it does in amylose-water mixtures. In spite of the limit in crystallinity of amylose crystals prepared in solution, samples of fair crystallinity have been obtained after a high temperature treatment.[22] Values of α from X-ray or calorimetry are not usually reported in the literature. With some estimation however a quantitative evaluation of crystallinity can be obtained from ΔH_{diss}.

Crystallinity from the heat of dissolution

$$\Delta H_{diss} = \Delta H_{melting} + \Delta H_{polymer\text{-}solvent\ interaction} \qquad \text{eq. 2}$$

For polyolefin solutions, $\Delta H_{polymer\text{-}solvent\ interaction}$ is low compared to $\Delta H_{melting}$. ΔH_{diss} is then a good evaluation of $\Delta H_{melting}$. The crystallinity index obtained from heat of dissolution has the same form as eq. 1:

$$\alpha\ (\Delta H_{diss}) = \Delta H_{diss} / \Delta H_o \qquad \text{eq. 3}$$

The value of α calculated from eqs. 1 and 3 with ΔH obtained from a fast T-ramp DSC experiment corresponds to non-strainable order, equivalent to long-range order.

For amylose, eq. 3 may not be very satisfactory due to the uncertainty in the size of the second term of eq. 2. It will be used however to estimate the crystallinity of samples whose thermal analysis is reported in the literature. We can turn to a model molecule to know ΔH_o, the enthalpy of melting of a hypothetically perfect amylose crystal. As previously assumed, ΔH_o of amylose should have the same order of magnitude as ΔH_m for crystalline glucose which was found to be 180 J/g.[17]

Literature values of ΔH_{diss} are reported for starch. For high degrees of polymerization, they range from 3 to 12 J/g. Since long-range order disappears at Td, the term ΔH_{diss} may be an acceptable expression but the term $\Delta H_{gelatinization}$ is rather used as it has the advantage of referring to the change in the starch granules rather than to a physico-chemical state above Td. Some higher values of ΔH_m (and Td) are given for amylose but they referred to amylose modified by cycles of temperature.[5, 10-11]

Taking the range of values found for starch, the value of crystallinity α (ΔH_{diss}) for amylose or starch is:

$$0.02 < \alpha\ (\Delta H_{diss}) < 0.07 \qquad \text{eq. 4}$$

We have observed that these amylose and starch samples have some long-range order as given by their X-ray diagram and therefore one would expect that more long-range order should lead to an increase in α (ΔH_{diss}).

The aim of the present work was to try to clarify the following paradox: How can crystalline samples dissolve with so little heat? The amylose-water mixtures seem to be a case where strain dissolution or arrested dissolution is particularly operative. In the following paragraph, some information on phase-changes under strain is given.

Strain-melting, strain dissolution

Strain-melting and strain-dissolution have been presented in previous papers on polyolefins[21, 23-25] and amylose.[17, 26] Strain on crystals displaces the solid-liquid equilibrium towards the solid phase. This is the reason why fibers solidly held in a fast T-ramp DSC pan melt at higher T than free fibers. Strain can develop without external stress. In a fast T-ramp DSC ramp, the unavoidable expansion taking place during melting has different effects depending on the location of the ordered chains in the material. In the regions without entanglements, melting takes place as it does for small molecules which reach above Tm their lowest free energy state. In the region with entanglements i.e. in the network phase, strain builds up because the chains cannot expand. As a consequence, melting in this region is arrested. The shape of the melting or dissolution traces give an indication of a sudden return to the solid region of the phase diagram: the heat flow above Tm drops abruptly while it raises regularly below Tm. However, if the T-ramp is slow, the chains can reorganize, melting is slowed down but not arrested. A slow T-ramp permits to differentiate between the free and bounded chains. The free chains melt with the same enthalpy whatever the rate of heating. The enthalpy of melting (or of dissolution) of the chains in a network raises when the ramp is slower because more ordered chains become meltable due to the reduction of strain. In consequence the rate of heating must be specified when giving a value for α (ΔH). In the following text, the distinction will be made between α ($\Delta H_{diss,\ fast\ T\text{-}ramp}$) and α ($\Delta H_{diss,\ slow\ T\text{-}ramp}$).

Eq. 4 should be written as:

$$0.02 < \alpha\ (\Delta H_{diss,\ fast\ T\text{-}ramp}) < 0.07 \qquad \text{eq. 5}$$

EXPERIMENTAL

Sample

Amylose isolated from potato starch was purchased from Sigma (St. Louis, Mo, USA). The powder was cold washed in ethanol to eliminate the fatty acid residues and left for at least 12 h at room temperature in a vacuum dessicator containing P_2O_5. Water was added to the dried amylose to have a 0.70 amylose fraction (W/W). The mixture was then thoroughly stirred using first a glass rod then a magnetic stirrer until a light paste was formed. The samples were then subjected to various thermal treatments in order to modify the phase composition. The X-ray spectra of the native samples revealed their almost amorphous nature.

Thermal treatment

Nitrogen was bubbled through amylose paste which was then placed in a glass tube sealed under nitrogen and heated to Tmax, using a heating rate of 3 K/h, with $50 < Tmax < 120°C$. The sample was maintained 10 hours at this temperature and then slowly cooled at a 3 K/h rate. Tubes in which nitrogen was bubbled insufficiently and which were found to be colored after the treatment were discarded.

X-ray spectroscopy

A Siemens K IV diffractometer with a Co cathode was operated in reflectance mode using the Co Kα wavelength (λ = 1.79021A). To compare with the values found in the literature, we have converted the 2Θ axis in the figures presented hereafter, to that found using a Cu Kα wavelength (λ = 1.54178A). Long-range crystallinity was determined by summing each peak over the total area by assuming the large undefined diffraction is representative of the amorphous chains, as indicated in fig 3d.

Calorimetry

A C80 calorimeter from Setaram (Lyon, France) was used. This apparatus is a very sensitive and stable DSC capable of accommodating large size cells (12 cm^3) for solution measurements. Quantitative enthalpy measurements can be obtained at very low heating rates (0.1 K/h) due to the low baseline fluctuation (5 μW, as shown in fig. 1 for a heating rate, v = 6 K/h). However, we have limited ourselves to ramps between 1 and 60 K/h with the discussion mostly centered on the results obtained at 6 K/h. The enthalpies were evaluated quantitatively using either commercially available decomposition software (Grams/386 from Galactic Industries) or a conventional planimeter.

FTIR

A Bomem MB-series spectrometer was used in transmission mode at a resolution of 1 cm^{-1} with an accumulation of 50 scans. Due to large water absorption elsewhere, the region of the CO stretching vibrations (1300-800 cm^{-1}) was the only one investigated. The intensities are given in absorbance unit (a.u.). A quantity of the treated paste was spread evenly between IR plates and the spectra taken. The layer of the amylose-water mixture was 5 to 15 μm thick. The baseline intensity which was subtracted was smaller than 0.2 a.u. Degradation of the spectra due to the deterioration of the IR plates by water was found to be negligible. The spectra were normalized by the 1078 cm-1 band to help visualize the evolution of the treatment.

Spectral simulations

While the seven IR bands in the spectra are easily distinguishable, some overlap occurs in the region of interest. Spectral simulations were performed to quantitatively separate the peaks. The simulations were carried out similarly on every samples as was reported

elsewhere.[26] Prior to simulation, the self deconvolution and second derivative traces were performed. From these, number and position of each band were determined. The full width at half height of each band varied from 20 to 40 cm^{-1}, and for the same band remained constant from one spectra to another. As observed on the original spectra, seven bands were used to obtain reasonable results.

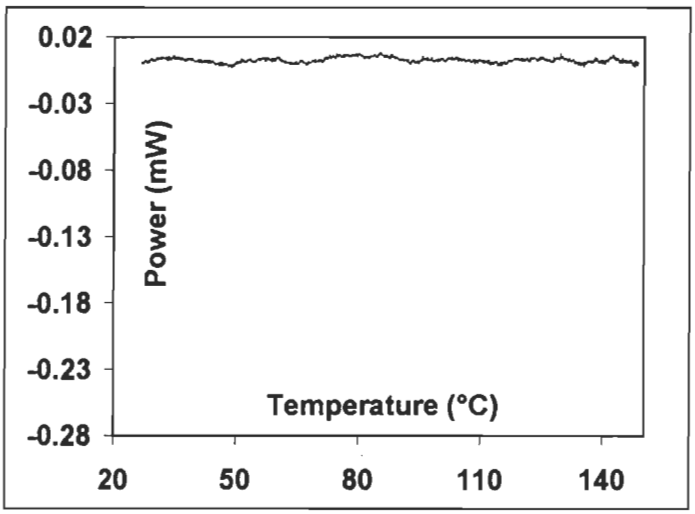

Figure 1 Baseline of the calorimeter at 6 K/h using typical cells. Note that the heating rate and the baseline signal are 6 times higher than in Fig. 5a.

RESULTS

Characterization of the samples

The fast T-ramp DSC traces, the X-ray diffraction spectra, the IR spectra and the slow calorimetry traces constitute the means used for the characterization of the samples after treatment.

FAST T-RAMP DSC

The values of $\Delta H_{diss,\ fast\ T\text{-}ramp}$ vary between 0 and 3.4 J/g for the different values of Tmax and v = 60 K/h (1 K/min). Table 1 gives the values of α ($\Delta H_{diss,\ fast\ T\text{-}ramp}$) calculated from eq. 3 with v = 1 K/min for the treated samples as a function of Tmax. Fig. 2a and b are fast T-ramp

DSC traces at 60 K/h (1 K/min) for non-treated and treated amylose. The traces for other values of Tmax are similar to Fig. 2b (Tmax = 95°C) with different values of $\Delta H_{diss,\ fast\ T\text{-}ramp}$. Fig. 2c gives the correlation between $\Delta H_{diss,\ fast\ T\text{-}ramp}$ and Tmax.

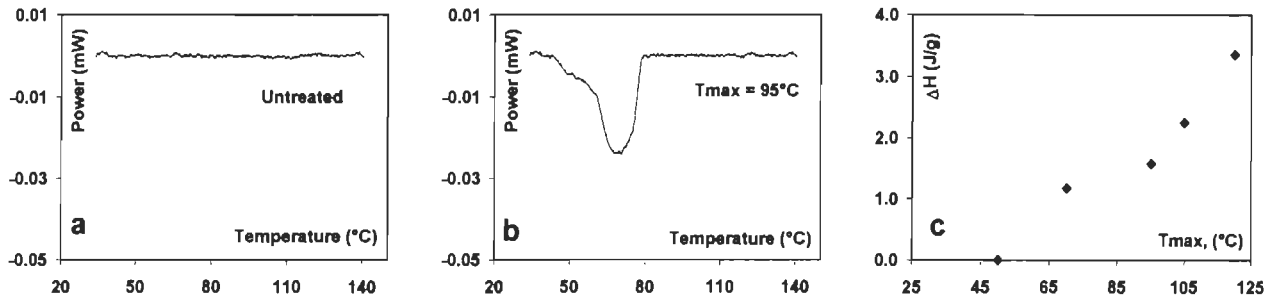

Figure 2 Fast T-ramp DSC traces of (a), untreated amylose-water mixture, (b), amylose-water mixture (70/30 W/W) treated at Tmax = 95°C. Fig. 2c gives the correlation between the enthalpy by fast T-ramp DSC and the treatment temperature, Tmax.

X-ray diffraction

The typical X-ray diffraction patterns of untreated samples and of treated materials at different Tmax are given in Fig. 3 a-f. As can be observed, the evaluation of the crystalline content is difficult as the separation of the B and V crystals contribution is difficult possibly due to the inhomogeneity from one sample to the other. However, the peak position remain relatively constant.

FTIR

Fig. 4a is the IR spectra of the non-treated amylose. The changes of the IR spectra due to treatment can be seen in Fig. 4b-c.[26] In Fig. 4d, the spectra for treated samples with five different Tmax have been put on the same graph. Figs. 4b-c give the spectra which are the most different, namely that for Tmax = 50°C and Tmax = 105°C. Table 2 gives the relative intensity of each band in the spectra.[26] Several bands vary with treatment but an overall indicator of the change is the relative intensity of the absorbance at high wavenumbers (1175-

1078 cm^{-1}) to the total absorbance (1175-950 cm^{-1}). Since it grows with Tmax it has been listed in Table 1 as α (IR, relaxed).

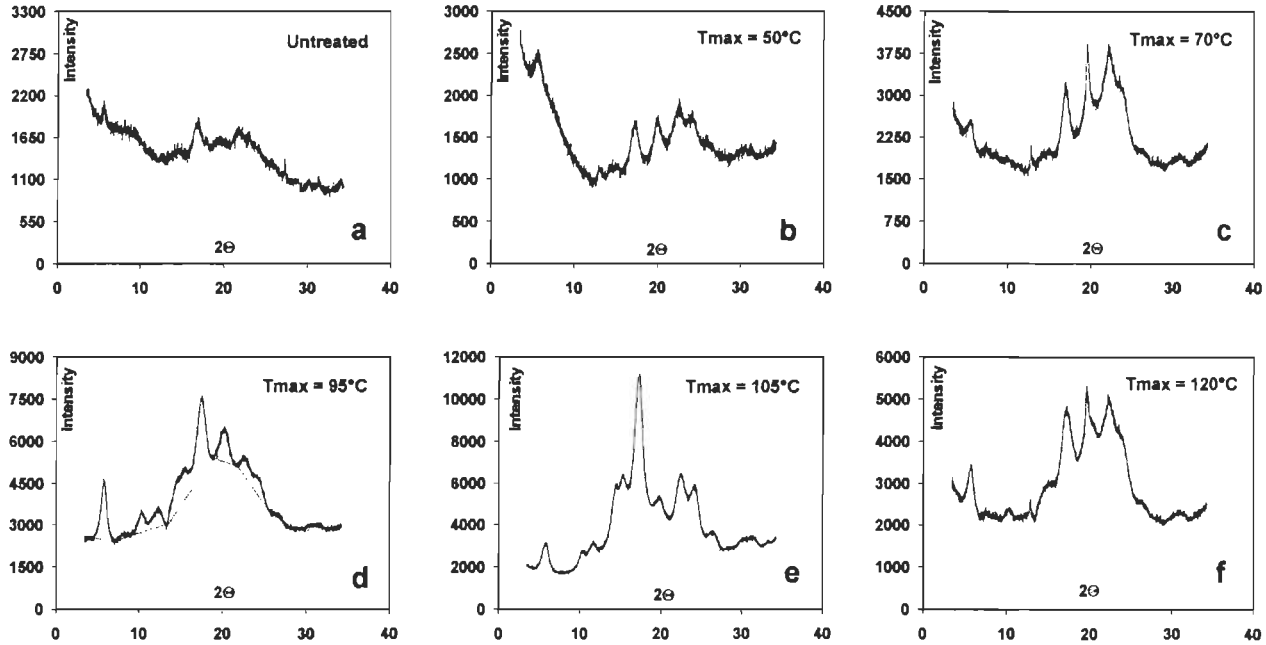

Figure 3 X-ray diffraction pattern for the untreated (a) and treated (b-f) amylose-water mixtures (70/30 W/W).

Table 1 Crystalline relative intensities of treated amylose by X-ray diffraction, fast T-ramp DSC (1 K/min) and IR spectroscopy

Tmax (°C)	α (X-ray)[a]	α ($\Delta H_{diss\ fast\ T\text{-}ramp}$)	α (IR, relaxed)[b]
50	0.15	0.000	0.29
70	0.19	0.007	0.33
95	0.33	0.009[c]	0.41
105	0.41	0.013	0.42
120	0.50	0.019	0.56

[a] Spectra shown in fig. 3
[b] Evaluated by the integrated absorbance of the 1175-1078 cm^{-1} region over the total area (1075-950 cm^{-1})
[c] Trace shown in fig. 2b

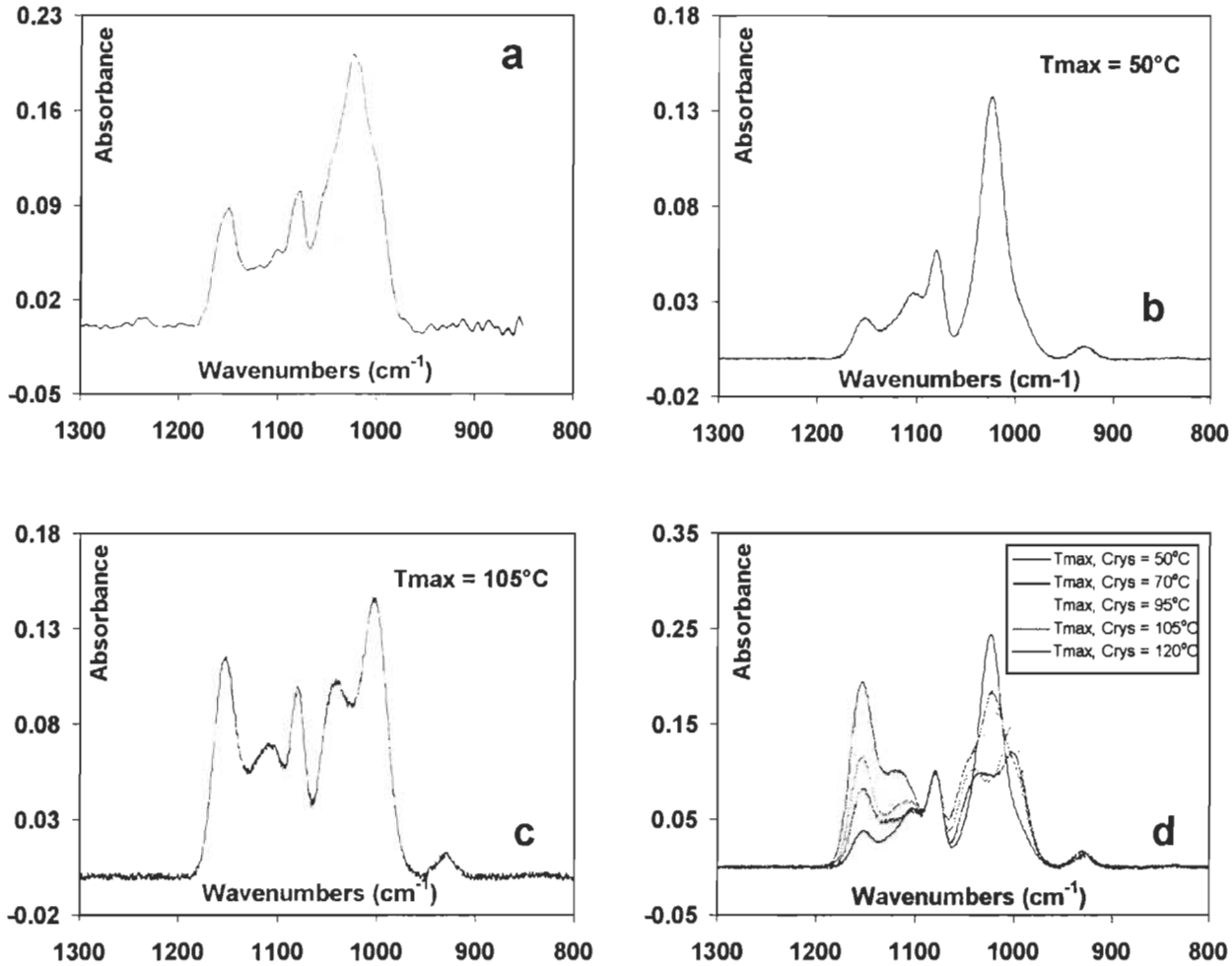

Figure 4. 4a corresponds to the spectra of untreated amylose-water mixtures (70/30 W/W), while 4b and 4c represent two spectra of the amylose-water mixture treated respectively at Tmax = 50 and 105°C. 4d Cumulative figure showing all the treated amylose spectra overlapped.

Table 2. Relative intensity (a.u.) of each band found[26] in the 1075-950 cm^{-1} region of the IR spectra of various treated amylose-water mixtures(70/30 W/W)

	Peak position (cm^{-1})						
Tmax[a]	1153	1126	1101	1078	1045	1022	999
50	0.07	0.05	0.13	0.11	0.08	0.47	0.09
70	0.12	0.08	0.09	0.09	0.19	0.28	0.15
95	0.18	0.11	0.08	0.08	0.18	0.18	0.19
105	0.18	0.12	0.11	0.07	0.16	0.12	0.24
120	0.25	0.20	0.07	0.08	0.11	0.12	0.18

[a] Spectra shown in fig. 4

Clearly, the FTIR and X-ray techniques are sensitive to treatment. Since the values of α ($\Delta H_{diss,\ fast\ T\text{-}ramp}$) seem less sensitive to the treatment, the slow calorimetry traces will be studied next.

Enthalpies of phase-change in slow calorimetry

To reveal the effect of treatment, the strategy of slowing down the T-ramp which has been proven usefull on polyolefin solutions[21, 23-24] and amorphous amylose[17] is used. Two series of data have been obtained. In the analysis of the as-received samples, the effect of the rate of heating is studied. In the analysis of the samples treated at five different Tmax, a single heating rate is used (6 K/h).

Phase-change of non-treated amylose-water mixtures (70/30 W/W) in a T-ramp

Figs. 5a-b give the traces of dissolution of non-treated amylose for v = 1 and 3 K/h. Note that the shape of the endotherms is different. A trace similar to that of Fig. 5a has been reported in a previous publication.[17] Table 3 gives the values of $\Delta H_{diss,\ slow\ T\text{-}ramp}$ for $1 < v < 60$ K/h.

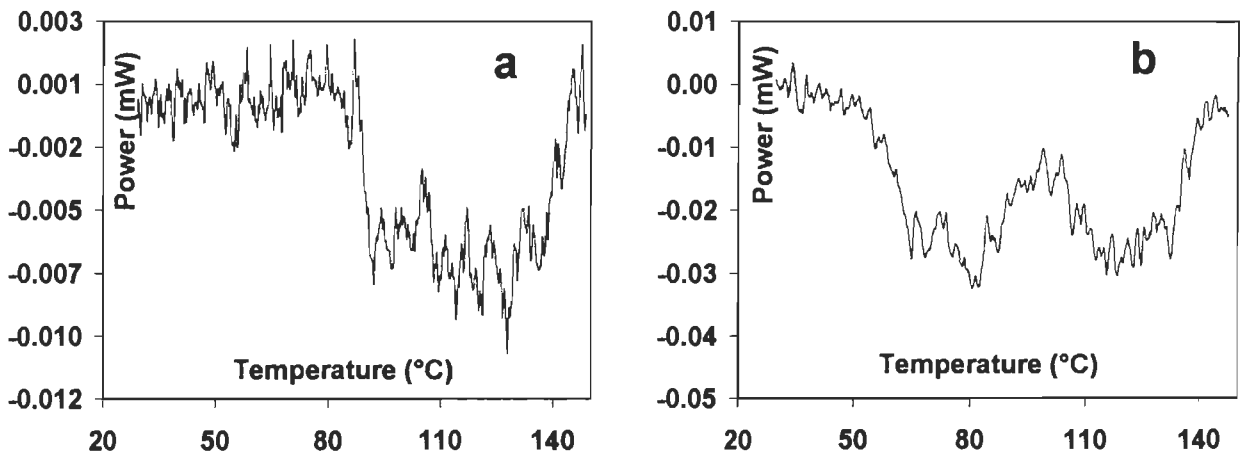

Figure 5 Dissolution traces of untreated amylose-water mixtures (70/30 W/W) at v = 1 K/h, for a mass of 17.46 mg (a) and at v = 3 K/h for a mass of 45.63 mg (b). Note that the orientation of endotherms is down.

Table 3. Effect of heating rate, v, on the heats of dissordering of native amylose-water mixtures (70/30 W/W)

Heating rate, v (K/h)	1[a]	3[b, c]	6	12	36	60
ΔH_{diss} (J/g)	60.4	53.0	7.8	5.0	1.5	0.0

[a] Trace shown in fig. 5a

[b] Trace shown in fig. 5b

[c] ΔH_{diss} was reported as 26 J/g in ref 17. It was later found that a longer contact time of amylose with water while stirring increases ΔH_{diss}.

Phase-change of amylose-water mixtures (70/30 W/W) in a 6 K/h T-ramp after treatment at Tmax and slow crystallization.

The rate of heating (6 K/h) was chosen because it did not give a sizeable heat on the as-received sample (< 10 J/g) (Table 3) and it was not slow enough to transform too much the treated samples. Figs. 6a, b are typical traces of dissolution of treated samples. As shown in dotted lines on the figures, the endotherm can be separated into three parts: a flat endotherm accompanied by a low-and a high-T endotherm with faster kinetics. Although there is some degree of overlapping between the three peaks, particularly when Tmax is > 95°C, one can separate them accepting a range of value for each of the ΔH. We will attempt to explain their presence later. The data for the total enthalpy and of each of the three peaks are given in Table 4 as a function of Tmax.

The effect of strain has been identified independently on the calorimetric traces and in the IR spectra.[26] When stress is reduced, the vibrations are displaced towards higher wavenumbers and the endotherms towards lower T. The attributions are given in Table 5 based on the correlation observed in Figs. 7-9 between the enthalpies of dissolution and the IR intensities. Other correlations were attempted without success.

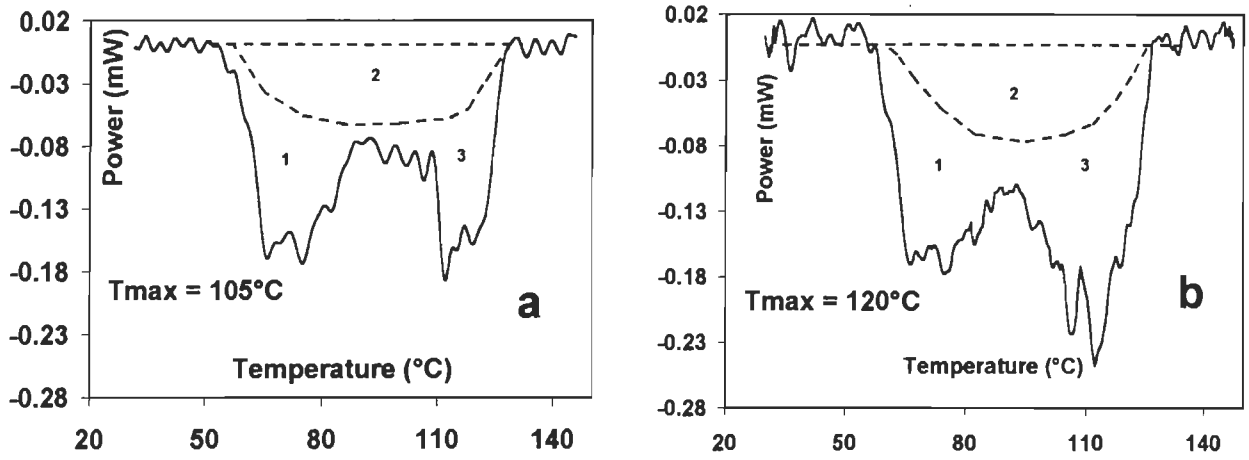

Figure 6 Dissolution trace at v = 6 K/h of amylose-water mixtures (70/30 W/W) treated at Tmax = 105°C (a) and 120°C (b). Note that the orientation of endotherms is down.

Table 4 Variations of the heats of disordering of amylose-water mixtures (.7/.3 W/W) with Tmax

Tmax (°C)	ΔH_{total} (J/g)	ΔH_1 [a] (J/g)	ΔH_2 [b] (J/g)	ΔH_3 [c] (J/g)	α ($\Delta H_{diss,\ slow\ T\text{-}ramp}$) [d]
50	22	4	9	9	0.07
70	72	24	14	35	0.32
95	118	39	34	45	0.47
105[e]	133	43	64	45	0.49
120[f]	148	51	68	28	0.44

[a] Enthalpy of the low-T endotherm integrated between 55-85°C with a maximum at about 70°C. [b] Enthalpy of the large T-range endotherm integrated between 60-130°C with a maximum at about 100°C. [c] Enthalpy of the high-T endotherm integrated between 90-135°C with a maximum at about 120°C. [d] Calculated as the averages of $\Delta H_1 + \Delta H_3$ over the enthalpy of complete melting, $\Delta H_0 = 180$ J/g. [e] Trace shown in fig. 6a. [f] Trace shown in fig. 6b.

Table 5 Assignment of the IR bands in the C-O stretching region to strained and unstrained environments[26] and correlation with $\Delta H_{diss,\ slow\ T\text{-}ramp}$

	Network		IR Crystalline	
	Strained	Unstrained	Strained	Unstrained
IR peak position (cm^{-1})	1022	1126	1045, 999	1153
Slow T-ramp DSC	not meltable	ΔH_2	ΔH_3	ΔH_1

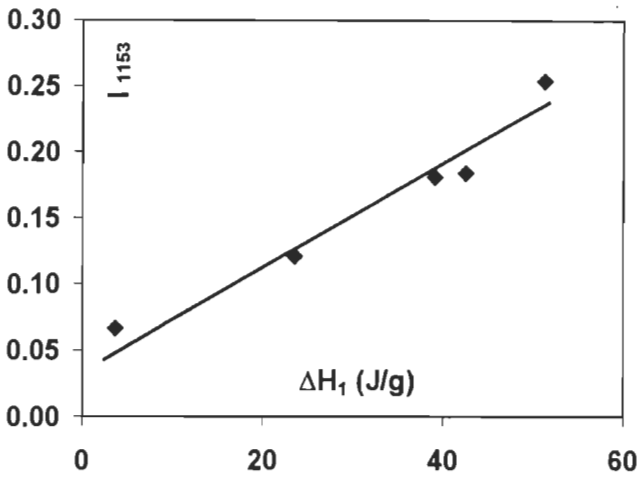

Figure 7 Correlation between the integrated intensity of the 1153 cm^{-1} band and ΔH_1 for the five values of Tmax.

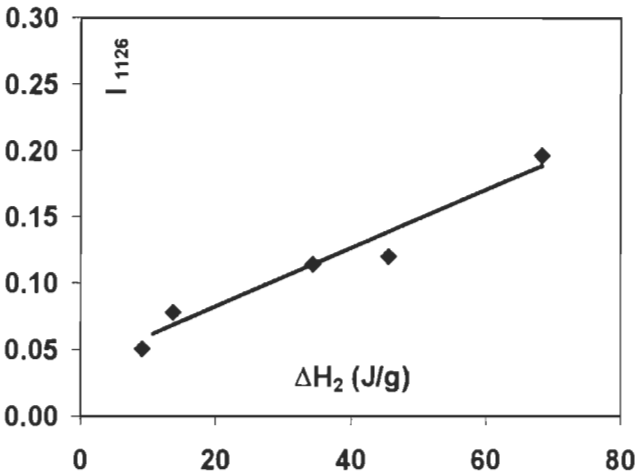

Figure 8 Correlation between the integrated intensity of the 1126 cm^{-1} band and ΔH_2 for the five values of Tmax.

DISCUSSION

Some comments will be made on X-ray results first. Followed by that on slow calorimetry. After, the results of slow calorimetry will be commented upon. In part B, the three endotherms found in the 6 K/h T-ramp traces will be correlated with specific IR bands. The fraction of double and single helices will be evaluated from the calorimetric and IR results. The similarity between the morphology of treated amylose and enzyme resistant amylose will be remarked upon briefly at the end.

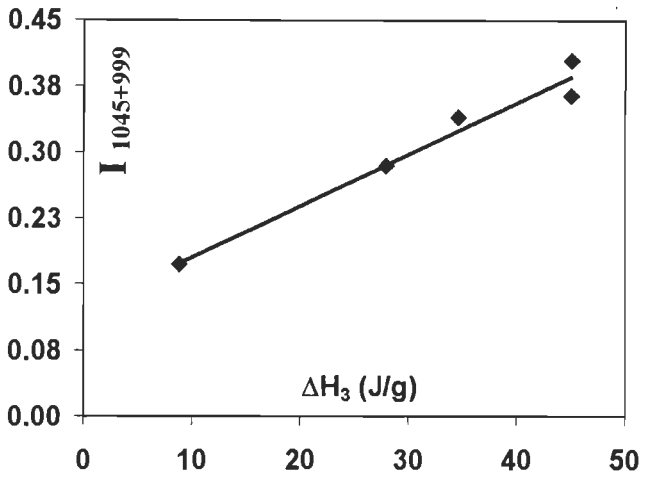

Figure 9 Correlation between the sum of the integrated intensity of the two bands at 1045 and 999 cm^{-1} band and ΔH_3 for the five values of Tmax.

A. X-ray spectra

The overall crystallinity, α (X-rays), has been estimated as indicated in the experimental part and is listed in Table 1. The increase of the sample's crystallinity with Tmax is not unexpected but what may be surprising is the growth of the characteristic V type morphology peaks. Disentanglements, brought about by the slow crystallization in H_2O, of single helical order while quenching gives exclusively the B form.[7] It is noteworthy that the height of a given peak of diffraction of the B or V form does not increase gradually with Tmax. Another peak of the same modification can grow instead. This feature of the diffraction pattern prevented us from determining the fraction of the V and B modification in each sample. However, an indirect estimation of the ratio of the double to the single helical order, given in part C, may offer a good lead in separating the fractions of the B and V forms in the X-ray spectra.

B. SLOW CALORIMETRY

Non-treated samples: strainable network phase of amorphous amyloses

The untreated amylose sample does not contain long-range order i.e. non-strainable order. Consequently, dissolution is associated only with the strainable network phase. As reported before[17] ΔH_{diss} is highly sensitive to the rate of heating as seen in Table 3 where it varies between 0 and 60J/g. The very slow T-ramp of Fig. 5a has annealed the sample. The interval of Td is 80-140°C while it is 50-140°C in Fig. 5b where the rate is 3 K/h.

One should note here that the time allowed for dissolution when a measurable endotherm is observed (1.5 J/g for v = 36 K/h) is about three hours, an order of magnitude longer than in a standard fast T-ramp DSC. In spite of this relatively long contact, dissolution in water does not occur with a kinetics fast enough to be recorded. This gives an indication of the heat stability of the ordered network in this hydrogen-bond rich network.

Treated amylose: α ($\Delta H_{diss.\ slow\ T\text{-}ramp}$) crystallinity

A crystallinity index depends on the technique of analysis. In the present case, it would not seem reasonable to use in eq. 3 the full value of $\Delta H_{diss,\ slow\ T\text{-}ramp}$ (Table 4) since it contains the enthalpy of melting of short-range order. As explained below, a meaningful range of the crystallinity index , α ($\Delta H_{diss,\ slow\ T\text{-}ramp}$) is:

$$\Delta H_1 / \Delta H_o < \alpha\ (\Delta H_{diss,\ slow\ T\text{-}ramp}) < \Delta H_{diss} / \Delta H_o \qquad \text{eq. 6}$$

where ΔH_1 is the enthalpy of the low temperature endotherm.

As listed in Table 1 the values of α ($\Delta H_{diss,\ fast\ T\text{-}ramp}$) are one order of magnitude smaller than α (X-ray). For semi-crystalline polymers, it is often the other way because small crystals can

contribute to α (ΔH) and not to α (X-ray). *This is one conclusion of this work: fast T-ramp DSC is not the technique to be used to reveal crystallinity in hydrogen-bonded and entangled systems.* The effect may be particularly pronounced in the present case of concentrated systems. On the other hand, the value of $\Delta H_{diss,\ slow\ T\text{-}ramp}$ grows with Tmax as does α (X-ray). As will be seen below, a reasonable value of α ($\Delta H_{diss,\ slow\ T\text{-}ramp}$) can be calculated from the traces using eq. 6.

Treated amylose: process of disentanglement

The transformation of amylose in the treatment is due to disentanglements and is understood as follows: during the T-ramp toward high T, the junctions in the network become loose, the more so when Tmax is high. In the T-ramp towards low T, this process continues somewhat but is reinforced by the crystallization of the mobile chains liberated from the network. Long-range order is formed as indicated by the change of the X-ray patterns in Fig.3. Our interpretation is in line with previous work on polyolefins in solution.[21,23-24] The conditions for disentanglements were learned on solutions of ultrahigh molecular weight polyethylene. As for amylose, the test of disentanglement was the trace of dissolution in a slow T-ramp of the sample slowly crystallized which included the value of ΔH and the number and shape of endotherms in the trace. In a perfectly disentangled solution, obtained after a large number of temperature cycles (>20), the dissolution trace has a single endotherm with a fast kinetics and a large value of ΔH, typically 1.5-2 times the value found without treatment.[29] In partially disentangled solutions two endotherms are observed, one with a fast kinetics and the other with a slow kinetics. ΔH increases with the course of disentanglement. The present system submitted to a single cycle is only partially disentangled. Accordingly, dissolution occurs with a range of tension and several endotherms. The high-T endotherm

with a relatively fast kinetic found in amylose-water mixtures does not occur in polyolefins solutions.

Treated amylose: the three endotherms

Fig. 6a, b are typical traces of dissolution for the samples treated at Tmax = 105°C and 120°C respectively. The large range of dissolution temperature and the three endotherms will be explained in terms of a range of strain during the dissolution trace.[27] Some long-range order grown from disentangled chains will dissolve at low T in a cooperative way and this is the low-T endotherm whose enthalpy is ΔH_1 in table 4. Some other crystals have managed to grow but keep some link between themselves or the network phase. They dissolve cooperatively with tension and this is the high-T endotherm whose enthalpy is ΔH_3. As expressed in eq. 6 above, the value of α ($\Delta H_{diss,\ low\ T\text{-}ramp}$) can have a range of values. Because of their faster kinetics, two peaks (the low and high-T endotherms) were chosen to contribute to the crystallinity so that:

$$\alpha\ (\Delta H_{diss,\ slow\ T\text{-}ramp}) = (\Delta H_1 + \Delta H_3) / \Delta H_o \qquad \text{eq. 6a}$$

The values of α ($\Delta H_{diss,\ slow\ T\text{-}ramp}$) are reported in the last column of Table 4 for the five treated samples. The trend with Tmax follows that found with α (X-ray) but the values are often different. This may come from the choice of ΔH_o or from dropping ΔH_2 completely in eq. 6a or from a lack of precision in α (X-ray) or $\Delta H_1 + \Delta H_3$.

The chains highly connected in a network, grow short-range order on cooling. The range of tension depends on the concentration of junctions which are not distributed homogeneously in the material. This phase will dissolve on a large T-range with a low kinetics and an endotherm whose enthalpy is ΔH_2. The value of ΔH_2 is highly sensitive on Tmax. Even a moderate value of Tmax = 95°C changes the value of the untreated sample from 7.8 J/g to 34.2 J/g .

The presence of a high-T endotherm in Fig. 5 which is absent in the traces of polyolefins solutions suggests this to be a special feature of amylose order. Cooperative hydrogen bonding lead to strain melting in crystals even in samples whose density of entanglements has been reduced by slow crystallization.

For the same reason, the low-T endotherm, which is reported above to correspond to the dissolution of non-strainable long-range order, remains highly sensitive to rate of heating and strain. *The second finding of this work is that with comparable molecular-weight dependant entanglements, polysaccharides are more strainable than polyolefins due to cooperative hydrogen-bonding in the ordered regions.* The temperature at which dissolution occurs (100-135°C) is sufficiently low for the hydrogen bonds to be still cohesive in the polymer mixtures. Cooperativity of the H bonds and low free–volume contribute to make the OH bonds more stable in polysaccharide solutions than in small molecules. The distinction between the kinetics of evolution of heat for ΔH_2 and ΔH_3 diminishes when Tmax and ΔH_2 increases. It is also dependent on the rate of heating.

In Fig. 6, the endotherm of dissolution of the network phase, situated in between the low- and high-T endotherms, is clear. In other traces the three endotherms overlap more so that a decomposition with two endotherms only would be possible. The calorimetric analysis has been somewhat helped in the distinction of three phases by the information gathered from the IR spectra. The changes in the spectra are interpreted as a displacement from a strained to a meltable network phase as Tmax is increased.[25] The displacement is not complete in the conditions of the treatment, the network phase remaining present even after high values of Tmax and slow recrystallization. This suggested that the endotherm of dissolution of the network phase is present on the trace in spite of being partially hidden by the other two peaks.

Short-range order, molecular order and strained order

Several authors have investigated short-range order either by NMR[28] or DSC[15]. In the ^{13}C NMR investigation, it is called molecular order while in the fast T-ramp DSC, an order leading to a phase-change was found in a sample characterized as amorphous by its X-ray pattern. The X-ray diagrams of the present treated samples have not been taken as a function of T. It is likely that they will become diffuse around 70°C i.e. well above the evolution of most of the heat. We do not think that it is inconsistent with the above statement that the dissolution followed by the last endotherm (ΔH_3) is cooperative as it would be for real crystals. Crystals deformed by strain may lose their X-ray diagram long before they melt. The authors of the NMR investigation conclude that molecular order is lost at Td, the temperature at which dissolution starts, which is not in agreement with the present IR and calorimetric studies which show that the double helix content of amylose is persistent throughout the dissolution. An explanation of the different result would be that the NMR spectra become unclear above Td masking the specific features of the double helix conformation. The loss of sharpness in ^{13}C NMR spectra of amorphous amylose has been remarked upon in an early study of amylose polymorphs.[3]

Quenched samples

Samples treated at different Tmax have also been quenched to room temperature (RT). FTIR analysis give a definite answer to the question of the relative contributions of the heating and cooling part of the treatment. The quenched sample at RT recovers the conformations it had before treatment. This is reasonable since quenching a solution is a known procedure to obtain network-rich gels. Analysis of quenched samples allowed the association of the 1022 cm^{-1} band with the network phase. The quenched samples were not analyzed in slow

calorimetry because the traces may have been obscured by a series of dissolution/recrystallization during the T-ramp likely to occur in these non-equilibrium samples. However, they will be dealt with in the course of further work on amylose-water systems.

Flory-Huggins equation and strained dissolution

In the equation for the chemical potential of the polymer and of the solvent in solution, there is no term to take account of strain. However, the elastic term, added to predict the swelling of cross-linked polymer samples[12] would suffice to correct the chemical potential of the present physically cross-linked samples. In those, the number of junctions is an unknown parameter whose value diminishes with treatment. One may wonder how some informative results can be obtained using the non-corrected equation for real solutions in amylose-water systems. This was done in a recent paper[7] where the relationship between Td and chain length showed that the Flory-Huggins relationship holds for low-medium degrees of polymerization. We think that the value of Td measured corresponds to the dissolution of free chains which are always present in a sample with a concentration which depends on the system.

The inadequacy of the equation will be shown in the calculated values of the polymer-solvent interaction parameter χ. The values of Td (55°C -119°C for 12 < polymerization degree < 55), obtained at a rate of heating one hundred times higher than the present one are difficult to compare to those in Table 4 because the values of ΔH_{diss} which would reveal the degree of non-equilibrium or of strain in these narrow fractions are not given. Note that the Flory-Huggins equation predicts that non-strained crystals dissolve in a range of Td in concentrated solutions. This is due to the fact that the first crystals dissolve in equilibrium

with a solvent and the last in equilibrium with a concentrated solution. However, as indicated by the difference between $\Delta H_{diss,\ fast\ T\text{-}ramp}$ and, $\Delta H_{diss,\ slow\ T\text{-}ramp}$, strain dissolution is the dominant mechanism in determining the range of Td observed in the present systems.

C. CORRELATION OF PHASE-CHANGES BY CALORIMETRY AND FTIR

The temperature treatment greatly changes the spectra of amylose-water mixtures as illustrated in Fig. 4. However, in these equilibrium samples, it is not the position of a band which changes but its relative intensity. Absorbance of the C-O stretching is distributed over a range of wavenumbers (1175-950 cm^{-1}). A band located at 1078 cm^{-1} has been found insensitive to treatment. By normalizing the spectra by the intensity of this band, comparison of the spectra is direct. The main changes due to treatment at Tmax are the following:

i. The right hand part of the spectra (1078-950 cm^{-1}) decreases while that in the left hand part (1175-1078 cm^{-1}) increases with Tmax. Following this observation, the 1078-950 cm^{-1} and 1175-1078 cm^{-1} regions have been then attributed respectively to vibrations in a strained (or strainable) and relaxed environment. ii. Specific bands have been paired in each region as belonging to strained and relaxed environment.

Analysis of polyethylene (PE) samples[24] has shown that the IR intensity cannot distinguish between short- and long-range order. This is reasonable because the size of the region to which responds an IR vibration is smaller than that corresponding to other techniques of measuring order. As a consequence, a crystallinity index, which follows short-range order by IR has to be larger than the X-ray crystallinity index. This was found for PE which has a specific tracer of crystallinity. In the case of amylose and of most of other polymers, long-range order does not leave a mark in the IR spectra, so long-range order is not measurable directly. In the treated samples, the growth of long-range order is linked with relaxation of the

strain. By attributing specific vibrations to strained and relaxed environments, one can follow indirectly the growth of long-range order.[26] In the fourth row of Table 1, the relative intensity of the region α (IR, relaxed), calculated as the fractional absorbance of the left region of the spectra has been listed as a function of Tmax. Table 5 reports the attribution of specific bands in the strained and relaxed regions of the IR spectra. It also gives a tentative association of endotherms of dissolution and IR bands. Two bands listed in Table 2, the 1078 and 1101 cm^{-1} bands, are not attributed to a specific environment because they change little with treatment.

In Fig. 7 a correlation is made of the integrated absorbance of the band at 1153 cm^{-1}, situated in the relaxed region, with the values of ΔH_1, the enthalpy of the less strained crystals. The network phase is relaxed, a condition which allows it to be meltable in the 6 K/h T-ramp. The values of ΔH_2 are correlated in Fig. 8 with a band in the relaxed region which also increases with Tmax. As better organization melts at higher T, ΔH_3 is correlated, in Fig. 9, with bands in the strained region, the 999 and 1045 cm^{-1} bands. It is interesting to note that when the network dissolves at 120°C, the absorbance of the recrystallized samples is allowed to shift from the strained to the relaxed side (1153 cm^{-1}). Relaxation favors organization to melt at lower T with the corresponding increase of ΔH_1 at the expense of ΔH_3.

D. ESTIMATION OF THE SINGLE AND DOUBLE HELICAL CONTENT IN TREATED SAMPLES

The presence of two crystalline modifications is revealed by the X-ray diagrams of Fig. 2 but a quantitative evaluation of the B and V component of the X-ray diagrams has not be

attempted. Instead, following some assumptions, the calorimetric and IR analysis offer the possibility to distinguish between the two in a semi-quantitative manner.

In Table 6, the fractions of simple-helices and double helices have been evaluated as a function of Tmax by combining the calorimetry and IR results which were both capable of observing modifications in the sample.

Single helix fraction

As the V crystals are made of single helices, they will by less strainable than those in the B crystalline modification. The endotherm of dissolution at low T, ΔH_1 is then associated with the meltable order made of single helices. Using the same value of ΔH_o as above one finds:

$$\text{Single helix fraction} = \Delta H_1 / \Delta H_o \qquad \text{eq. 7}$$

The value ranges from 0.02 to 0.28 as reported in Table 6. In the analysis of the IR spectra[26] the 1153 cm^{-1} band has been associated with a vibration in the environment of ordered single helices. The relative intensity of this band has been listed in the first column of Table 2. One sees that the trend with Tmax and also most of the values are found to be very similar in Tables 2 and 6. The calorimetric analysis supports the attribution of this band. As a consequence, one could speculate that the small amount of order first melted in the fast T-ramp of traces such as that of Fig. 1b, would be rich in the V modification. The loss of sharpness in the X-ray traces reported above Td in the literature indicates the long and short-range order do not disappear with the same kinetics in a T-ramp.[15]

Double helix fraction

The two other endotherms corresponding to the dissolution respectively of the network phase ΔH_2 and of the strained crystals ΔH_3 constitute a large fraction of ΔH_{diss}. They are associated with the dissolution of order made with double-helices. The reason behind this

assumption is that these orders are strainable and also that amylose is rich in double helix morphology. A fraction, non meltable in the conditions used with slow calorimetry, must be included. This fraction can be estimated from the band at 1022 cm^{-1} given in Table 2. This band is called the network band and is associated with a strained environment. Combining the two techniques, one finds:

Double-helical fraction = unmelted fraction + melted fraction

$$= \text{fractional absorbance at } 1022\ cm^{-1} + (\Delta H_2 + \Delta H_3) / \Delta H_o \qquad \text{eq. 8}$$

the fraction of double helix is given in Table 6 with another component, the sum of the 1078 + 1101 cm^{-1} bands.

$$\text{Other fraction} = 1078 + 1101\ cm^{-1} \text{ bands} \qquad \text{eq. 9}$$

The fraction of the double helical morphology is about 0.63 for the three highest values of Tmax, its meltable fraction increases with the treatment. This fraction is comparable with that found in amylose submitted to a thermal treatment[5] leading to a higher resistance to the amylase enzyme.

There is no reason why the sum of eqs. 7-9 should total 1.0 because the normalizing factors are the total absorbance when the IR absorbance is used and ΔH_o when the evaluation is made from the calorimetric trace. The fact that the sum is near 1 for Tmax = 95, 105 and 120°C means that the value of ΔH_o is reasonable. The reason why the sum of the fractions has a low value (0.81-0.86) for low crystallinity samples (for Tmax = 50°C and 70°C) is not clear. It looks as if a fraction is missing in the spectra which could be the amorphous amylose swollen in water. One needs further work to find the origin of this effect.

Table 6 Evaluation of the single and double helical relative intensity as a function of Tmax

Tmax (°C)	Single helix (eq. 7)	Double helix (eq. 8)			Other (eq. 9)
		Unmelted (1022 cm^{-1})	Melted	Total	
50	0.02	0.47	0.10	0.57	0.24
70	0.13	0.28	0.27	0.55	0.18
95	0.22	0.18	0.44	0.62	0.16
105	0.23	0.12	0.50	0.62	0.18
120	0.28	0.12	0.53	0.65	0.15

Reversibility of the traces

The trace of Fig. 5 indicates that the slow T-ramp has succeeded in dissolving a large fraction of the assumed total enthalpy of the fully ordered sample (147.5 / 180 = 0.82). One can wonder how much of this fraction will disentangle on cooling again. This was not done on amylose-water mixtures. However, in polyolefins solutions the heat flow was followed in the heating and cooling ramp. The cooling trace was a mirror image of the heating trace with two exotherms with different kinetics, the high-T part of which was attributed to crystallization of the strained morphology which had melted at high T in the heating ramp. This result points out to the fact that melting a strained morphology followed by recrystallization is not a condition sufficient for disentangling. A strained/double helical order does not lead after melting to a single helix morphology. However, in mixtures with a low viscosity, disentanglement occurs progressively during slow cooling and the non disentangled fraction has its strain diminished. On quenching after the high T-endotherm, the network or double helix morphology remains with a more fragmented order.

Non-equilibrium dissolution has been mentioned in the literature without reference to the physical phenomena behind it. A recurring feature of the traces of polyolefins solutions in the

course of disentanglement is the displacement towards low–T, even below Td, of the network endotherm. Such endotherms have been found in polysaccharides of different origins in presence of a low quantity of water.[14] They can be displaced at higher T by annealing. It is likely that due to the high concentration, a small fraction of order is relaxed and dissolves without strain and a small heat (<5 J/g) in a fast T-ramp (10 K/h).

High T treatment of amylose

Amylose-water mixtures which have undergone a high-T treatment exhibit high temperature endotherms which are history dependent and sometimes have a medium-size heat (20-25 J/g), in a fast T-ramp[10-11, 14] a feature which seems improbable according to the present discussion. Our answer[17] is that the heat treatment has weakened the network and hence diminished the building up of strain in the T-ramp allowing for a dissolution which is probably still incomplete but larger than in the non-treated samples.

Comparaison of ΔH_{total} with ΔH_m of amorphous amylose

The value of ΔH_{total} is about twice as large as that of amorphous amylose (60 J/g). From the values of the heat of immersion, the swellable fraction of amorphous amylose was estimated to be 0.5.[17] After treatment, the meltable order increases but the value of $\Delta H_{diss,\ slow\ T\text{-}ramp}$ depends on the history and conditions of melting as said above.

CONCLUSION

Analysis of amylose-water mixtures (70/30 W/W) having been submitted to a slow cycle of temperature between RT and Tmax (50 < Tmax < 120°C) was made by X-ray diffraction, fast T-ramp DSC, slow calorimetry and FTIR. The sample crystallinity increases with Tmax and reaches a value estimated to be 0.5. The peaks associated with the V and B crystalline

modifications are present in the sample. The very small heats of dissolution of the treated samples obtained by fast T-ramp DSC (0.5 J/g) point strongly to an arrested dissolution due to strain. By contrast, the large heats of dissolution found in a slow T-ramp (6 K/h) (20-140 J/g) reflect the relaxation of the material and the change of crystallinity of the samples after treatment. In the slow T-ramp, the three endotherms observed are the consequence of fractionation of the ordered chains due to strain. It is assumed that the single helix V type organization is less strainable than the double helix crystals. The low-T endotherm is associated with the dissolution of the V modification, the high-T endotherm to that of the B crystals and the large–span endotherm to the dissolution of the small-range order in the network. Using the IR analysis of the same samples, the relative intensities of single helix and double helix morphology in the sample are given. Quenching a solution leaves the double-helix content intact while a slow crystallization leads to the growth of a sizeable amount of the V crystalline form associated with a specific IR band.

The main conclusion of this work is that the dissolution of order in mixtures rich in hydrogen bonds such as the polysaccharide-water systems cannot be followed by fast T-ramp DSC. On the other hand, IR spectra in the C-O stretching regions give quantitative information on the phases in the treated samples which can be correlated with the enthalpies of disordering obtained in a slow T-ramp. Double helical order is thought to be highly heat resistant, its apparent disappearance around Td may be due to the inability of usual techniques to quantify deformed order.

ACKNOWLEDGEMENTS

The financial support of the National Science and Engineering Research Council of Canada is gratefully acknowledged. We would also like to thank Dr. Patricia LeBail (INRA, Nantes) for

her helpful discussions on X-ray diffraction results.

REFERENCES

1. Wunderlich, B. Macromolecular Physics; Academic Press: New York, 1976, Vol. 3.
2. Nguyen, H. P.; Delmas, G. Macromolecules 1985, 18, 1235.
3. Horii, F.; Yamamoto, H.; Hirai, A.; Kitamaru, R.; Carbohydrate Research 1987, 169, 29.
4. Gidley, M. J.; Bociek, S. M. J. Am. Chem. Soc. 1985, 107, 7040.
5. Gidley, M. J.; Cooke, D.; Darke, A. H.; Hoffman, R. A.; Russel, A. L.; Greenwell, P. Carbohydrate Polymers 1995, 28, 23.
6. Hayashi, A.; Kinoshita, K.; Miyake, Y.; Cho, C. H. Agri. Biol. Chem. 1983, 47, 1699.
7. Moates, G. K.; Noel, T.; Parker, R.; Ring, S. G. Carbohydrate Research 1997, 298, 327.
8. Noel, T. R.; Ring, S. G. Carbohydrate Research 1992, 227, 203.
9. Durrani, C. M.; Donald, A. M. Polym. Gels Network 1995, 3, 1.
10. Sievert, D.; Wursch, P. Cereal Chem. 1993., 70, 333.
11. Sievert, D.; Pomeranz, Y. Cereal Chem. 1989, 66, 342.
12. Hollinger, G.; Kuviak, L.; Marchessault, R. H. Biopolymers 1974, 13, 879.
13. Biliaderis, C. G. in Water relationship in food, Levine, H; Slade, L Eds.; Plenum Press, New York, 1991, p251.
14. Appelqvist, I. A. M.; Cooke, D.; Gidley, M. J.; Lane, S. J. Carbohydrate Polymers 1993, 20, 291.
15. Nakazawa, F.; Noguchi, S.; Takahashi, J.; Takada, M. Agric. Biol. Chem. 1984, 48, 2647.
16. Krueger, B. R.; Knitson, C. A.; Inglett, G. E.; Walker, C. E., J. Food Sci. 1987, 52, 715.
17. Le Lay, P.; Delmas, G. Carbohydrate Polymers 1998, 37, 49.
18. Shiotsubo, T.; Takahashi, K. Agric, Biol. Chem. 1984, 48, 9.

19. Shiotsubo, T.; Takahashi, K. Carbohydrate Research 1986, 158, 1.

20. Gidley, M. J.; Bulpin, P. V. Macromolecules 1989. 22, 34.

21. Nguyen, H. P.; Delmas. G. Macromolecules 1992, 25, 414.

22. Doublier, J. L.; Cole, I.; Hamas, G.; Charlet, G. Prog. Colloid Polym. Sci. 1992, 90, 1.

23. Delmas, G., J. Polym. Sci., Polym. Phys Ed., 1993, 31, 2011.

24. Zhang, Z.; Nguyen, H. P.; Bernazzani, P.; Lapes, I.; Delmas, G. Can. J. Chem. 1997, 75, 1354.

25. Bernazzani, P.; Bich, V. T.; Nguyen, P.; Haine, A.; Chapados, C.; Dao, L. H.; Delmas, G. Can. J. Chem. 1998, 76, 1674.

26. Bernazzani, P.; Chapados, C.; Delmas, G. "Phase-change in amylose-water mixtures as seen by FTIR", Submitted to Biopolymers.

27. Crystallization in a T-ramp lead to range of lamellar thickness of the crystals in the samples and in turn to a range of Td. However, this feature widens the peak of dissolution but is not expected to lead to the large overall endotherm observed here (between 50-140°C). The effect of changing Tc, the isothermal crystallization temperature, has been investigated on polyolefin solutions. Slower crystallization at higher Tc raises Tm or Td by a few K. Strain melting is not considered in these works and with some justification because solutions are highly disentangled due to the choice of sample and the high dilution.

28. Cooke, D.; Gidley, M. J. Carbohydrate Research 1992, 227, 103.

29. Nguyen, H. P.; Delmas. G. Thermochimica Acta, 1994, 238, 257.

CHAPITRE 6

6. CONCLUSION

Le sujet de la thèse est la détermination de la structure du système amylose–eau et la recherche des façons de pouvoir contrôler la morphologie de ce biopolymère. Le modèle qui existait au début de nos travaux pour la structure de ce système était un modèle à trois phases: deux phases cristallines (B et V) et une phase amorphe. Comme ce modèle n'expliquait pas tous les phénomènes physiques qui étaient observés nous avons développé un modèle à cinq phases*. Aux trois phases précédentes nous avons ajouté deux phases semi-ordonnées dont les chaînes ont une mobilité intermédiaire entre celle des chaînes des phases cristallines et amorphe. La présence de jonction entre les chaînes réduit leur mobilité.

L'objectif de cette thèse est de développer une méthodologie qui permettrait de contrôler, par un traitement approprié, la composition phasique du système amylose-eau et de la caractériser. Pour atteindre cet objectif, nous avons d'abord fait une étude fondamentale sur un polymère modèle, le polyéthylène. Cette recherche a conduit aux deux premiers articles de cette thèse, chacun développant deux techniques nouvelles soit la calorimétrie lente et la spectroscopie IR avancée. Nous entendons par spectroscopie IR avancée, l'étude de l'effet de l'environnement d'un groupement chimique sur ses vibrations caractéristiques. Ces deux techniques ont permis de montrer que des structures enchevêtrées étaient présentes dans les polymères synthétiques. Les deux autres articles présentés dans cette thèse utilisent également la spectroscopie IR et la calorimétrie lente pour élucider la composition phasique du système amylose-eau. Dans le quatrième article, nous avons pu corréler quantitativement

---

* Dans l'article, nous arrivons à la conclusion qu'il y a trois phases. Ces trois phases se divisent en réalité de la façon suivante: la phase cristalline comprend les deux structures B (hexagonale) et V (orthorhombique); la phase intermédiaire comprend la structure d'enchevêtrements et la structure de liaisons hydrogène et la structure amorphe. Nous avons donc cinq structures. Ces structures sont en réalité des phases distinctes et il est plus approprié de les appeler phases et il y en a cinq. C'est pourquoi dans cette conclusion nous parlerons des cinq phases.

les résultats de DSC_{Lent} et de spectroscopie IR. Nous allons maintenant succinctement présenter la problématique, les conclusions et la contribution originale de chaque article.

6.1 Article 1: « Analysis of physical and chemical networks by slow DSC and turbidimetry »

6.1.1 Problématique

Dans cet article, nous répondons à plusieurs problématiques. La plus importante consiste à déterminer l'existence de phases intermédiaires qui seraient dues à la tension et en déterminer leur quantité. Nous voulions également déterminer l'effet de ces enchevêtrements sur les propriétés physique des macromolécules. Nous avons développé une méthodologie utilisant la DSC_{Lent} qui permet l'observation entre les phases cristalline et amorphe d'une phase intermédiaire qui est attribuée aux enchevêtrements des chaînes. Le point fondamental de l'article montre qu'il est possible de quantifier les enchevêtrements dûs à leur ordre à petite distance. Lors de différents traitements qui modifient la composition phasique de l'échantillon il sera alors possible de quantifier cette phase.

6.1.2 Conclusions

Cet article souligne l'importance de la vitesse de chauffage en calorimétrie lors de l'étude de systèmes métastables comme les polymères. Ainsi, cet article montre que la DSC_{Lent} permet d'observer des phénomènes que la DSC_{Rapide} ne peut observer. La figure 1 de l'article 1 montre un endotherme qui est étalé sur une large gamme de température entre 150 et 240 °C et qui est situé à une température plus élevée que la température de fusion des cristaux (132 °C). Cet endotherme présent uniquement dans la trace de DSC_{Lent}, double ou triple la chaleur

de fusion du polymère.

L'endotherme obtenu à haute température est associé, à la fusion de cristaux sous tension. Cette tension est due à la présence d'enchevêtrements qui forment des nœuds qui se tendent lorsque l'augmentation de température provoque une augmentation de volume. L'association avec les enchevêtrements est clair lorsque l'on compare une trace de DSC_{Lent} du PE réticulé chimiquement avec celle du PE non réticulé. Dans la figure 1 de l'article 1, nous comparons les deux traces. La chaleur de l'endotherme à haute température est nettement plus large chez l'échantillon réticulé parce qu'il a d'avantage d'enchevêtrements. Ces résultats montrent que la technique de DSC_{Lent} permet l'observation de la tension associée avec la phase intermédiaire d'enchevêtrements. La quantité d'enchevêtrements est contrôlée par la température où le polymère est chauffé et par la vitesse de refroidissement.

6.1.3 L'utilité de ce travail pour le système amylose–eau

L'utilisation d'une rampe lente de température a permis la détermination de la tension dans la structure du polymère. De plus, la mesure de l'endotherme de fusion donne une valeur quantitative de la présence d'un ordre à courte distance. Cet ordre doit être commun à tous les polymères incluant l'amylose. Par conséquent, le même stratagème devrait permettre d'observer et de contrôler les phases de réseaux de l'amylose.

Les calorimétries rapide et lente permettent d'observer des transitions de phases mais ne permettent pas de connaître des groupes fonctionnels en jeu. La spectroscopie IR a été choisie pour combler cette lacune. C'est l'objet du deuxième article.

6.2 Article 2:«FTIR analysis of the phase content in low-density polyethylene»

6.2.1 Problématique

Pour les systèmes polymériques, l'article 2 sert à déterminer les points suivants: 1) la spectroscopie IR permet-elle de suivre les effets des modifications phasiques? 2) la spectroscopie IR permet-elle de suivre d'une façon spécifique l'interphase composée d'enchevêtrements de chaînes? 3) la spectroscopie IR permet-elle d'observer l'ordre à courte distance? 4) est-il possible de faire la corrélation entre les mesures IR et les mesures de DSC_{Lent}?

6.2.2 Conclusions

Dans l'article 1, nous avons trouvé qu'il y avait un réseau semi-ordonné d'enchevêtrements et que la tension entre les chaînes résulte de l'augmentation de volume lors de l'application d'un traitement thermique. La conséquence de cette augmentation de volume est de serrer les nœuds formés par les enchevêtrements des chaînes. Cet article montre que la spectroscopie IR permet de suivre les phases tendues dans un polymère. La figure 3 de l'article 2 montre que la région de 725 cm^{-1} contient quatre bandes qui peuvent être attribuées à trois phases: les deux bandes situées à 730 et 720 cm^{-1} furent attribuées à la phase orthorhombique [61], la bande à 725 cm^{-1} fut attribuée à la phase amorphe et la bande à 717 cm^{-1} à la phase monoclinique. Cette bande répond aux équilibres de tension/relaxation dans l'échantillon.

Cet article montre également l'importance de la contribution de l'ordre à courte distance. La quantité d'ordre total obtenue par spectroscopie IR est plus grande que celle mesurée par la DSC_{Rapide} et la diffraction des rayons X (tableau 3, article 2). L'observation de la présence de l'ordre à courte distance obtenue par IR, mène à une vision plus réaliste de la structure du

PE.

Les méthodes de spectroscopie IR et de mesure de densité mènent à des valeurs différentes de l'ordre présent dans le PE. La mesure par densité est toujours plus basse que celle trouvée par spectroscopie IR (figure 4 de l'article 2). Ce phénomène est dû au fait que la spectroscopie IR permet l'observation de l'ordre à grande et à courte distance. Notons cependant que les variations observées suite aux traitements thermiques dans les phases cristalline et d'enchevêtrements sont semblables lorsqu'elles sont observées par spectroscopie IR et par mesure de densité (figure 4, article 2). La méthode peut servir à évaluer la morphologie de différents polymères en comparant différents échantillons. De plus, la compréhension de plusieurs phénomènes physiques dépend de la capacité d'évaluer l'interphase composée d'enchevêtrements.

Le tableau 3 de l'article 2 montre que par un traitement thermique approprié, il est possible de modifier la composition phasique du PE. De plus, la température maximum d'un cycle de chauffage et de refroidissement très lent (3 K/h) déplace la position de la bande associée à l'état de tension des enchevêtrements. Le tableau 4 de l'article 2 montre qu'une analyse tenant compte de trois phases, incluant la présence d'une phase de tension, est meilleure.

6.2.3 L'utilité de ce travail pour l'étude de l'amylose

Cet article montre la validité de la technique hybride IR-DSC_{Lent} développée pour observer l'interphase composée d'enchevêtrements. La problématique de la structure de l'amylose consiste selon nous, en la caractérisation des deux phases intermédiaires, celle due aux enchevêtrements et celle due aux liaisons hydrogène. Le développement d'une méthodologie permettant l'évaluation de la phase d'enchevêtrements dans une molécule modèle telle que le

PE est une étape importante. Comme la spectroscopie IR peut caractériser différents types de ponts hydrogène, cette technique devrait donner des informations sur la phase réseau riche en liaisons hydrogène.

Cet article confirme l'importance de l'étude de la composition phasique d'un matériau et de l'ordre à courte distance. Une corrélation des propriétés physiques et thermiques avec la composition phasique ne peut être valide sans tenir compte de cet ordre. L'intérêt des techniques de DSC_{Lent} et de spectroscopie IR est donc également important pour la détermination de l'ordre à courte distance qui doit être présent dans tous les systèmes polymériques incluant l'amylose.

La méthode de contrôle des phases cristallines et non cristallines développée pour le PE s'applique à l'amylose.

6.3 Article 3 : « Phase change in amylose-water mixtures as seen by FTIR »

6.3.1 Problématique

L'analyse des phases du PE par IR s'est faite en absence de solvant. Nous devons adapter notre technique à des mélanges amylose-eau. Nous devons également confirmer qu'un traitement thermique modifie autant la composition phasique du système amylose-eau qu'il modifie celle du PE. Après avoir choisi la région du spectre la plus prometteuse, notre effort va se porter sur la corrélation entre les variations d'intensité des différentes bandes et les transformations de phase attendues comme une conséquence du traitement thermique.

6.3.2 Conclusions

Nous avons choisi la région du spectre entre 1175 et 950 cm^{-1} puisque l'eau interfère peu dans cette région (figure 2 de l'article 3). Les traitements effectués conduisent à de grandes

différences dans les spectres de l'amylose-eau (figure 3 de l'article 3). Une analyse quantitative de ces spectres qui utilise les intensités maximales, nous permet d'associer des bandes avec la tension dans l'échantillon. Nous avons identifié une région tendue (1078-950 cm^{-1}) et une région non tendue (1175-1078 cm^{-1}) (figure 6 de l'article 3). La variation de l'intensité des bandes dans ces régions en fonction de la température (figure 2 de l'article 3) nous permet d'identifier un changement de phase à 70 °C associé à la température de transition vitreuse, Tg (figure 8 de l'article 3). La variation de l'intensité des bandes dans ces mêmes régions en fonction de la température maximum du traitement thermique, Tmax, (figure 3 de l'article 3) nous permet d'identifier deux changements de phase, l'un à 70 °C (Tg) et l'autre à environ 115 °C. Ce dernier est associé à la dissolution de l'amylose dans l'eau (figure 9 de l'article 3).

Nous avons interprété ces deux changements de phase comme faisant partie d'un seul phénomène, celui de la dissolution lente des chaînes d'amylose tendues par les enchevêtrements et les liaisons hydrogène. La bande à 1022 cm^{-1} est identifiée comme traceur de gel.

6.3.3 Nouveautés

Notre connaissance de la littérature des polymères synthétiques nous a conduit à un traitement des mélanges amylose-eau qui engage deux caractéristiques: la lenteur de la rampe de température et la cristallisation lente. Ces conditions sont loin des conditions habituelles où les traitements consistent en une chauffe rapide suivie d'une trempe.

Les auteurs de ces recherches font l'hypothèse que le spectre d'un échantillon trempé à partir de Tmax, reflète le spectre à Tmax. L'effet de la variation de Tmax observé par ces auteurs, est faible. Nous avons montré que dans des systèmes riches en amylose, le spectre obtenu

après la trempe est indépendant de Tmax. Nous avons découvert que pour stabiliser des états différents il faut faire une recristallisation lente.

Ce résultat a des conséquences dans les analyses qui utilisent non seulement la spectroscopie IR, mais également d'autres techniques comme la RMN. Pour observer des différences importantes dans les analyses, il faut utiliser des échantillons recristallisés et non trempés comme c'est la pratique courante.

Les organisations en doubles hélices dont les chaînes ont une mobilité réduite, peuvent être tendues. Nous avons donc associer la région tendue du spectre IR à l'environnement des doubles hélices et la région non tendue à celui des simples hélices.

6.4 Article 4: « Double helical network in amylose as seen by slow calorimetry and FTIR »

6.4.1 Problématique

Dans cet article, nous reprenons les échantillons d'amylose-eau traités thermiquement tel que décrit dans l'article 3. L'analyse par spectroscopie IR de ces échantillons révèle qu'ils présentent une grande différence de composition phasique reliée à Tmax. Nous nous demandons si des différences aussi spectaculaires seront obtenues à partir de leur analyse par DSC_{Lent}. Un des résultats de l'analyse IR était d'identifier des régions du spectre qui correspondent à des régions tendues et non tendues et de suivre leurs variations avec Tmax. La calorimétrie lente dont la spécificité est de séparer l'ordre qui fond ou se dissout selon la tension présente (article 1), pourrait confirmer l'analyse de phases faite par FTIR (article 3). Nous tiendrons compte de travaux précédents [29] qui utilisent la DSC_{Lent} (1K/h) pour dissoudre les phases non cristallines (phase d'enchevêtrements et phase riche en liaisons

hydrogène) de l'amylose amorphe non traité. Ce travail avait permis de mesurer une chaleur de dissolution de l'amylose indécelable en DSC_{Rapide}. La valeur de l'enthalpie de dissolution obtenue (60J/g), était de l'ordre de 10 fois supérieure à celle obtenue sur des amyloses cristallins par DSC_{Rapide} et s'étalait sur 60 °C. Si les amyloses traités ont des endothermes de dissolution comparables à ceux de l'amylose non traités, on attend qu'une corrélation entre les endothermes de dissolution et des bandes spécifiques du spectre soit réalisable.

6.4.2 Conclusions

Les spectres de rayons X du système amylose-eau montrent que le traitement augmente l'ordre à grande distance. La fraction de cet ordre était de 0.05 dans l'amylose non traité et passe à 0.4-0.5 après un traitement thermique. Une valeur élevée de Tmax augmente l'ordre en favorisant la forme V (figure 3 de l'article 4). La dissolution de cet ordre devrait donner une chaleur comparable à celle d'un PE de même cristallinité observée par rayons X (~ 100 J/g). Les chaleurs de dissolution de DSC_{Rapide} varient entre 0 et 4 J/g tandis que celle de DSC_{Lent} varient entre 22 et 150 J/g. Nous en concluons que même l'ordre à grande distance dans des systèmes fortement liés n'est pas mesurable par DSC_{Rapide}. Sachant qu'une rampe très lente modifie la tension dans les phases de réseaux, nous avons utilisé une vitesse de chauffe lente (6 K/h). Celle ci est cependant plus rapide que la vitesse utilisée dans les mesures sur l'amylose non traité (1 K/h). Cette stratégie nous a permis d'étaler les endothermes de dissolution entre 55 et 135 °C. La différence entre les coopérativités des dissolutions, révélée par la forme des endothermes et les températures des maxima de flux de chaleur, nous permet d'identifier trois endothermes de dissolution et leurs enthalpies respectives notées ΔH_1, ΔH_2, et ΔH_3. La correspondance entre les chaleurs de dissolution et les spectres IR est basée sur l'hypothèse suivante : une organisation faite de chaînes en simple

hélice est plus mobile que celle formée de doubles hélices, donc moins susceptible de devenir tendue. En conséquence, l'endotherme à basse température correspond à l'organisation en simple hélices. En suivant les résultats de l'article 3 où certaines bandes sont attribuées à des environnements de simples et doubles hélices, nous pouvons faire une corrélation entre les traces calorimétriques et les spectres. Les figures 7, 8, 9 de l'article 4, donnent la corrélation de ΔH_1, ΔH_2, et ΔH_3 avec quatre bandes du spectre (ΔH_3 est associée à deux bandes dans la région tendue, situées à 1045 et 999 cm^{-1})

6.4.3 Nouveautés

La DSC_{Rapide} a été utilisée depuis plus de 50 ans pour caractériser l'ordre dans l'amylose et l'amidon. Les chaleurs de dissolutions obtenues sont de l'ordre de 5-15 J/g. Des mesures de DSC_{Lent} sur des échantillons similaires donnent des valeurs entre 100 et 150 J/g. Notre travail démontre clairement que la DSC_{Rapide} n'est pas une méthode satisfaisante pour suivre la dissolution de l'ordre présent dans des systèmes très cohésifs comme l'amylose.

De nombreux travaux utilisent la RMN de l'état solide pour caractériser les simple et double hélices dans l'amylose. L'analyse de ces différentes conformations par IR a suscité peu de travaux jusqu'à maintenant. Ceci peut venir du fait que les échantillons analysés avaient des spectres très semblables. Nous avons pu faire la corrélation entre les spectres IR et la calorimétrie parce que nous avons préparé des échantillons dont la composition phasique était très différente. La fraction de simples hélices non tendues trouvée semblable par calorimétrie et par spectroscopie IR (figure 7 et tableau 6 de l'article 4) montre que cette stratégie est efficace.

6.4.4 Note complémentaire qui n'est pas discutée dans l'article 4 sur le réseau de liaisons hydrogène

Des études antérieures sur la DSC_{Rapide} de molécules telles que le glucose et la cellulose ont démontré qu'un élargissement des bandes résulte de l'hydratation de ces composés. La figure 5, tirée de la référence [117] montre une trace de DSC_{Rapide} du glucose hydraté (a) et lyophilisé (b). On observe que l'endotherme de dissolution du glucose hydraté est plus large. De plus, Chapados et Fitzback ont également observé que la déshydratation du $MgSO_4$ $7H_2O$ pouvait être suivie par calorimétrie. Sur la figure 6 qui montre une telle trace, on observe que chaque molécule d'eau qui se dissocie du système provoque un endotherme facilement observable en DSC. Ce phénomène est comparable à l'augmentation du détail dans le signal retrouvé dans les traces de DSC_{Lent} du système amylose-eau. Ces deux observations corroborent les résultats trouvés en DSC_{Lent} et montrent la présence et la contribution à la tension des liaisons hydrogène. Il est possible d'envisager d'autres méthodes pour prouver par DSC_{Lent}, l'existence de la transformation des groupements O-H liés par des ponts hydrogène en O-H libre. Si on effectuait la méthylation de l'amylose par exemple, les liaisons hydrogène seraient éliminées et la trace de DSC_{Lent} du système amylose-eau devrait être plus semblable à celle du PE. C'est un projet à explorer dans le futur.

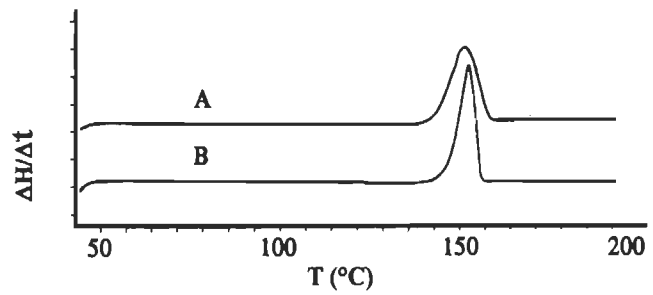

Figure 5 Trace de DSC_{Rapide} du glucose hydraté (A) et lyophylisé (B) [117]

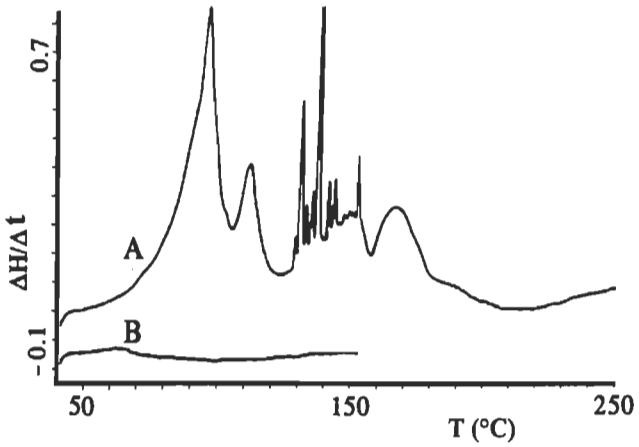

Figure 6 Trace de DSC_{Rapide} montrant les étapes de la déhydratation(A) du $MgSO_4 \bullet 7H_2O$ [117]. En B, on montre une trace de $MgSO_4$ préalablement déshydraté.

6.5 Résultat global

Notre étude a été développée dans trois secteurs. Le premier secteur traite d'une nouvelle méthodologie d'analyse mise au point pour déterminer la composition phasique du système amylose-eau. Cette méthodologie est une méthodologie hybride qui combine la spectroscopie IR et la DSC_{Lent}. Le deuxième secteur fait état de la détermination de deux nouvelles structures pour le système. Ces deux structures qui sont des réseaux semi–ordonnés sont composés d'enchevêtrements et de liaisons hydrogène. Ces deux structures s'ajoutent aux trois structures qui avaient été mises en évidence auparavant. Le troisième secteur fait état du développement d'une méthodologie basée sur des traitements thermiques pour contrôler la composition phasique du système.

6.5.1 Méthodologie d'analyse de l'amylose

Dans le premier secteur de cette étude, nous avons développé une nouvelle méthode d'analyse de la composition phasique du système amylose-eau. Nous avons d'abord évalué

l'efficacité des techniques préalablement utilisées, pour ensuite développer une nouvelle méthodologie qui comble les lacunes des méthodes existantes. Le tableau 1 compare les méthodes qui existaient avant notre travail et celles que nous avons développées (DSC_{Lent} et spectroscopie IR avancée).

Le tableau 1 montre que la DSC_{Rapide} de même que la diffraction des rayons X ne sont pas

Tableau 1 Méthodes analytiques pour la détermination des phases de l'amylose

Structure	DSC_{rapide}	DSC_{lente}	Rayons X	IR avancé	Hybride DSC_{lente}–IR
Cristaux B	2[a]	5[b]	4[d]	5[e]	5
Cristaux V	2[a]	5[b]	4[d]	5[e]	5
Réseaux d'enchevêtrements	0	4[c]	0	4[f]	5
Réseaux de liaisons hydrogène	0	4[c]	0	3[f]	4
Amorphe	0	0	0	5	5

Légende: 0, non utile à 5, très utile

[a] la DSC_{rapide} bien que sensible à la cristallinité totale ne permet pas de distinguer entre les cristaux B et V.

[b] la DSC_{lente} permet de distinguer la dissolution des cristaux B et V et de l'ordre à petite distance.

[c] la DSC_{lente} permet l'observation de la dissolution combinée des deux réseaux, sans pouvoir évaluer leur contribution respective à la chaleur observée.

[d] la diffraction des rayons X ne mesure pas l'ordre à courte distance.

[e] un traceur IR non ambigu d'ordre tridimensionnel n'existe pas pour les polymères excepté pour le PE. L'association de la position d'une bande à une forme cristalline donnée est donc circonstancielle.

[f] dans la région IR de 1100 cm^{-1} il est difficile de séparer les deux types de réseaux.

des méthodes suffisantes pour étudier les phases de l'amylose. En effet ces méthodes sont insensibles aux réseaux d'ordre à courte portée et ne mesurent que partiellement la quantité de cristaux contenue dans l'échantillon. L'utilisation de la DSC_{Lent} permet de quantifier les deux phases cristallines et les deux types de réseaux contenus dans le système amylose–eau. Enfin, la spectroscopie IR permet la détermination de toutes les phases mais doit être corrélée

avec une autre technique afin de faire l'attribution des bandes. La méthodologie hybride IR–DSC_{Lent} que nous avons développée dans les articles 2 et 4 s'est avérée une bonne méthode pour la détermination des phases dans les polymères. Avec ces techniques nous avons mis en évidence la présence de réseaux semi–ordonnés en plus des réseaux ordonnés et de la phase amorphe dans le système amylose–eau.

6.5.2 Détermination des réseaux semi–ordonnés

L'utilisation de la calorimétrie en rampe lente de température, permet l'observation dans le polyéthylène (PE), d'un endotherme très large à une température plus élevée que la température de fusion. La DSC en rampe rapide de température est incapable d'observer ce phénomène. En comparant cet endotherme chez le PE avec la trace de fusion d'un PE réticulé, nous avons associé le pic endothermique à haute température avec la fusion de cristaux sous tension, la tension étant due aux enchevêtrements entre les chaînes.

Les traces de DSC_{Lent} à 6 K/h du système amylose-eau présentent également un endotherme très large à une température plus élevée que la température de dissolution. Cet endotherme n'est pas observable par DSC_{Rapide}. Le large endotherme retrouvé dans les traces de DSC_{Lent} est similaire à celui retrouvé dans les traces du PE et est attribué à la dissolution sous tension de l'ordre entre les chaînes d'amylose. L'existence de la tension est donc un concept qui peut être généralisé à tous les polymères.

L'attribution de bandes du spectre IR aux phases cristalline, tendue et amorphe dans le PE, a permis une évaluation quantitative de la composition phasique de ce polymère. En comparant avec les traces de DSC_{Lent}, nous avons confirmé que la tension retrouvée dans l'amylose était due à la quantité d'enchevêtrements présente dans le polymère. Nous avons fait la corrélation de bandes spécifiques aux vibrations d'élongations C-O et C-C du spectre IR avec les trois

endothermes du DSC_{Lent}. La corrélation des résultats obtenus par les deux techniques confirme nos hypothèses.

À l'aide des résultats de DSC_{Lent} et de spectroscopie IR nous montrons qu'un modèle qui inclut deux phases cristallines B, et V et une phase amorphe ne peut expliquer les phénomènes observés. Nos résultats calorimétriques et spectroscopiques nous conduisent à ajouter deux phases semi–ordonnées : les réseaux de chaînes enchevêtrées et de liaisons hydrogène.

Tableau 2 Effet du traitement sur les fractions des bandes du spectre IR du système amylose-eau.

	Traitements						
	Refroidissement lent (3 K/h) Tmax (°C)					Trempé Tmax	
	50	70	95	105	120	Tous[a]	
Position (cm^{-1})	**Fraction**						**Attribution**
1153	0.07	0.12	0.20	0.18	0.27	0.12	Simple hélice
1126	0.05	0.07	0.11	0.11	0.19	0.06	Simple hélice tendue
1045	0.12	0.19	0.18	0.15	0.14	0.20	Double hélice tendue
1022	0.42	0.28	0.21	0.15	0.14	0.28	Amorphe
999	0.09	0.15	0.17	0.21	0.17	0.17	Double hélice tendue

[a] Tmax n'a aucun effet sur le spectre IR du système amylose-eau trempé

6.5.3 Contrôle de la composition phasique

Le tableau 2 résume l'effet du traitement sur les bandes du spectres IR du système amylose-eau. Nos résultats montrent d'une part, qu'une cristallisation lente est essentielle pour obtenir des variations dans le spectre et d'autre part, qu'avec Tmax, les chaînes passent de doubles

hélice en simples hélice. Un refroidissement lent nous permet donc de contrôler la composition phasique du système amylose–eau. Nos résultats de DSC_{Lent} montrent également de grandes différences selon la rampe de température (tableau 3). Un refroidissement très lent favorise la relaxation de la tension et permet la dissolution de l'amylose dans l'eau. L'étalement de la dissolution permet de décomposer la trace de DSC_{Lent} en trois endothermes. En combinant les résultats tirés des spectres IR avec les dissolutions par DSC_{Lent}, nous avons associé les trois endothermes respectivement avec la dissolution des simples hélices, des simples hélices tendues et des doubles hélices tendues. Une détermination de la composition phasique du système amylose-eau a donc pu être effectuée.

Tableau 3 Effet du traitement sur les chaleurs de dissolution des traces de DSC_{Lent} du système amylose-eau.

	Traitements						
	Refroidissement lent (3 K/h) Tmax (°C)					Trempé Tmax	
	50	70	95	105	120	Tous[a]	
Intervalle de dissolution (°C)	**ΔH (J/g)**						**Association avec l'IR** (cm^{-1})
55-85	3.7	23.5	39.3	42.5	51.2	4	1153
60-130	9.1	13.8	34.3	44.4	68.3	0	1126
90-135	8.8	34.8	45.0	45.0	28.0	0	1045, 999

[a] Tmax n'a aucun effet sur la trace calorimétrique du système amylose-eau trempé

6.6 Conclusion finale

L'amylose est un composé très important puisqu'il est impliqué dans de nombreuses industries telles les industries du textile et des pâtes et papiers, l'industrie pharmaceutique et l'industrie alimentaire. L'amylose est pour cette raison un composé très étudié. La force

motrice de ces recherches est l'établissement d'une méthodologie qui permet le contrôle des propriétés physiques de l'amylose. En effet, le contrôle des propriétés peut simplifier certaines étapes de production, tout en améliorant les qualités du produit final.

Ce projet de thèse porte sur l'étude et le contrôle des phases du système amylose-eau. Nous avons fait les contributions suivantes aux connaissances de ce système: 1) mise au point des techniques analytiques qui permettent d'étudier la composition phasique; 2) détermination de la structure de l'amylose en mettant en évidence deux phases intermédiaires inédites (enchevêtrements et liaisons hydrogène); 3) développement d'une méthodologie de contrôle des phases de l'amylose.

6.6.1 Mise au point de la méthodologie

La détermination de la composition phasique de l'amylose a nécessité le développement d'une méthode combinant la spectroscopie IR et la DSC_{Lent}. La section 6.5 nous a permis de noter que ces deux techniques se complètent et permettent la détermination de la composition phasique de l'amylose. Nous avons fait la corrélation des thermogrammes obtenus par DSC_{Lent} et des spectres IR. Des cinq phases observées, deux phases sont cristallines (B et V), deux phases sont des réseaux semi–ordonnés (enchevêtrements et liaisons hydrogène) et une phase est amorphe.

6.6.2 Réseaux semi–ordonnés

Le réseau semi-ordonné dans une molécule non polaire comme le PE est fait de chaînes dont la mobilité est diminuée par les enchevêtrements. Dans l'amylose, les liaisons hydrogène et les enchevêtrements concourent à former les jonctions du réseaux. La calorimétrie ne peut quantitativement séparer les deux. L'étude de la région des vibrations d'élongation O-H par spectroscopie IR qui pourrait isoler le réseau de liaisons hydrogène, n'a pas été faite dans ce

travail.

6.6.3 Contrôle des propriétés

Nous avons pu suivre les variations de composition phasique du système amylose-eau en fonction de divers traitements thermiques. Ainsi il a été possible de déterminer exactement l'effet de la température maximale et des vitesses de chauffe et de refroidissement sur la quantité de phases. Cette détermination rend possible le contrôle de la composition phasique et donc des propriétés physiques de l'amylose.

6.6.4 Applications industrielles

Le contrôle des propriétés physiques par le contrôle de la composition phasique a des répercussions intéressantes sur plusieurs industries notamment dans les domaines alimentaire et pharmaceutique. Du côté de l'alimentation, une augmentation de la quantité de réseau semi-ordonné d'enchevêtrements provoque une augmentation de la résistance à l'attaque par l'enzyme amylase. Ainsi, une augmentation en enchevêtrements mène à une dégradation plus lente. Un simple traitement thermique permet de varier la quantité de cette phase et donc de contrôler la résistance à la dégradation. L'industrie alimentaire pourrait appliquer cette méthodologie pour accroître la conservation des aliments à base de glucides complexes sans avoir recours à l'ajout d'agents chimiques.

Dans le domaine pharmaceutique, l'amylose est utilisé comme matrice pour le relarguage lent des médicaments. Le temps et l'uniformité du relarguage dépendent de la cristallinité et de la quantité de réseaux semi-ordonnés (d'enchevêtrements et de liaisons hydrogène) présents dans l'amylose. En contrôlant la quantité de ces phases par un traitement thermique approprié, il serait possible de cibler l'organe où le médicament serait digéré.

6.6.5 Poursuite des travaux

La continuation de ce travail aura pour objectif de confirmer les attributions tant en calorimétrie quand spectroscopie IR, présentées dans les articles 3 et 4. Cette confirmation se fera, pensons-nous, en utilisant les stratégies ci-dessous dont certaines ont fait l'objet d'études préliminaires dans notre laboratoire.

6.6.5.1 Analyse IR: Étude d'autres régions du spectre

Le spectre des mélanges amylose-eau ne peut facilement être étudié dans la région des élongations O-H à cause de l'absorptivité de l'eau. Pour contourner cette difficulté on peut utiliser plusieurs approches comme l'élimination du solvant ou sa soustraction spectrale. Chaque méthode présente des avantages et des inconvénients : en utilisant un solvant de l'amylose pour préparer des films secs, on risque de ne pas arriver à modifier la composition phasique du polymère. Par ailleurs, la technique de soustraction développée par Chapados et ses collaborateurs sur des solutions de petites molécules peut présenter des difficultés sérieuses dans des systèmes hétérogènes et visqueux [118, 119]. Une combinaison de soustraction d'eau avec une substitution ménagée des groupements O-H par O-D aiderait à étendre notre étude à des régions différentes des régions C-O et C-C (1175-950 cm^{-1}).

6.6.5.2 Analyse hybride calorimétrique-IR

6.6.5.2.1 Étude d'amyloses modifiés

Nous avons rapporté dans ce travail l'emploi du traitement thermique pour la modification de la composition phasique de l'amylose. On peut réduire la fraction des phases de réseaux en diminuant la concentration des liaisons OH par une méthylation ménagée de l'amylose. La technique utilisée pour changer la trace de fusion du PE, la réticulation (par des agents

chimiques ou par irradiation), donnerait aussi des résultats intéressants. On sait que la réduction de la mobilité des chaînes se voit dans plusieurs analyses d'un matériau (spectre de rayons X, RMN de l'état solide, composition phasique).

6.6.5.2.2 Étude de systèmes ou l'interaction amylose-solvant est modifiée

L'analyse de spectres de systèmes où la concentration d'amylose ou le pH sont changés apportera une information complémentaire au présent travail. L'étude de l'influence de l'origine de l'amylose ou de la présence d'agents complexant (acides gras) sur les spectres IR ou sur les traces de DSC_{Lent} serait très informatrice.

6.6.5.3 Utilisation d'autres techniques (RMN)

La RMN a été utilisée pour caractériser l'amylose par plusieurs laboratoires. Peu d'études se concentrent sur le changement lors du passage à la gelification. Nos travaux ont montré que seulement une faible variation du contenu phasique à cette température était observable. Nous avons initié une collaboration avec le Professeur F. Horii à l'université de Kyoto pour l'analyse de nos échantillons par ^{13}C RMN. Il serait pertinent d'intéresser un laboratoire canadien aux échantillons recristallisés lentement.

Nous voyons maintenant cette thèse comme une illustration de l'avantage du "métissage scientifique". Le concept de changement de phase sous tension, la technique de calorimétrie lente, le modèle du réseau physique ont été développés pour des polymères synthétiques tels le PE ou le polypropylène. Au cours de notre travail, nous avons découvert avec plaisir que ce concept, cette technique et ce modèle s'exportaient avantageusement aux polymères naturels. Donnons comme exemple l'utilisation de la DSC pour suivre la fusion ou dissolution des polymères : Alors que la DSC_{Lent} ajoute 30 à 50% à la chaleur de dissolution

du PE obtenue par DSC_{Rapide}, elle multiplie par un facteur d'environ 40 celle de l'amylose. Ceci est dû au fait que la phase réseau du PE provient uniquement d'enchevêtrements tandis que celle de l'amylose provient d'enchevêtrements et de liaisons hydrogène.

RÉFÉRENCES

1. Lenaerts, V., Moussa, I., Dumoulin, Y., Mebsout, F., Chouinard, F., Szabo, P., Mateescu, M. A., Cartilier, L., Marchessault, R. M., J. of Control. Releas., 53, 225, (1998).
2. Dumoulin, Y., Alex, S., Szabo, P., Carilier, L., Mateescu M. A., Carbohydrate Polymers, 37, 361, (1998).
3. Simkovic, I., Laszlo, J.A., Thompson, A. R., Carbohydrate Polymers, 30, 25-30 (1996).
4. Biliaderis, C. G., Can. J. Physiol. Pharmacol., 69, 60-78 (1991).
5. Kraak, A., Ind Crops Prod., 1, 107, (1993).
6. Galiard, T., Bowler, P. dans: Starch, Properties and Potential, T. Galiard, ed., John Wiley, New York, (1987), p. 1.
7. Takeda, C., Takeda, Y., Hizukuri, S., Cereal Chem., 66, 22, (1989).
8. Manners, D. J., Carbohydrate Polymers, 11, 87, (1989).
9. Guilbot, A., Mercier, C. dans: The polysaccharides 3, G.O. Aspinal, Ed., Academic. Press, Orlando, (1985), p. 25.
10. Morisson, W, R., Laignelet, B., J. Cereal Sci., 1, 9, (1983).
11. Radley, J. A., dans: Examination and analysis of starch and starch products, Applied Science Publications., London, (1976) p. 1.
12. Hargin K. D., Morrison., W. R., J. Sci. Food Agri., 31, 877, (1980).
13. Morrison W. R., Milligan, T. P., Azudin, M. N., J. Cereal Sci., 2, 257, (1984).

14. Morrison W. R., Tester, R. F., Law, R. V., Snape, C. E., Gidley, M. J., Cereal Chem., 70, 385, (1993).

15. Morrison W. R., Tester, R. F., Gidley, M. J., Karkalas, J., Carbohydrate Research, 245, 289, (1993).

16. van Soest, J. J. G., Starch plastic: structure property relationships, Thèse de doctorat, Université d'Utreck, Pays-Bas, (1996).

17. Biliaderis, G. C. 1991. Water relationships in food. Editeurs : H. Levine, et L. Slade, Plenum Press, New York, (1991), p. 251

18. Osman, E. M., dans: Starch, vol I, Whisler R. L. et Paschall, E. F., Ed., Academic Press, New York, (1967), p. 331.

19. van Soest, J. J. G., Hulleman, S. H. D., de Wit, D., Vliegenthart, J. F. G., Indus. Crops Prod., 5, 11, (1996).

20. Jane, J. M. S., Pure Appl. Chem., 32, 751, (1995).

21. Chebli, C., Moussa, I., Buczkowski, S., Cartilier, L., Pharmaceutical Research, 16, 1436, (1999).

22. Dumoulin, Y., Cartilier, L. H., Mateescu, M. A., J. Control. Releas., 60, 161, (1999).

23. Szabo, P. I., Ravenelle, F., Hassan, I., Preda, M., Structural-drug release properties relationship for crosslinked amylose, soumis à Carbohydrate Polymers (1999).

24. Welsh, E. J., Bailey, J., Chanarana, R., Norris, W. E., Prog. Fd. Nutr. Sci., 6, 45, (1982).

25. Gidley M. J., Macromolecules 22, 351, (1989).

26. Miles, M. J., Morris, V. J., Ring, S. G., Carbohydrate Research., 135, 257, (1985).

27. Gidley, M. J., Ross-Murphy, S. B., Macromolecules, 22, 346, (1989).

28. Kim J. O., Kim, W. S., Shin, M. S., Stärke, 49, 71, (1997).

29. LeLay, P., Delmas, G., Carbohydrate Polymers, 37, 49, (1998).

30. Dumoulin, Y., Clement, P., Mateescu M. A., Cartilier, L., STP Pharma Sciences, 4, 329, (1994).

31. Maquenne, L., Roux, E., Compt. Rend., 140, 1303, (1905).

32. Aspinall, G. O.,The polysaccharides, Academic Press, New York, (1982), vol. 1.

33. Yu, X., Houtman, C., Atalla, R. H., Carbohydrate Research, 292, 129, (1996).

34. Schoch, T.J., J. Am. Chem. Soc., 64, 2957, (1942).

35. Schoch, T.J., Cereal Chem., 18, 121, (1941).

36. Whisler, R. L., Hilbert, G. E., J. Am. Chem. Soc., 67, 1161, (1945).

37. Kerr, R. W., J. Am. Chem. Soc., 67, 2268 (1945).

38. Everet, W. W., Foster, J. F., J. Am. Chem. Soc., 81, 3459 (1959).

39. Marchessault, R. H., dans Contemporary topics in polymer science, Vol 5, Vandenberg, E. J., Ed., Plenum Publishing Corporation, (1984), p. 15.

40. Cooke, D., Gidley, M. J. Carbohydrate Research. 22, 103, (1992).

41. Goodfellow, B. J., Wilson, R. H., Biopolymers, 30, 1183, (1990).

42. Sarko, A., Wu, H. C. H., Stärke 30, 7378, (1978).

43. van Soest, J. J. G., Hulleman, S. H. D., de Wit, D., Vliegenthart, J. F. G., Carbohydrate Polymer, 29, 225, (1996).

44. Godet, M. C., Buleon, A., Tran, V., Colonna, P., Carbohydrate Polymers, 20, 91, (1993).

45. Godet, M. C., Bouchet, B., Colonna, P., Gallant D. J., Buleon, A., J. of Food Sci., 61, 1196, (1996).

46. Tako, M., Hizukuri, S., J. Carbohydrate Chem., 14, 613, (1995).

47. Miles, M. J., Moris, P. D. O., Ring, S. G., Carbohydrate Research, 135, 271, (1984).

48. Buléon, A., Delage, M. M., Brisson, J., Chanzy, H., Int. J. of Biol. Macrom., 12, 25, (1990).

49. Veregin, R. P., Fyfe, C. A., Marchessault, R. H., Taylor, M. G., Macromol., 19, 10330, (1986).

50. Godet, M. C., Tran, V., Delage, M. M., Buleon, A., Int. J. of Biol. Macromol., 15, 11, (1993).

51. Guilbot, A., Mercier, C., dans: The polysaccharides, Academic Press, Inc., vol. 3, (1985), p. 209.

52. Godet, M. C., Tran, V., Colonna, P., Buleon A., Pezolet, M., Int. J. of Biol. Macromol. 17, 405 (1995).

53. Gidley, M. J., Bociek, S. M., J. Am. Chem. Soc., 107, 7040, (1985).

54. Cowie, J. M. G., Polymers: chemistry and physics of modern materials, Intex Educational Publication, New York, (1973).

55. Billmeyer, F. W., Textbook of Polymer Science, John Wiley & Son, Toronto, (1984).

56. Delmas, G., J. Polymer Science Polymer Physics Ed., 31, 2011, (1993).

57. Nguyen, H, P., Delmas, G., Macromolecules, 25, 408, (1992).

58. Nguyen, H, P., Delmas, G., Macromolecules, 25, 414, (1992).

59. Nguyen, H. P., Delmas, G., J. Sol Chem., 23, 249, (1994).

60. van Soest, J. J. G., Benes, K., Wit, D. D., Stärke, 47, 429, (1995).

61. Zerbi, G., Gallino, G., del Fanti, N., Baini, L., Polymer, 30, 2324, (1989).

62. Agosti, E., Zerbi, G., Ward, I., Polymer, 34, 4219, (1993).

63. de Gennes, P. G., Macromolecules, 17, 703, (1984).

64. Brenner, T., Rudin, A., J. Polym. Sci. Polym. Phys. Ed., 30, 1247, (1992).

65. Kitamaru, R., Horii F., Murayama, K., Macromolecules, 19, 636, (1986).

66. Sievert, D., Pomeranz, Y., Cereal Chem., 66, 342, (1989).

67. Sievert, D., Wursch, P., J. Food Sci., 58, 1332, (1993).

68. Mestres, C., Matencio, F., Pons, B., Yajid, M.,Fliedel, G., Stärke 48, 2, (1996).

69. Kalistratova, E. N., Persikov, A. V., Danilenko, A. N., Protserov V. A., Yuryev, V. P., Stärke, 51, 160, (1999).

70. Cooke D., Gidley, J. G. M., Carbohydrate Research, 227, 113-120, (1992).

71. Eerligen, R. C., Win H. V., Delcour, J. A., J. of Thermal Anal., 47, 1229-1246, (1996).

72. Acquistucci, R., Bucci, R., Magri, A. D., Magri, A. L., J. Anal. Chem. 357, 97, (1997).

73. Shiotsubo, T., Takahashi, K., Carbohydrate Research, 158, 1, (1986).

74. Shiotsubo, T., Takahashi, K., Agric. Biol. Chem., 48, 9, (1984).

75. Biliaderis, C. G., Maurice, T. J., Vose, J. R., J. Food Sci., 45, 1669, (1980).

76. Villareal, C. P., Hizukuri, S., Juliano, B. O., Cereal Chem., 74, 163, (1997).

77. Biliaderis, C. G., dans: Water Relationship in Food, Levine, H., et Slade, L., Ed., Plenum Press, New-york, (1991), p. 251.

78. Silverio, J., Svensson, E., Eliasson, A. C., Olofsson, G., J. of Thermal Anal., 47, 1179, (1996).

79. Shogren, R. L., Jasberg, B. K., J. Env. Polym. Degradation, 2, 99, (1994).

80. Akuzawa, S., Sawayama, S., Kawabata, A., Biosci. Biotech., 61, 487, (1997).

81. Nuessli, J.,. Sigg, B., Conde-Petit B., Escher, F., Food Hydrocolloides, 11, 27, (1997).

82. Zhang, X., Nguyen, H. P., Bernazzani, P., Lapes I., Delmas G., Can. J. of Chem., 75, 1354, (1997).

83. Bernazzani, P., Delmas, G., J. of Thermal Anal., 49, 449, (1997).

84. Bernazzani, P., Chapados, C., Delmas, G., Chapitre 4 de cette thèse, Soumis à Biopolymers, (1999).

85. Bader, H. G.,Goritz, D., Starke 46, 229, (1994).

86. Muller, I. J., Gernat, C., Schulz, W., Muller, E. C., Vorwerg, W., Damaschun, G., Biopolymers, 35, 271, (1995).

87. Cheetham, N. W. H., Tao, L., Carbohydrate Polym., 36, 277, (1998).

88. Gessler, K., Uson, I., Takaha, T., Krauss, N., Smith, S. M., Okada, S., Sheldrick G. M., Saenger, W., Proceedings of the National Academy of Sciences of the USA 96, #8, 4246, (1999).

89. Miles, M. J., Morris, V. J., Ring, S. G., Carbohydrate Research, 135, 257, (1985).

90. Zobel, H. E., French, A. D., Hinkle, M. E., Biopolymers, 5, 387, (1967).

91. Waigh, T. A., Hopkinson, I., Donald, A. M., Butler, M. F., Heidelbach, F., Riekel, C., Macromolecules, 30, 3813, (1997).

92. Miles, M. J., Morris, V. J., Orford, P. D., Ring, S. G., Carbohydrate Research, 135, 271, (1985).

93. Hulleman, S. H. D., Helbert, W., Chanzy, H., Int. J. Biol Macromol., 18, 115, (1996).

94. Noda, T., Takahata, Y., Sato, T., Ikoma, H., Mochida, H., Stärke, 48, 395, (1996).

95. Brisson, J., Chanzy, H., Winter, W. T., Int. J. Biol Macromol., 13, 31, (1991).

96. Dunn Jr. L. B., Krueger, W. J., 17 Macromolecular Symposia 140, 179, (1999).

97. Laignel, B., Bliard, C., Massiot, G., Nuzillard, J. M., Carbohydrate Research, 298, 251, (1997).

98. Kulp, K, Lorenz, K., Cereal Chem., 58, 46, (1981).

99. Veregin, R. P., Fyfe, C. A., Marchessault, R. H., Macromolecules, 20, 3007, (1987).

100. Tanner, S. F., Ring, S. G., Whittam, M. A., Belton, P. S., Int. J. Biol Macromol., 9, 218, (1986).

101. Gidley, J. M., Bociek, S. M., J. Am. Chem. Soc. 107, 7040, (1985).

102. Gidley, M. J., Cooke, D., Darke, A. H., Hoffmann, R. A., Russell, A. L., Greenwell, P., Carbohydrate Polym., 28, 23, (1995).

103. Kondo, T., Sawatari, C., Polymer, 37, 939, (1996).

104. van Soest, J. J. G., de Wit, D., Tournois, H., Vliegenthart, J. F. G., Stärke, 54, 1, (1994).

105. van Soest, J. J. G., de Wit, D., Tournois, H., Vliegenthart, F. G. J., Carbohydrate Research, 279, 201-214 (1995).

106. van Soest, J. J. G., de Wit, D., Tournois, H., Vliegenthart, F. G. J., Polymer, 35, 4721, (1994).

107. Vasko, P. D., Blackwell, J., Koenig, J. L., Carbohydrate Research, 19, 297, (1971).

108. Vasko, P. D., Blackwell, J., Koenig, J. L., Carbohydrate Research, 23, 407, (1972).

109. Cael, J. J., Koenig, L. J., Blackwell, J. Carbohydrate Research, 29, 123, (1973).

110. Cael, J. J., Koenig, J. L., Blackwell, J., Biopolymers, 14, 1885, (1975).

111. Delwiche, S. R., Norris K. H., Pitt, R. E., Appl. Spectros., 46, 783, (1992).

112. Delwiche, S. R., Bean, M. M., Miller, R. E., Webb, B. D., Williams, P. C., Cereal Chem., 72, 182, (1985).

113. Villareal, C. P., Cruz, N. M. D. L., Juliano, B. O., Cereal Chem., 71, 292, (1994).

114. Reeves, J.B., Appl. Spectros., 50, 154, (1996).

115. Bernazzani, P., Chapados, C., Delmas, G., Chapitre 4 de cette thèse, soumis à J. Polym. Sci. Polym. Phys. Ed., (1999).

116. Gidley, M. J., Bulpin, P. V., Macromolecules, 22, 34, (1989).

117. Fitzback, Mémoire de maîtrise, Sciences des pâtes et papiers, Université du Québec à Trois-Rivières, (1992).

118. Max, J. J., Chapados, C., Appli. Spectros., 52, 963, (1998).

119. Max, J. J., Trudel, M., Chapados, C., Appl. Spectros., 52, 234, (1998).